NTNU – Trondheim
Norwegian University of
Science and Technology

On the Mechanical Properties of Cement Grout

Rikke Marie Vollan

Civil and Environmental Engineering
Submission date: June 2012
Supervisor: Thomas Benz, BAT

Norwegian University of Science and Technology
Department of Civil and Transport Engineering

NTNU – Trondheim
Norwegian University of
Science and Technology

On the Mechanical Properties of Cement Grout

Rikke Marie Vollan

Civil and Environmental Engineering
Submission date: June 2012
Supervisor: Thomas Benz, BAT

Norwegian University of Science and Technology
Department of Civil and Transport Engineering

NORWEGIAN UNIVERSITY OF SCIENCE AND TECHNOLOGY
DEPARTMENT OF CIVIL AND TRANSPORT ENGINEERING

Report Title:	Date: June 18, 2012			
On the mechanical properties of cement grout	Number of pages (incl. appendices): 115			
	Master Thesis	X	Project Work	

Name:
Rikke Marie Vollan

Professor in charge/supervisor:
Professor Thomas Benz

Other external professional contacts/supervisors:

Abstract:

During pressure grouting of ground anchors in non-cohesive soils the water in the grout is filtrated out, producing a stiff filter cake material. Often the grouting is done in more than one stage so that the filter cake will be unloaded as the pressurizing is paused, and then reloaded again during the following grouting phase. Little is known of how this filtered material behaves, neither for the first time loading nor for the unloading and reloading. Aiming at a better understanding of the properties of this material, filtration tests on fresh grout with water contents ranging between 0,4-0,6 and filtration pressures between 1-15 bar have been executed. Additionally, oedometer tests were run on the filter cake material produced during the filtration tests. A split-ring oedometer allowing measurements of the horizontal pressures were used. Thus, the lateral response can also be evaluated from the oedometer results in addition to conventional oedometer properties like the one-dimensional stiffness. Also the water contents before and after filtration and after oedometer testing were measured, and a simple permeability test was done on some of the filter cakes. It was found that the initial water content and the filtration pressure had only a minor effect on the water content after filtration, in general ranging between 0,24-0,30. The time needed for the filtration process to finish was found to be unaffected by the initial water content, but decreasing with increasing filtration pressure. The permeability of the filter cake was found to lie in the order of $1 \cdot 10^{-8}$ to $2 \cdot 10^{-7}$, mainly affected by the initial water content. The oedometer results show an increase in initial stiffness with filtration pressure, while the stiffness seems less affected by this as the load increases. However, the increase in stiffness is small and the material does not have clear over and normally consolidated areas. When unloading and reloading in the oedometer, the material clearly remembers the prestressing to a much greater extent, giving much higher stiffnesses for the reloading sequences than for first time loading. The lateral stress coefficient was found to vary between 0,25-0,30 for first time loading. Based on the over-all results, a kinematic hardening model is proposed for modeling the filtered materials behavior.

Keywords:

1. Split ring oedometer
2. Filtration test
3. Cement grout
4. Ground anchor

NTNU
Faculty of Engineering Science
and Technology
Department of Civil
and Transport Engineering

MASTER THESIS

(TBA4900 Geotechnical Engineering, Master Thesis)

Spring 2012
for
Rikke Marie Vollan

On the mechanical properties of cement grout

BACKGROUND

Cement grouts have various fields of application in geotechnical engineering, ranging from bulk filling and sealing grouting to various forms of compaction grouting. Especially in the latter, the mechanical properties of grout may play an import role in design. Examples for the application of compaction grouting are: Underpinning of buildings, improvement and uplift of foundations, stabilization of embankments, working face strengthening and horizontal umbrella grouting in tunnel construction, increasing the load-bearing capacity of piles, and anchor grouting. Yet the mechanical properties of cement grout in these applications are not fully understood as can be observed for example in the case of grouted anchors in sandy soils. Although empirical evidence suggests that the bearing capacity of grouted anchors increases with grouting pressure, little is known about the mechanism behind and the quantification of the observed increase. Thus, it is difficult to propose optimum design procedures (e.g. grouting procedure) for such structures. The research performed in this thesis shall contribute to the development of a mechanical model for cement grout which subsequently shall be used to improve numerical modeling of grouted anchors in sand (not part of this thesis).

TASK DESCRIPTION

The aim of the thesis is to generate knowledge on the mechanical properties of filtered cement grout. The mechanical properties shall be derived for various grouting pressures and various water cement ratios of the cement grout. The thesis shall focus on deformation properties. Moreover, the thesis shall contribute to the understanding of the filtration process during grouting by adopting a 1D laboratory model for the filtration process. Mechanical testing shall be performed in a split ring oedometer apparatus.

The objectives of the thesis are defined as follows:

1. To perform filtration tests on cement grout with different water contents and different grouting pressures
2. To test the mechanical properties of the readily filtered cement grout (filter cake)
3. To organize and plot all test results in a structured manner
4. To evaluate soil mechanical properties of the filter cake material (deformation only)
5. To discuss the findings and relate them to soil mechanics of soft soils
6. To propose a type of constitutive model that could be used to model cement grout
7. To conclude on the generated results

It is acknowledged that the given task involves a considerable amount of testing with partly new equipment and that due to unforeseen issues in testing not all objectives may be fulfilled in the given timeframe.

Professor in charge: Prof. Thomas Benz

Department of Civil and Transport Engineering, NTNU

Date: 06.06.2012

Professor in charge

Acknowledgements

This report is written as a master thesis in geotechnical engineering at the Department of Civil and Transport Engineering at the Norwegian University of Science and Technology spring 2012.

The author wishes to thank the professor in charge of this thesis, Prof. Thomas Benz for patience and understanding during a though time. Also, many thanks are sent to Xenia Stodieck for many helpful discussions and advises. Hopefully, the work with this master thesis will give some valuable additions to her doctor thesis. Finally, the author also wants to thank the laboratory engineer Per Østensen for all the help on proper setup of the laboratory equipment.

Rikke Marie Vollan
Trondheim, June 2011

Abstract

During pressure grouting of ground anchors in non-cohesive soils the water in the grout is filtrated out, producing a stiff filter cake material. Often the grouting is done in more than one stage so that the filter cake will be unloaded as the pressurizing is paused, and then reloaded again during the following grouting phase. Little is known of how this filtered material behaves, neither for the first time loading nor for the unloading and reloading. Aiming at a better understanding of the properties of this material, filtration tests on fresh grout with water contents ranging between 0,4-0,6 and filtration pressures between 1-15 bar have been executed. Additionally, oedometer tests were run on the filter cake material produced during the filtration tests. A split-ring oedometer allowing measurements of the horizontal pressures, were used. Thus, the lateral response can also be evaluated from the oedometer results in addition to conventional oedometer properties like the one-dimensional stiffness. Also the water contents before and after filtration and after oedometer testing were measured, and a simple permeability test was done on some of the filter cakes. It was found that the initial water content and the filtration pressure had only a minor effect on the water content after filtration, in general ranging between 0,24-0,30. The time needed for the filtration process to finish was found to be unaffected by the initial water content, but decreasing with increasing filtration pressure. The permeability of the filter cake was found to lie in the order of $1 \cdot 10^{-8}$ to $2 \cdot 10^{-7}$, mainly affected by the initial water content. The oedometer results show an increase in initial stiffness with filtration pressure, while the stiffness seems less affected by this as the load increases. However, the increase in stiffness is small and the material does not have clear over and normally consolidated areas. When unloading and reloading in the oedometer, the material clearly remembers the prestressing to a much greater extent, giving much higher stiffnesses for the reloading sequences than for first time loading. The lateral stress coefficient was found to vary between 0,25-0,30 for first time loading. Based on the over-all results, a kinematic hardening model is proposed for modeling the filtered materials behaviour.

Sammendrag

Ved trykkinjisering av jordankere i kohesjonsfrie jordarter presses vannet ut av den sementbaserte injeksjonsmassen, og det dannes et stivt filtrert materiale. Ofte gjøres injiseringen i flere steg, slik at det filtrerte materialet vil oppleve en avlastning når man tar en pause i injiseringen, for så å bli rebelastet når man gjenopptar injiseringsarbeidet. Det er uklart hvordan dette materialet oppfører seg både under første gangs belastning, avlastning og rebelastning. For å bedre forstå hvilke egenskaper dette materialet innehar har det derfor blitt utført filtreringstester med filtreringstrykk på 1-15 bar på fersk sementpasta med vanninnhold på 0,4-0,6. I tillegg ble det kjørt ødometerforsøk i et splittet ring-ødometer på det filtrerte materialet som ble produsert under filtreringstestene. Et slikt ødometer gjorde det mulig å måle horisontalspenningene, slik at også den laterale responsen kunne undersøkes – i tillegg til egenskapene man normalt finner ved et ødometersforsøk. Det ble også gjort målinger av vanninnholdet i sementpastaen både før og etter filtrering og etter ødometerforsøkene, i tillegg til en enkel permeabilitetstest på det filtrerte materialet. Det ble funnet at vanninnholdet før filtrering og filtreringstrykket hadde en marginal effekt på vanninnholdet etter filtrering, som generelt varierte mellom 0,24-0,30. Tiden det tok å filtrere materialet var lite påvirket av det initielle vanninnholdet, men viste seg derimot å minke for økende filtreringstrykk. Permeabiliteten ble anslått til å ligge i størrelsesorden $1 \cdot 10^{-8}$ to $2 \cdot 10^{-7}$, og varierte i all hovedsak med det initielle vanninnholdet. Ødometerresultatene viste en økning i den initielle stivheten med økende filtreringstrykk, mens denne påvirkningen avtok med økende pålastning. Økningen var derimot liten, og materialet har ikke noe klart overkonsolidert og normalkonsolidert område. Ved av- og rebelastning i ødometeret husket derimot sementen avlastningsnivået i mye større grad, og gav en sterk økning i stivhet i det overkonsoliderte området. Hvilestrykkskoeffisienten ble funnet til å variere i området 0,25-0,30 for første gangs pålastning. Basert på resultatene samlet, foreslås det å bruke en kinematisk herdingsmodell for å modellere oppførselen til det filtrerte materialet.

Contents

List of Figures

List of Tables

Nomenclature

δ_{self}	Self deformation of oedometer
$\delta\rho$	Incremental change in deformation during filtration test
$\Delta\sigma'_h$	Incremental change in horisontal effective stress
$\Delta\sigma'_v$	Incremental change in vertical effective stress
Δh	Vertical displacements in oedometer sample
$\Delta K'_0$	Lateral stress coefficient for stress changes
Δt	Time increment
δt	Incremental change in time after start of filtration
ΔV_w^{out}	Volume of water coming out during an increment of time Δt
γ	Total unit weight
γ_g^i	Unit weight of grout before filtration
γ_w	Unit weight of water
ρ	Mobilized friction
ρ	Vertical displacement/deformation during filtration test
σ	Filtration pressure
σ'_1	Major effective principle stress
σ'_3	Minor effective principle stress
σ'_a	Effective vertical stress at a
σ'_a	Effective vertical stress at time a
σ'_b	Effective vertical stress at time b
σ'_h	Horizontal effective stress
σ'_m	Mean effective vertical stress for an time increment ranging from a to b

σ'_v	Vertical effective stress
σ_a	Reference stress level equal to 100kPa
σ_h	Horizontal total stress
σ_v	Vertical total stress
τ	Shear stress
ε'_v	Vertical strain
A	Cross sectional area of filter cake
A	Inner cross sectional area of steel cylinder
a	Curve fitness parameter/stress exponent
c_v	Coefficient of consolidation
d	Diameter of the anchor
d_c	Thickness of the filter cake after filtration
d_i	Depth of fresh grout in steel cylinder before filtration
e	Void ratio
e_c	Void ratio of filter cake
e_g	Void ratio of fresh grout
F	Load during oedometer test
F_c	Resistance of the filter cake
F_p	Resistance of the filter stone used in the filtration test
h_0	Height of oedometer sample before loading
k	Coefficient of permeability
K'_0	Coefficient of lateral stress
k_c	Coefficient of permeability for the filter cake
k_p	Coefficient of permeability for the filter stone used in the filtration test
$k_{w\sigma}$	Weighted initial apparent water content and filtration pressure
L_{bf}	Bond length of the tendon
L_c	Thickness of the filter cake during filtration
L_{fixed}	Fixed length of the anchor
L_{free}	Free length of the anchor
L_p	Thickness of filter stone in filtration test

L_{tf}	Free length of the tendon
M	Inclination of the Coloumb criterion in a p'/q-plot
M	Oedometer modulus
m	Modulus number
N	Inclination of the Coloumb criterion in a σ_3'/σ_1'-plot
p	Hydraulic pressure head
p	Total mean stress
p'	Effective mean stress
q'	Deviatoric stress
R	Coefficient of determination according to the least squares method
R	Time resistance
S	Inclination of the Coloumb criterion in a σ_3'/q-plot
t	Time after start of filtration
t	Time after start of oedometer
t	Time after start of permeability test
u_b	Pore pressure measured at the bottom of the oedometer sample
V	Total volume
V_w	Volume of water
V_w^{out}	Amount of water coming out during filtration
w	Water content
w_c	Water content of the filtration cake
W_g^i	Weight of fresh grout in steel cylinder before filtration
W_s	Weight of solids
W_w^i	Weight of water in steel cylinder before filtration
W_w^{out}	Weight of water coming out during filtration

Chapter 1

Introduction

During pressure grouting of ground anchors and other geotechnical fields related to grouting in non-cohesive soils the water in the grout is filtrated out, producing a stiff filter cake material. The aim of this thesis is to widen the understanding of the grouting process by investigating the mechanical properties of this filtered grout. This was done by testing filtered grout material in a split ring oedometer, allowing evaluation of the lateral stress response in addition to conventional oedometer results like the one-dimensional stiffness. The grouting procedure is often executed in more than one phase, meaning that the filtered grout will be unloaded when the process is stopped, and reloaded again when it is restarted. It is believed that after unloading some residual stress is trapped within the filter cake, but little is known about this. Thus, hoping to establish some knowledge also on unloading and reloading properties the filter cake was manually unloaded and mechanically reloaded in the oedometer. Additionally, the process of making a filter cake was investigated by measuring the pore pressures, time and displacements during filtration, using different filtration pressures and grouts with different water/cement ratios.

Several investigations on the process of filtrating cement grouts and the mechanical properties of fresh cement paste, mortar and concrete have been carried out. There has however been little investigations on the mechanical properties of the filtered material, setting out the grounds for the work of this thesis. The experimental setup for filtration testing used in this thesis resembles that of McKinley (1993). The main difference is that McKinley drained the grout through the top piston, meaning the production of the filter cake would be initiated right under the top piston. Thus, the water flow was directed upwards, creating problems with cement grout finding it's way out between the moving top piston and the cylinder, hindering further displacements of the top piston. Thus, in this thesis the drainage vent was placed at the bottom to create water flow in the same direction as the piston displacement, hoping to avoid this problem. Also, a wider range of filtration pressures and water/cement ratio are used. McKinley (1993) also investigated the deformation properties in a one-dimensional consolidation test, using the same equipment as during filtration. He was however not able to measure the displacements for loads below the filtration pressure, due to the low sensitivity of the equipment he used. The split ring oedometer used in this

thesis is however very sensitive and should be able to measure displacements down to an order of 0,001 mm. Additionally, the lateral response can be evaluated from the horizontal stresses.

Firstly, in Section 2.1 an introduction on pressure grouted ground anchors are given, mainly focusing on grouting in non-cohesive granular soils as this is where filtering of the grouting material is most likely to happen. Further, Sections 2.2, 2.3 and 2.4 explains the basic theory behind and the general output expected from filtration tests, permeability tests and split ring oedometer tests, respectively. Additionally, a brief comment on basic methods used for analysis of the results are given in Section 2.5. Thereafter, in Chapter 3 details on the experimental setup in general and setup of laboratory equipment for filtration tests, permeability tests and split ring oedometer tests are given in Sections 3.1 to 3.4, respectively. In Sections 4.1, 4.2 and 4.3 the results from the filtration tests, permeability tests and oedometer tests are presented and discussed. Finally, the main results are summarized and concluding remarks added in Chapter 5.

Chapter 2

Theory

2.1 Ground anchors

There are various areas of applications for grouted anchors, as they constitute an effective way of transferring tensile forces to soil masses. Also compressive forces can be applied, but ground anchors often make an expensive and resource-demanding alternative compared to other methods, and are therefore rarely used for this purpose alone. Specifically, common areas of use involve tie back of retaining walls, preventing overturning, uplift or sliding of a structure, slope reinforcement and avalanche galleries. Tensile forces from the structure is then transferred either to soil or rock masses. In Norway the latter is the most common, since the depth to rock often is limited. In many other countries, the depth to rock is often larger and anchorage in soil is therefore more of interest. The execution of drilling and grouting varies, depending on the ground conditions. In this thesis the main focus will be on anchorage in fine granular non-cohesive soils, since these are the conditions where the making of a filtrated grout cake is most likely to happen. The voids in such soils are in general to small for the thick cement to easily permeate into the ground. Thus, the pressure increases while grouting and the water in the cement is filtered out of the cement and dissipates into the ground. Further in this section basic properties of ground anchorage is outlined.

2.1.1 How an anchor looks and works

Anchors can be permanent or temporary (in service for less than 2 years), see Figure 2.1 and Figure 2.2 for design details. In general grouted anchors are made of one or multiple tendons with injected grout bodies at the ends, where the tendons are tensioned and the stresses are locked off with an anchor head. The load is initially transmitted to the distal end of the grout column and due to elasticity of the tendon, the load is transmitted to the proximal end as the load increases. The tension also produces tension cracks in the grout

body. Further, the load is transmitted from the grout to the ground by shear along the interfaces.

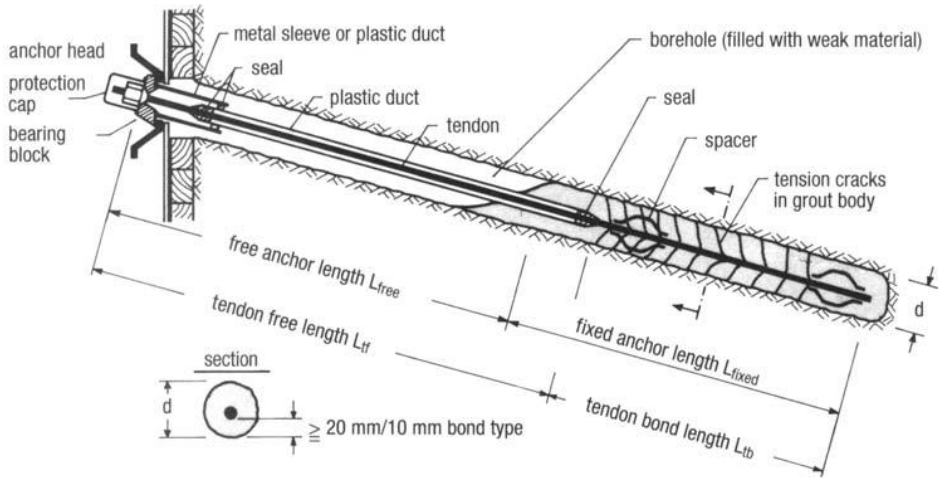

Figure 2.1: Scheme of temporary anchor (Smoltzcyk and Ulrich, 2002)

The grout body

The diameter of the grout body may be equal to or greater than the diameter of the borehole, the boreholes being either tremied or pressure grouted, respectively. Tremie grouting is mostly used in rock and very stiff cohesive soils, while for non-cohesive soils or fissured rock, pressure grouting is more common. The pressure can vary strongly, and high pressures give larger and often more irregular grout bodies. Empirical evidence show that large bodies gives higher bearing capacities, but the quantity of increase in bearing capacity by pressure is not clear, making it difficult to propose optimum design procedures. Large volumes of injected grout can also cause heave of the ground around the anchor and damage adjacent services. Controlled enlargements up to three to four times the borehole diameter can be done efficiently with a mechanical underreaming tool - though this is most relevant for stiff cohesive soils. For the subject of filtration cake formations the soils of interest are fine granular non-cohesive soils, and the focus in this thesis will therefor be on pressure grouting(Warner, 2004, Xanthakos, 1991).

The tendons

The tendons are often locked off at a stress state big enough to account for both the required final stress and the loss of tension with time. Also, post-tensioning is common if the load capacity of the anchor cannot allow full tensioning in one go. Commonly, the load and corresponding displacements are measured and the load/displacements curve extrapolated to infinite displacements to estimate the load capacity.

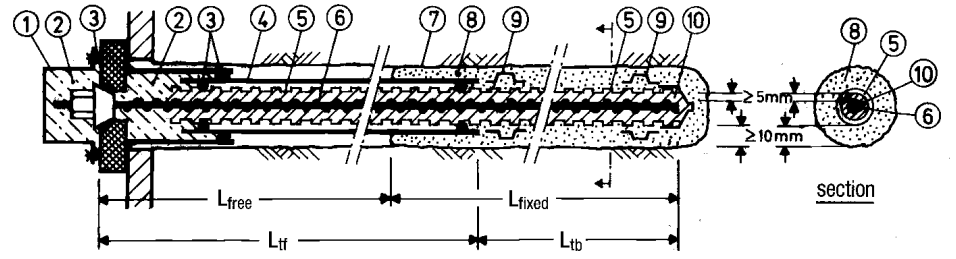

(a) With a single corrugated plastic duct

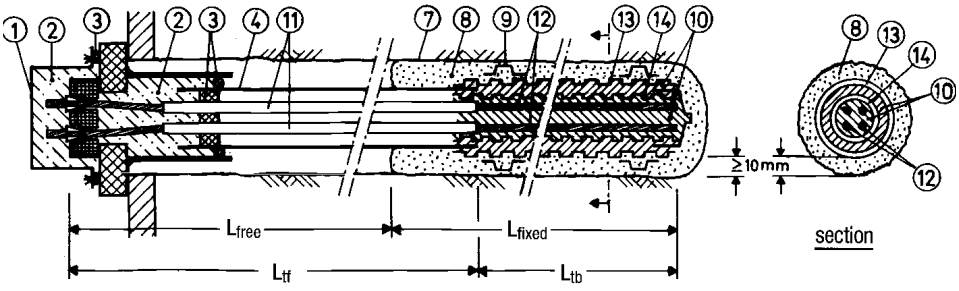

(b) With two corrugated plastic ducts

Figure 2.2: Scheme of permanent anchors (Smoltzcyk and Ulrich, 2002)
1 protective cap, 2 flexible corrosion protection compound, 3 seal, 4 smooth plastic duct, 5 corrugated plastic duct, 6 ribbed bar tendon, 7 borehole, 8 grout body, 9 spacer, 10 cement grout in corrugated plastic duct, 11 plastic sheath filled with corrosion protection compound, 12 multi-unit tendon of strands, 13 outer corrugated plastic duct, 14 inner corrugated plastic duct

The tendons usually consist of one or multiple steel bars, wires or strands. It is important that the tendons are protected against corrosion - especially for permanent anchors, but also for temporary anchors. There are a great deal of circumstances that can cause severe corrosion on steel tendons, and since all relevant factors rarely are known, a superior requirement that all tendons should be protected against corrosion has been set to ensure proper corrosion protection.
A temporary anchor should therefore be covered with a plastic duct along the free length, and the cement grout shall cover at least 10mm of the tendon bond length.
A permanent anchor must either be protected by two protective barriers against corrosion or one barrier combined with an integrity test for this barrier (e.g. electrical resistivity test). Along the free length L_{tf}, it is common to use two plastic ducts. Along the bonded length L_{tb}, the following alternatives are much used (Smoltzcyk and Ulrich, 2002)

- A single corrugated plastic duct and cement grout between the tendon and the duct with a minimum cover of 5 mm and a crack width not exceeding 0.1 mm under service load. If the cover cannot be verified, an integrity test is required (Figure 2.2(a)).
- Two concentric corrugated plastic ducts around the tendon with the space between the ducts completely filled with cement grout (Figure 2.2(b))

The anchor head

For both permanent and temporary anchors the anchor head should either be protected by a non-fluid corrosion protection compound or by a protective cap (Smoltzcyk and Ulrich, 2002). Examples on design of anchor heads are shown in Figure 2.3.

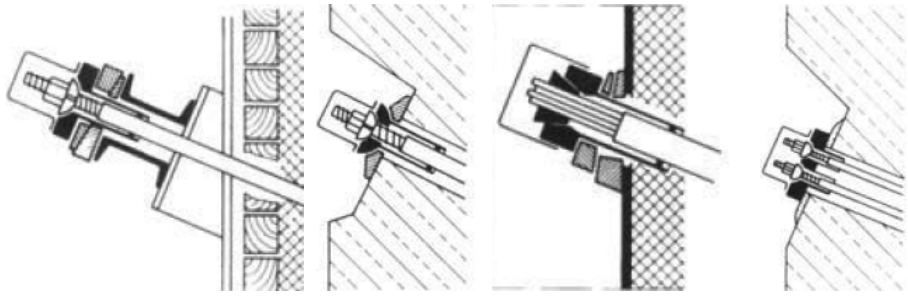

Figure 2.3: Examples of anchor head design (Smoltzcyk and Ulrich, 2002)
(a) Single bar anchor: locknut and wedge-shaped bearing plates for a soldier pile wall
(b) Single bar anchor: locknut and globular plate bearing for a concrete wall
(c) Multi-strand anchor: wedges and wedge-shaped bearing plates for a sheet pile wall
(d) Multi-bar anchor: locknuts and bearing plate upon a mortar bed

Failure states

Most commonly the anchors are so-called deep anchors, but also shallow anchors are used. The main difference between these two types of anchors are the failure mechanism when reaching the pull-out load. For a deep anchor the failure mechanism is comparable to the point bearing capacity of a pile, while a shallow anchor is considered to have reached failure when measurable movements arise at the soil surface. The critical depth at which the failure mechanism changes depend on the diameter of the anchor and the soil conditions. It is common to use the ratio of the length and the diameter of the anchor (relative depth) to determine whether an anchor is deep or shallow, and the critical relative depth will be higher for denser soils. Thus, for a shallow anchor the failure mode is characterized by failure within the ground mass, while for a deep anchor the failure is in the anchor it self. This can happen by failure of the bond between the grout and the tendon or between the ground and the grout, where the latter is the most interesting from a geotechnical perspective. Also failure can occur in the tendon itself or some other component and the grout body may fail by bursting (Smoltzcyk and Ulrich, 2002).

2.1.2 Installing an anchor in the ground

In this section, common practice for installment of ground anchors in agreement with the European Standard EN 1537 is given (European Committee for Standardisation, 1999).

Drilling

Commonly, the drilling holes are in the range of 80-200 mm in diameter, and up to 50 m or more in length. The drilling is usually of rotary or rotary-percussion type, and it is common to insert a casing at the same time, see Figure 2.4(b). Generally, a casing is needed when exceeding a certain depth, depending on the ground conditions. When the anchors are long or the the ground consists of material sensitive to erosion, using a casing is recommended to avoid soil falling down on and possibly damaging the rods. Commonly, a hollow drill rod allowing water injection and a casing annulus for flush removal are used. It is also possible to use rotary or rotary-percussion drilling without the insertion of a casing (Figure 2.4(a)) if the conditions are appropriate, though this is rarely the case for cohesionless soils. Alternatively, if a casing is not used one can use cement grout as flush medium. In this case the drilling rod is usually left in the hole, later acting as a tendon (Smoltzcyk and Ulrich, 2002).

Grouting

After drilling the borehole and inserting the casing and the tendon, the hole is grouted. When a casing is used, grout is injected by pressure at the head of the casing. Simultaneously, the casing is rotated and withdrawn to the end of the free fixed anchor length. When the casing has reached this point, it is further withdrawn without pressure grouting. To

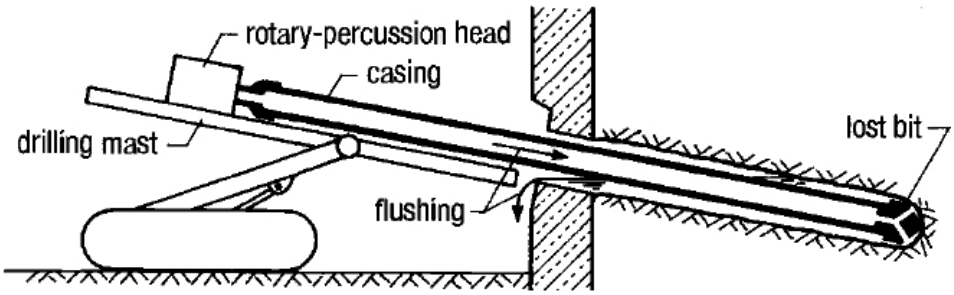

(a) Rotary or rotary-percussion drilling with lost bit crown

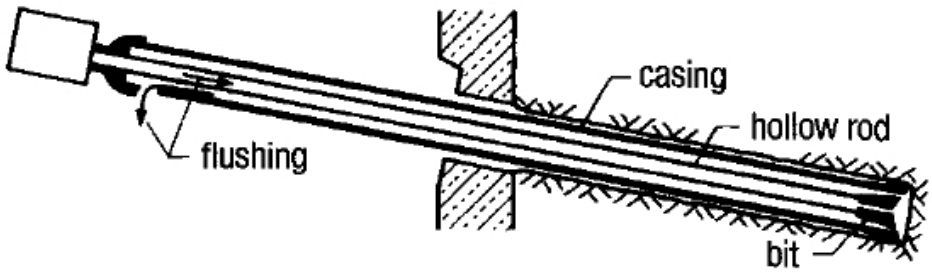

(b) Overburden drilling with casing and interior hollow rod for counterflush

Figure 2.4: Drilling methods for non-cohesive soils (Smoltzcyk and Ulrich, 2002)

avoid load transfer to the anchored structure, it may be necessary to flush out some grout along the free length. The resulting void can be filled with a weak or compressible filler. One can also install soft packs around the tendon, allowing a full length grouting done in one single phase (Smoltzcyk and Ulrich, 2002).

The grouting material is usually a stable cement paste or mortar, injected either via a grouting head attached to the casing or a separate pipe attached to the tendon. Also, so-called tube-á-manchette is an alternative, though it is mostly used for fine cohesive soils. The space between the sleeve pipe and the borehole is then sealed by a plastic sheath grout of bentonite-cement, preventing the grout from escaping to the surface instead of penetrating into the ground. This system also makes it possible to inject different grout mixes at different ports within the same borehole at different times. By comparison, grouting through rods, casing or pipes can only allow a certain pressure to avoid the grout escaping to the surface. For ground anchors, the purpose of grouting is mainly to increase the tensile strength of the soil. The effect of the grouting pressure is not completely understood, but it seems like most investigations concludes that the effect is relatively small compared to other factors such as soil density as long as the pressure is greater than some minimum value (500 - 1000 kPa) and lower than the fracturing pressure (Smoltzcyk and Ulrich, 2002). For cohesionless soils, water/cement ratios of 0,4-0,5 and pressures of more than 10 bar are common. When a grout is exposed to such high pressures in fine or medium coarse cohesionless soils, the excess water in the grout will be pressed out of the grout as the grout itself cannot permeate into the voids of the soil. This process produces a filtrated grout cake, which is much stiffer than the original grout mass. It has also been speculated that a fraction of the grouting pressure remains locked-in to the ground after grouting, causing a higher load capacity of the anchors (McKinley, 1993, Smoltzcyk and Ulrich, 2002). Little research has been done on the filter cakes deformation properties, which encourages the work for this thesis.

The spread of the grout is normally directly proportional to the grouting pressure, and the rheological properties of the grout mix influence the minimum and maximum allowable grouting pressures. The spread is also inversely proportional to the yield value of the grout mix which defines its static strength and minimum pumping pressure. When specifying both the maximum allowable pressure and the pressure losses that occur when grout enters small fissures, the viscosity of the grout must be considered. Thus, the maximum pressure is usually defined on the basis of the hydraulic interaction of the void geometry and rheology of the grout mix, rather than of weight of the overlying ground. Often, the maximum pressure is set to 80% of a fracture pressure which is found by testing in situ. The fracture pressure is attained when increased pump rates at a test point result in decreasing grouting pressures (Smoltzcyk and Ulrich, 2002).

When planning grouting it is also important to be aware of the effects from ground water. Seepage flow is important if the flow velocity leads to surface erosion of the fresh injected grout mix. Different chemical agents can also lead to retardation or stopping of the grouts hardening. It is also important to evaluate the spread of the grout when injecting under the ground water level. The more wide spread the grout is, the larger the buoyancy. Thus, if there is a chance of uplift of the grout body due to water pressure, a wide spread grout body must be avoided (Smoltzcyk and Ulrich, 2002, Xanthakos, 1991).

2.2 Filtration testing

Trying to recreate the filtration conditions in the ground the filtration testing was carried out by filling cement paste in a steel cylinder, applying a constant load on top and draining it at the bottom. Initially, the cylinder contains fresh cement paste with a void ratio e_g and water content w_g. Water is then pressed out of the grout through the bottom, starting the formation of a filter cake at the base. As the filtration continues, the thickness of this cake increases until all the excess water has been filtrated out and all the grout has been transformed into a filter cake. Figure 2.5 illustrates the filtration process with time. This is very much the same procedure as was used in McKinley (1993), but with minor alterations. E.g. the draining at the bottom ensures that filtrated grout does not get stuck between the piston and the cylinder, which was described as a problem in McKinley (1993).

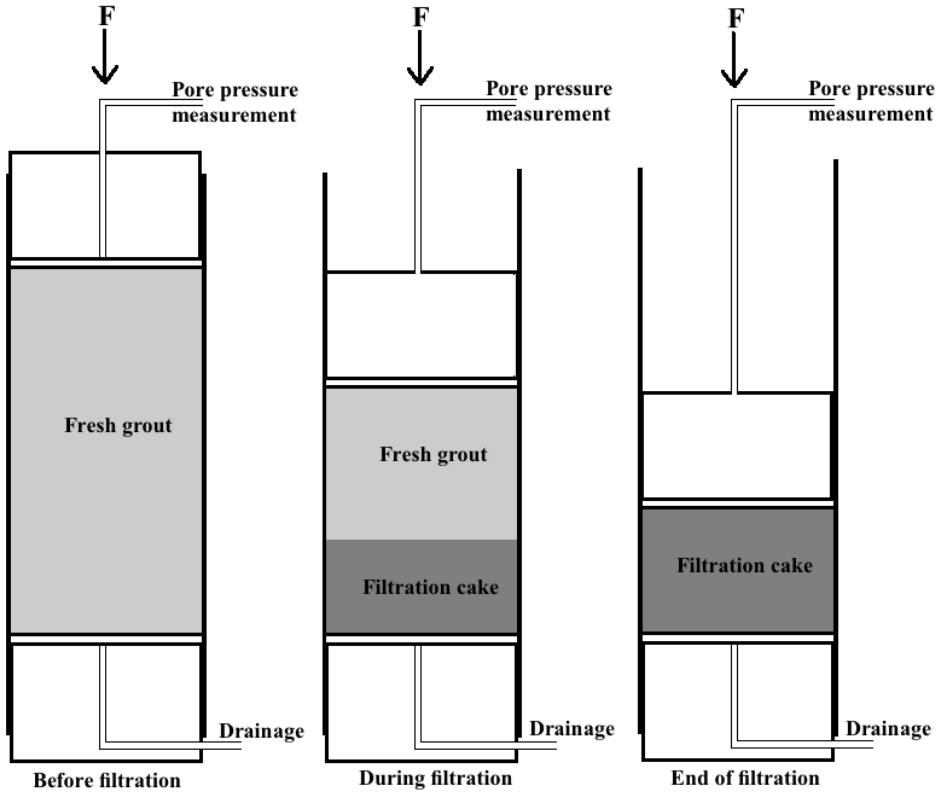

Figure 2.5: Illustration of filtration process with time

The following assumptions are made for the filtration analysis

- Both the water and the cement particles are incompressible
- There is no air in the slurry

- Effects of bleeding and hindered settling are negligible compared to the piston velocity
- Chemical setting and the effect of use of setting retarder is negligible
- The filter cake is very stiff, and the variation in moisture content within the filter cake is small compared to the difference in moisture content between the cake and the fresh grout.
- Particle size varies little during the induction period, so that the grout cake can be treated as a filter of constant permeability and uniform void ratio
- Friction between the piston and the cylinder and between the grout and the cylinder is negligible.

As filtration goes on the thickness L_c of the filter cake increases. At a time t after start of filtration the settlement ρ is

$$\rho = L_c \frac{e_g - e_c}{1 + e_c} \tag{2.1}$$

Where e_c is the void ratio of the filter cake. The rate of settlement equals the rate at which water is pressed out. On the lower surface of the filter cake there are no pore pressures and the effective stress equals the filtration pressure. On the surface between the grout and the upper filter stone the effective stresses will be zero, since the pore pressure equals the filtration pressure. Thus, the potential difference equals the filtration pressure σ and Darcy's law gives (McKinley, 1993)

$$\frac{\delta\rho}{\delta t} = \frac{\sigma}{\gamma_w}\left[\frac{L_p}{k_p} + \frac{L_c}{k_c}\right]^{-1} \tag{2.2}$$

Where $\delta\rho$ is an infinitely small incremental change in settlements during an infinitely small increment of time δt, γ_w is the unit weight of water, L_p is the thickness of the filter stone and k_p and k_c are the coefficients of permeability for the filter stone and the filter cake, respectively. Combining equations (2.1) and (2.2) and integrating with respect to time gives

$$\rho = F_c \frac{t}{\rho} - F_p \tag{2.3a}$$

$$F_c = \frac{2\sigma k_c}{\gamma_w}\left[\frac{e_g - e_c}{1 + e_c}\right] \tag{2.3b}$$

$$F_p = 2k_c\left[\frac{L_p}{k_p}\right]\left[\frac{e_g - e_c}{1 + e_c}\right] \tag{2.3c}$$

And thus

$$\frac{F_p}{F_c} = \frac{L_p \gamma_w}{k_p \sigma} \tag{2.4}$$

F_c and F_p representing the resistance of the filter cake and filter stone means that a plot with the displacements on the abscissa and time divided by displacements on the ordinate

should produce a straight line if the material properties are constant. Such a plot should thus be able to show the importance of the filter stone resistance relative to the filtration cake resistance, the former having a more marked effect at the initial part of the curve and at low filtration pressures.

If F_p is small we obtain

$$\rho^2 = F_c t \tag{2.5}$$

and the permeability of the filter cake can be calculated as

$$k_c = \frac{d_c^2 \gamma_w}{2 t_f \sigma} \left[\frac{e_g - e_c}{1 + e_c} \right] \tag{2.6}$$

Where d_c is the final thickness of the filter cake, and t_f is the time from start until filtration is finished. From equation (2.5) it is clear that the piston displacements should be directly proportional to the square root of time during the filtration process. When all the grout has been transformed into a filter cake, the piston stops and the filter cake is consolidated. For the filtration and consolidation of slurries the result should lie between the two curves shown in Figure 2.6, neglecting creep and secondary compression (McKinley, 1993).

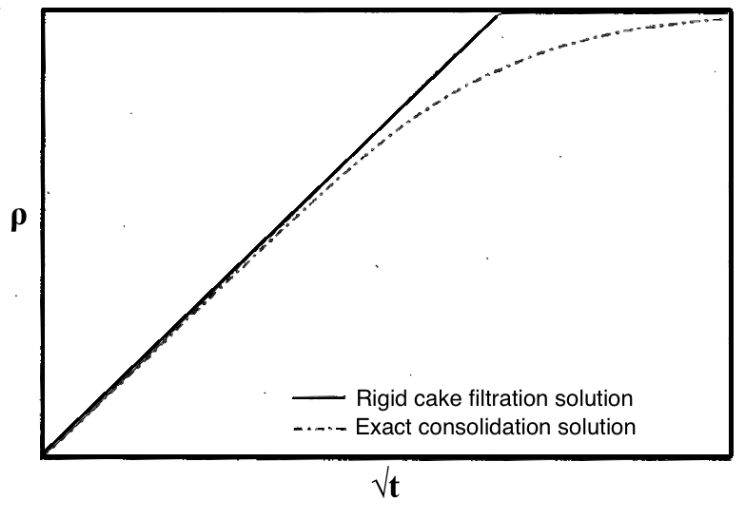

Figure 2.6: Settlement curves (McKinley, 1993)

Assuming that only water particles are pressed out, the amount of water coming out V_w^{out} corresponding to the displacements should equal $V_w^{out} = \rho A$, where A is the area of the cylinder. Consequently, the water content after filtration w_c can be estimated by

$$w_c = \frac{W_w - W_w^{out}}{W_s} \tag{2.7}$$

where W_w is the initial weight of water in the cylinder, W_w^{out} is the weight of the water coming out during filtration and W_s is the weight of solids/cement in the cylinder (assumed constant during filtration).

The unit weight of the grout before filtration $\gamma_g = W_g/(d_i A)$ and the unit weight of the filter cake after filtration can be calculated as

$$\gamma_c = \frac{W_g - W_w}{d_c A} \tag{2.8}$$

where d_i is the initial depth of grout in the cylinder, W_g is the initial weight of wet grout and $d_c = d_i - \rho$ is the depth of the filter cake.

The void ratio, e is the volume ratio of voids and solids. In this case the solids are the cement particles, and the voids are assumed saturated with water. Thus the volume of solids equals the total volume minus the volume of water and

$$e = \frac{V_w}{V - V_w} \tag{2.9}$$

where V_w is the volume of water and V is the total volume.

The water content in a sample is defined as $w = W_w/W_s$, where W_w is the weight of water and W_s is the weight of solids/cement. Consequently, the void ratio can be calculated as

$$e = \frac{\gamma \cdot w}{\gamma_w(1+w) - \gamma \cdot w} \tag{2.10}$$

where γ is the unit weight of the grout before filtration or the filter cake after filtration. Alternatively, the void ratio of the filter cake can be expressed as

$$e_c = \frac{d_c}{d_i}(1 + e_g) - 1 \tag{2.11}$$

2.3 Permeability measurements

During a permeability tests, the amount of water coming out and the time from start are measured. Knowing the depth of the filter cake d_c, the pressure head during filtration p and the area of the cylinder A it is possible to calculate the permeability coefficient k_c of the filter cake using the principle of constant pressure head according to equation 2.12.

$$k_c = \frac{\Delta V_w^{out} d_c}{A p \Delta t} \tag{2.12}$$

where ΔV_w^{out} is the amount of water coming out during an increment of time Δt. The filtration pressure σ can be related to hydraulic pressure head p by $\sigma = p/\gamma_w$. Thus, a filtration pressure of 100kPa corresponds to a hydraulic head of 10m.

Table 2.1: Common values for the coefficient of permeability of natural soils (Sandveen and Department of Geotechnics at NTNU, 2010)

Soil type	k [m/s]
Homogeneous silt	10^{-5}-10^{-8}
Clay	10^{-8}-10^{-11}

2.4 Split-ring oedometer

The difference between a split-ring oedometer and an ordinary oedometer lies in its ability to measure horizontal stresses. The oedometer ring consists of three separate sections. When tightened together the diameter of the ring is 54 mm. Measuring the horizontal stresses makes it possible to calculate the lateral stress coefficient K_0' defined as the ratio between the horizontal and vertical stress $K_0' = \sigma_h'/\sigma_v'$. By this the lateral response can be evaluated in addition to the more conventional properties that are calculated from oedometer results.
The loading can be done successively or continuously with a constant rate of strain (CRS), where only the latter will be used here. During consolidation vertical displacement, total vertical and horizontal stress, pore pressures and time are measured.

The following assumptions are made when interpreting the results.

1. The sample is homogeneous
2. Water and solids are incompressible compared to the grain skeleton
3. Darcy's law is applicable for water flow through the sample
4. The sample is fixed laterally, and only vertical draining is present
5. Both total and effective stresses are homogeneous along the horizontal plane
6. The material is cohesionless

The results that come out of an oedometer test are mainly related to stiffness and says little about strength as the sample is withheld failure. Thus, running an oedometer test are mainly done to describe a materials deformation properties.

The pore pressures are measured at the bottom of the sample, while the top of the sample is drained (zero pore pressures). Thus, the pore pressures measured are not representative for the whole sample, and a parabolic distribution has theoretically been found as a good approximation (see Figure 2.8) as long as the pore pressures at the bottom are not more than 15% of the vertical load. Consequently, multiplying the pore pressures with a factor of 2/3 should give a fair approximation to the average pore pressures in the sample. The pore pressures generated during an oedometer test depends on the permeability of the sample and the loading rate. Common for clays are strain rates between 0,75-1,2% pr. hour.

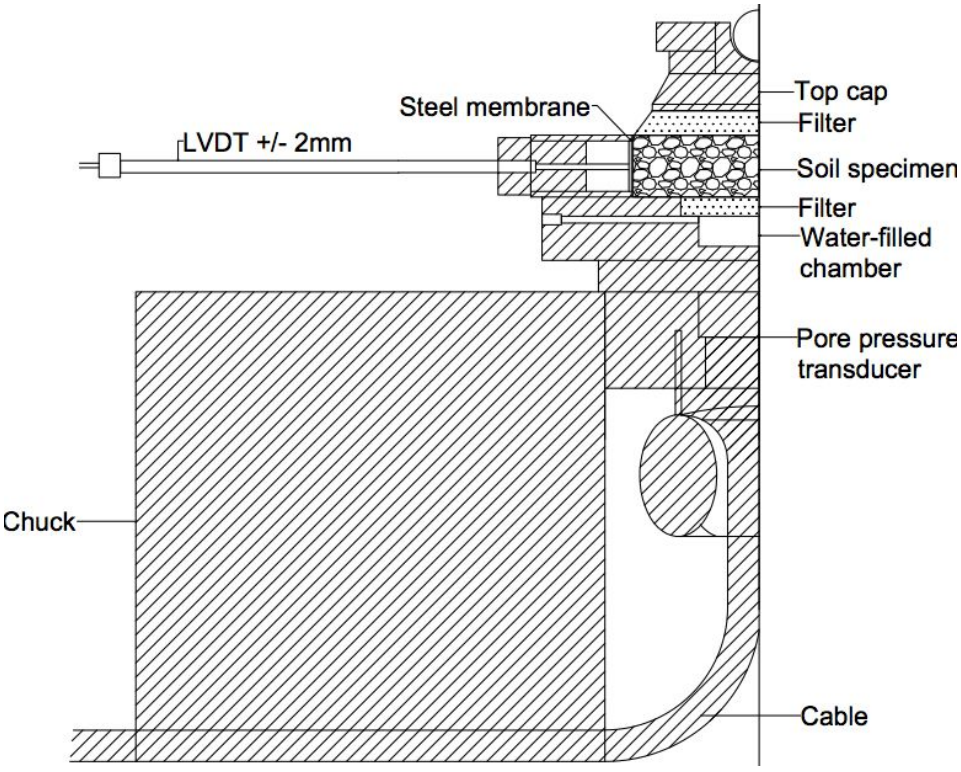

Figure 2.7: Simplified vertical cross-section of the split-ring oedometer with chuck

The pore pressure ratio u_b/σ_v should preferably not exceed 0,1 during testing. (Sandveen and Department of Geotechnics at NTNU, 2010). For a CRS test, the pore pressure are expected to be highest at the beginning of the test, decreasing towards zero as the displacements increase. The maximum strain rate for the split ring oedometer apparatus used in this thesis is 4% pr. hour (Svaan et al., 1992).

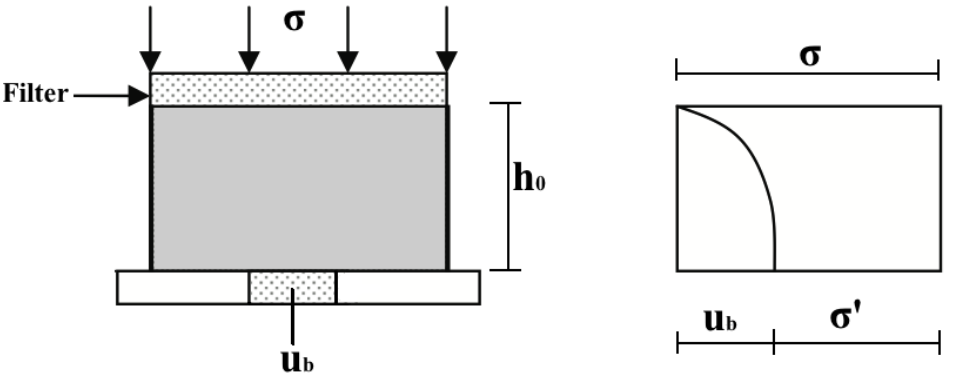

Figure 2.8: Pore pressure distribution in an oedometer sample (Sandveen and Department of Geotechnics at NTNU, 2010)

Commonly, the following parameters are studied after a split-ring oedometer test

- Effective horizontal stress $\sigma'_h = \sigma_h - (2/3)u_b$ and effective vertical stress $\sigma'_v = \sigma_v - (2/3)u_b$, where u_b are the pore pressures measured at the bottom of the sample.
- Vertical strain $\varepsilon_v = \Delta h/h_0$, where Δh are the vertical displacements and h_0 is the specimens height before loading.
- Lateral stress coefficient $K'_0 = \sigma'_h/\sigma'_v$.
- Lateral coefficient for incremental stress changes $\Delta K'_0 = \Delta\sigma_h{}'/\Delta\sigma'_v$.
- Mean vertical stress in a given time interval from a to b $\sigma'_m = (\sigma'_a + \sigma'_b)/2$, where σ'_a and σ'_b are the effective vertical stresses at time a and b, respectively.
- Oedometer modulus $M = \Delta\sigma'_v/\Delta\varepsilon_v$.
- Coefficient of consolidation $c_v = M \cdot k/\gamma_w$.

Additionally, as the horizontal stress is recorded it is possible to calculate the effective mean stress $p' = (\sigma'_1 + \sigma'_2 + \sigma'_3)/3$, deviatoric stress $q = \sigma'_1 - \sigma'_3$ and shear stress $\tau = q/2$, where σ'_1, σ'_2 and σ'_3 are the principal stresses and $\sigma'_1 \geq \sigma'_2 \geq \sigma'_3$. In this case $\sigma'_1 = \sigma'_v$ and $\sigma'_3 = \sigma'_h$ These parameters are commonly used for evaluating the failure state and the effective stress path in triaxial tests, but as the sample cannot fail in an oedometer these

parameters will not give the useful information as for triaxial tests, and are therefore not considered important.

According to Ramberg (2009), the eigendeformations in this particular oedometer can be expressed as

$$\delta_{self} = 0,057F^{0,47} \tag{2.13}$$

Where F is the load measured in kN. This equation was found by loading on a piece of steel in 2009, and for this thesis it is assumed that it is still valid. Thus, new measurements of the self deformation of the oedometer was not executed and Equation (2.13) was used to calculate the deformations.

The oedometer modulus is traditionally expressed as a function of vertical effective stress in soil mechanics. Using the Janbu notation it can be expressed as (Nordal, 2011)

$$M = m \cdot \sigma_a (\sigma'_v / \sigma_a)^{1-a} \tag{2.14}$$

where
m is the modulus number
σ_a is a reference stress level equal to 100kPa
a is the stress exponent (curve fitness parameter)

Assuming a=0 (common for soft soils), the modulus number can be found as the secant value in a σ'_m/M-plot (σ'_m being the mean value of σ'_v for the calculated M). Since m is independent of stress level it is considered a material parameter.

Common values for the modulus number and lateral stress coefficient of different soft soils are listed in Table 2.2.

Table 2.2: Common values for different soil parameters

(a) Modulus number

Soil type	m
NC Soft clay	<10
NC Medium soft clay	10-20
NC Stiff clay	>20
OC clay	30-60

(b) Lateral stress coefficient

Soil type	m
NC clay	0,4-0,7
OC clay	0,8-2,8
Sandy clay	0,43

2.5 Some basics on analysis of laboratory results

If the saving interval during the oedometer tests is small (e.g. every 10th second), the changes in the parameters between each reading are small and might reflect disturbances just as much as the actual changes in the parameters, as the oedometer is very sensitive.

Thus, when calculating parameters based on incremental changes like $\Delta\sigma$, $\Delta\varepsilon_v$, $\Delta K_0'$ and M it might be necessary to use larger increments to be able to produce smooth and readable curves. Care must however be taken not to alter the results to much by selecting to large increments.

Basic statistics can be very useful to make an unbiased evaluation of laboratory results. The mean value $\bar{X}$ is found by dividing the sum of the observed values with the number of observations n.

$$\bar{X} = \frac{\sum_{i=1}^{n} X_i}{n} \tag{2.15}$$

To get an idea of how close the data set is to the mean value, the standard deviation can be estimated as

$$\sigma^2 = \frac{1}{n-1} \sum_{i=1}^{n} (X_i - \bar{X}) \tag{2.16}$$

Alternatively, it is possible to draw trendlines according to a simple regression analysis. The validity of these lines is not unique, especially when multiple factors are interfering with the results. However, they provide a simple way of illustrating trends in observations.

Chapter 3

Experimental setup

3.1 General setup

The experiments were carried out in series, where the tests within a series had the same grout mix. For each series, two or three filtration tests and one oedometer test were executed. Usually, the oedometer test was carried out on the first filtration cake produced in a series to ensure that any setting of the cement were interfering with the results on a minimal basis. Additionally, one or two permeability tests were also executed for tests series 7-10 and 12-19. The tests were given names so that it is easy to see in which order they were performed. E.g. the first test in the first series is called 1.1, the second test in the first series is called 1.2 etc. Additionally the initial theoretical water/cement-ratio and the filtration pressure were included in the name. Thus, when a graph is shown in this thesis a test name could be 050_5bar_9.1, meaning it had a w/c-ratio of 0,50, the filtration pressure was 5 bar and it was the first test in the ninth series.

3.1.1 General procedure

Grout composition and mixing

The cement used was an ordinary Portland cement (Norcem Standard Lab Cement St14). Also a setting retarder was added to ensure that the setting didn't start before the testing was finished. The cement was stored in a plastic bag in a sealed bucket to ensure that the cement didn't react with water vapour in the air.

The grout was mixed in a kitchen machine since only one litre grout was needed for one series of filtration tests. The mixing was done by adding water and retarder to the cement. The mixing started off slowly to ensure that as little cement particles as possible was stirred up, floating in the air. When it had been mixed for about two minutes, the machine was stopped and cement stuck at the sides and the bottom of the bowl was manually blended

into the grout. Further the grout was mixed at high speed for one minute, followed by a two to three minutes rest and then mixed again at high speed for one minute. Care was taken when weighing up the amount of cement, water and retarder to ensure that the water content was as equal as practically possible for each series. This way the grout should be well mixed and the water/cement-ratio should be close to the theoretical/wanted value. The grout was also remixed before starting a new test in a series.

Measuring water contents

Because the grout will set and harden faster if exposed to high temperatures, the applicability of the conventional way of measuring water contents in a drying oven is questionable. Thus, in this thesis it was attempted to measure the water content by using a microwave which gives a higher heating effect than a drying oven. A small sample of grout (approximately 10-20 g) was put in a ceramic bowl and wrapped in a paper bag. This was then microwaved on full effect (750 W) along with a bowl of water until the weight did not change. The paper bag ensured that material was not spread around in the microwave in case of an explosion in the material due to high pore pressures building up during heating. This was especially important for testing the grout after filtration and oedometer testing - since the compaction makes the chance of an explosion particularly high. The sample drying took about five minutes, giving reasons to believe that the grout will not have enough time for considerable setting. However, some setting may occur and so the method does not give exact values. Additionally, a small amount of the water will react with cement particles as soon as the water is added to the cement, producing a thin colloidal gel covering the cement grains. This water is chemically bound, and will not dissipate when heated. Nevertheless, the relative difference between the measured and theoretical water content should aim to be somewhat constant for a certain water content.
After some tests had been done, it was found that the weight still changed a little (change in water content of approximately 1 %) if it was dried in the oven after microwaving. Thus, this was also done for the later tests (from test series 11). The reason why this happened is probably related to the fact that a water bowl has to be put into the microwave along with the samples. Thus, the air in the microwave is more moist than in a drying oven, preventing the samples to be completely dried out.
The Norwegian Public Roads Administration describes a similar practice for measuring water contents in cement (Statens Vegvesen, 1997). Although they use bigger samples of concrete the method should be applicable also at a smaller scale. Using smaller samples makes it essential to measure the weight accurately and a weight with an accuracy of 0,01g was used. However, as the drying is faster for smaller samples the setting and hardening are probably less advanced and so the measured values may be closer to the actual values than if bigger samples were used.

Cleaning filters

The filters used in both the filtration and the oedometer tests were cleaned in an ultrasound bath between each test series. Initially, they were put into a netting basket placed in a

bowl with soap water. It is then heated to 40°C and vibration applied for about 15min. The heating is not considered a problem with respect to the curing of the cement, as the cleaning process is quick and the temperature not really that high. The process is then repeated, using clean water in stead of soap water. The filters used for filtration testing were also cleaned in clean water between each test (not just between the test series).

3.2 Filtration testing

For the filtration tests, a steel cylinder with an inner diameter of 54mm was used. This was placed onto a bottom piece with a drainage pipe, a filter stone and filter paper (or in some tests sand). Also an o-ring was added at the bottom to ensure that grout could not find it's way between the cylinder and the bottom piece (the o-ring on the bottom piece is a bit to far down). The procedure is further explained below.

1. Bottom piece was saturated by opening the vent, filling the cylinder with some water and closing the vent at the moment the water level had reached the bottom.
2. The mixed grout was poured into the cylinder until it had reached a height of about 8cm. A filter paper was put on top, along with some water.
3. The top piece was mounted on top of the cylinder and the tube connected to a pressure gauge.
4. The top vent was opened and the top piece and it's tube saturated by pressing it down until most of the surplus water on top of the grout is out. The vent was then closed and the pressures reset.
5. The cylinder was placed under the loading frame and the desired amount of weights put on. The displacements where zeroed, data saving started and the bottom vent opened. The total amount of water coming out was noted.
6. Valve was closed and data saving stopped when the test is finished. The sample was then either used for permeability testing, oedometer testing or the water content measurements.

Figure 3.1(a) shows the steel cylinder and the top and bottom piece separated. The filter stones are not shown but are screwed on to the top and bottom piece. The total assembly of equipment used for the filtration test is shown in Figure 3.1(b). The loading is done by manually putting weights on the weight arm and the forces are mechanically transferred to the top piece. The pressure applied, the displacements and the time are recorded by a LVDT attached to a computer where the datas are saved.

3.3 Permeability testing

After filtration a simple permeability test was executed for a number of tests. The procedure were as follows, using the same equipment as during filtration testing.

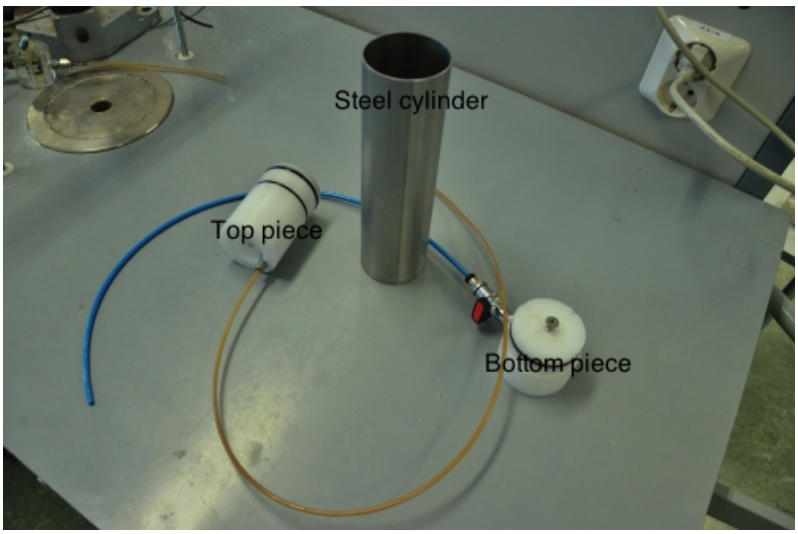

(a) Steel cylinder with top and bottom piece disconnected

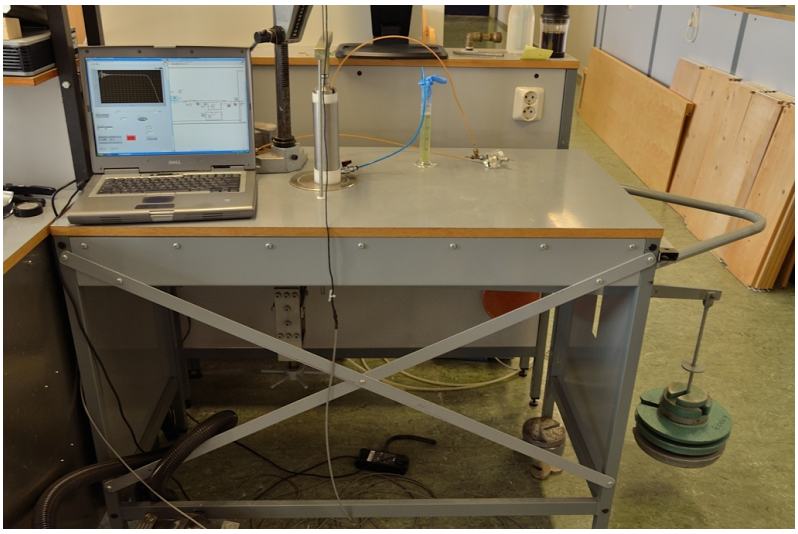

(b) Filtration test setup

Figure 3.1: Filtration test equipment

- Fill the cylinder containing the filter cake with water. Put on the top piece and saturate the tube. Reset pore pressures.
- Load the cylinder until a pressure off approximately 100 kPa is reached. Open the bottom valve, and close it again when the sample is saturated. Reset displacements.
- Start saving data and open the bottom valve. Close it again when enough data has been gathered (typically 15-30 min were used).

3.4 Testing in a split-ring oedometer

In the following, the setup necessary to run a continuous split-ring oedometer test is explained.

3.4.1 Equipment

The split-ring oedometer used in this thesis consists of an oedometer ring (a chuck with three movable sections), a press for continuous loading, an amplifier, a power supplier for the motor, a box for adjustments of the zero-point of the radial sensors and a computer where the datas are saved. A picture of the apparatus is shown in Figure 3.2. For a detailed overview of how to set up the device, one can read the users manual by Svaan et al. (1992). However, the manual and the oedometer apparatus are old and a few adjustments have been made. Thus, a brief overview of what was done will be given in Section 3.4.2.

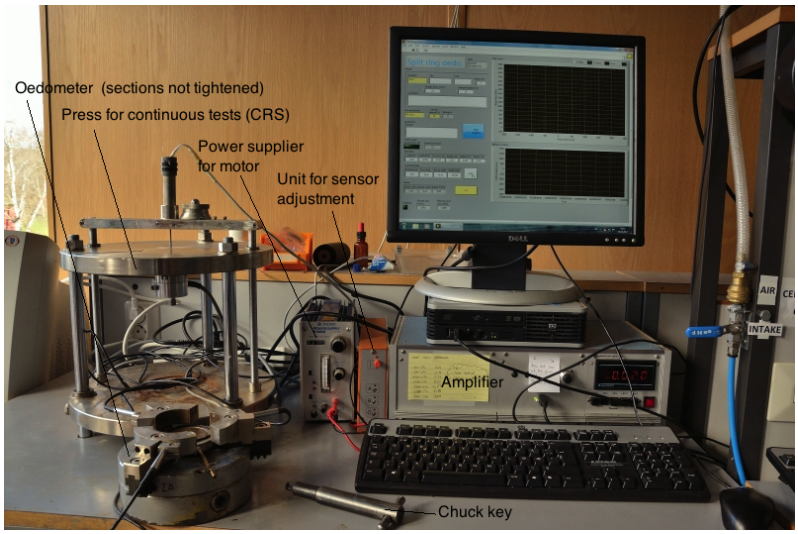

Figure 3.2: The oedometer and its appurtenant devices

3.4.2 Testing procedure

Preparing the oedometer

Before the sample can be built into the oedometer one needs to...

1. ...connect the chuck, press and oedometer by using the chuck key.
2. ...turn on the power on the motor and the amplifier.
3. ...apply exsiccator grease to the o-ring in the base, and clean its slot.
4. ...apply silicone oil at the base and the ring sections before putting the o-ring into its slot.
5. ...apply a vertical strip of silicone on to the joints of the sections, and around the base to ensure that the oedometer is water tight.

Installing the soil specimen

When building in an appropriate specimen the following must be done

1. Ensure that the pore pressure chamber is saturated by filling the pore pressure chamber and the drainage pipe with distilled, air-free water. Insert the bottom filter with the smooth side turning upwards.
2. Place the specimen centric on the base so that the lower 25 mm are not disturbed. Remove surplus water with a pipette.
3. Reset the lateral stress gauges so that all units show 0.00.
4. Screw together the sections till contact is achieved with the specimen.
5. Trim the top of the specimen by cutting from the center towards the sides. Save the cut-off for testing of water contents.
6. Insert the top filter stone with the smooth side turning downwards. Make sure that it lies as centric as practically possible.
7. Insert the oedometer into the press and put on the top piece.
8. Reset the pore pressure gauge and the load gauge.
9. Establish contact between the load gauge and the specimen manually(contact should be as small as possible). Check that the top piece is centric.
10. Reset the strain gauge.
11. Set the rate of strain to the desired value and turn the switch back to automatic loading. Set the desired maximum loading and turn on the motor.

3.4.3 During and after testing

During some of the tests the sample was unloaded and reloaded. The equipment could not do this automatically so it was done manually. The procedure is given below.

1. Stop the motor and switch to manual loading.
2. Make sure the saving interval is small (1-2 s were used).
3. Unload until the vertical stress equals approximately 10 kPa.
4. Set the new desired maximum loading and switch back to automatic loading. Set the desired saving interval and start the motor.

Right after the test was finished the water content of the sample was measured and the equipment thoroughly cleaned. The results were finally processed and interpreted in a spreadsheet. When calculating parameters based on increments, a starting interval of 30 kPa of vertical stress was found appropriate. As the stiffness in the sample increased, larger stress increments were needed to make smooth curves. When the vertical stress had increased to 200 kPa, 500 kPa and 1500 kPa intervals of 50 kPa, 100 kPa and 200 kPa were chosen, respectively. Also the parts of the readings that were influenced by unloading and reloading were excluded when calculating parameters based on incremental changes. Thus, separate calculations were made for the reloading sequences.

Chapter 4

Results and evaluation

In this chapter the main results from the tests are presented and discussed. In addition to the tests run on cement grout, two tests on clay were run to check that the oedometer equipment was in good condition. The results from these two tests can be found in Appendix F. Some results may be excluded as they are considered disturbed or because something went wrong during the testing procedure. A complete explanation of why these results are excluded can be found in Appendix G. Also, some figures may show results from only a representative sample of tests, as having all tests in one plot would make it difficult to read. The same results including all successful tests can be found in Appendix A for the filtration and permeability tests and in Appendix B for the oedometer tests.

4.1 Filtration test results

Figure 4.1 shows the root of time plotted against deformation for some of the filtration tests. Clearly there is a smoother transition from the filtration to the consolidation phase for the tests with low water content and filtration pressure than for the tests with high water content and filtration pressure. Even so, the curves are more similar to the upper curve in Figure 2.6 indicating that a filtration model is more appropriate than a consolidation model. Figure 4.2 shows the time divided by deformation plotted against the deformation. According to Equation (2.3a) the resistance of the filter cake is negligible if the extrapolation of the filtration part of these curves hit origo, which they seem to do. Thus, the resistance of the filter stone is neglected, and Equation (2.6) is used to calculate the permeability of the filter cake.

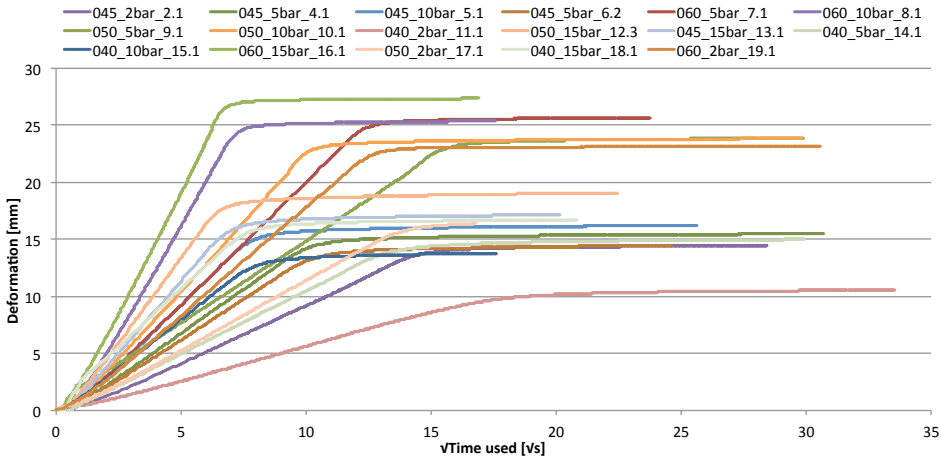

Figure 4.1: Square root of time versus piston displacements

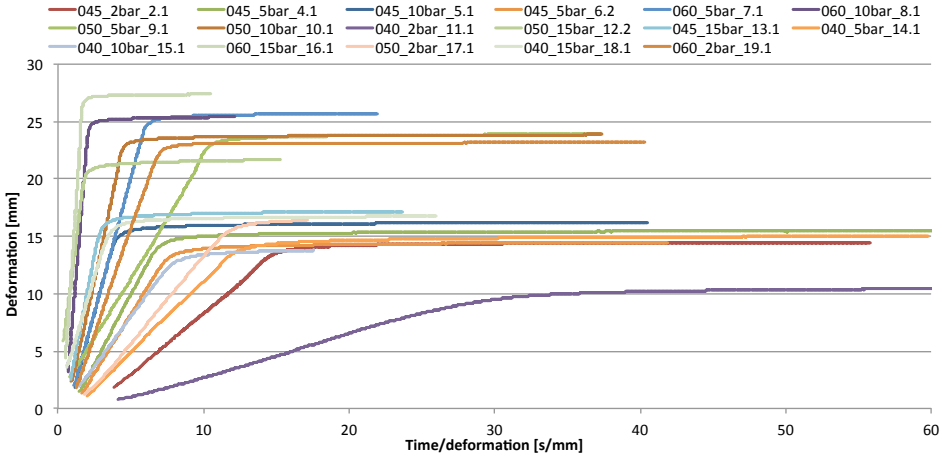

Figure 4.2: Time divided by displacements versus displacements

Comparing results within one test series did not result in any clear trends, neither for water content, displacements or time. It is thus reasonable to believe that the setting of the cement was prevented to a minimal extent with the amount of setting retarder that was used. Also, the measured amount of water coming out during filtration was in good agreement with the amount of water coming out based on displacements. Thus, only the latter has been used for further calculations.

The main results for the water content measurements can be seen in Figures 4.3 and 4.4. As expected, the apparent water contents are lower than the theoretical values due to some initial chemical bonding of the water to the cement and possibly also some setting during drying as described in Section 3.1.1. It is not known how much these factors influence the water content individually, but the apparent water content before filtration ranges between 85-95 % of the theoretical values. Assuming a normal distribution for the ratio between the apparent and theoretical water content, the mean value is estimated to 91,5% with a standard deviation of 2,4%.
The final water content calculated from displacements during filtration and the initial apparent water content is in general higher than the measured values. Using the displacements to calculate the water contents supposes that only water is coming out. For some of the high pressure tests it was clear that also some grout came out, and although the results from these tests are excluded in the calculations related to displacements, it is clear that it is difficult to avoid any grout coming out. Thus, the water content based on displacements can be considered as an upper limit (the difference in using the apparent and theoretical initial water content is negligible), while the apparent water content yields a lower limit for the true water content. It is also clear that the initial water content does not have a substantial effect on the final water content. As seen from Figure 4.3(b) neither the filtration pressure has a considerable effect on the final water content, indicating that there is a certain amount of water in the grout that cannot be pressed out. As the displacements should be proportional to the amount of water expelled they should be strongly related to the initial water content, as presented in Figure 4.5. The void ratio after filtration is strongly related to the final water content (Equation (2.10)), and the same trends are therefore found for the void ratio and the final water content (see Appendix A). The permeabilities calculated from Equation (2.6) are plotted against filtration pressure in Figure 4.6. No clear trend is evident. A slight increase in permeability with initial water content is found, which is logical from Equation (2.6).
While most of the parameters mentioned above seems to be little affected by the filtration pressure, the total amount of time for the filtration process to finish shows a clear relation to the filtration pressure, as illustrated in Figure 4.7. The relative increase in time is higher for lower filtration pressures, which seems reasonable as the time should approach infinity as the pressure approaches zero.

More results for the filtration tests can be found in Appendix A.

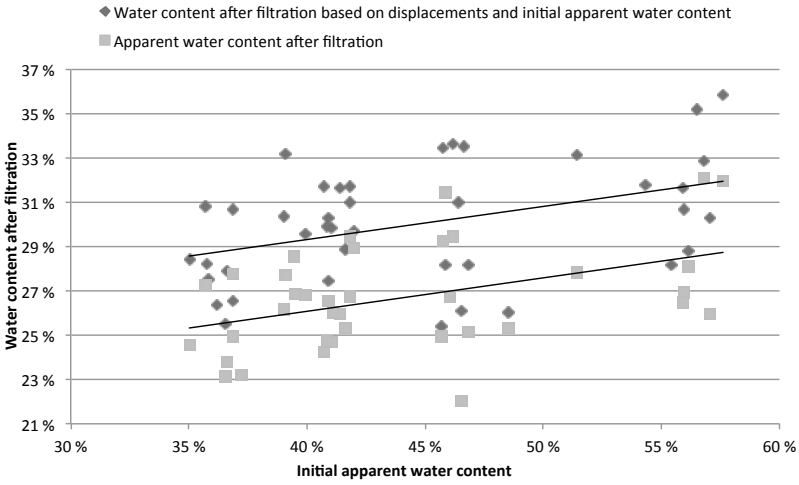

(a)

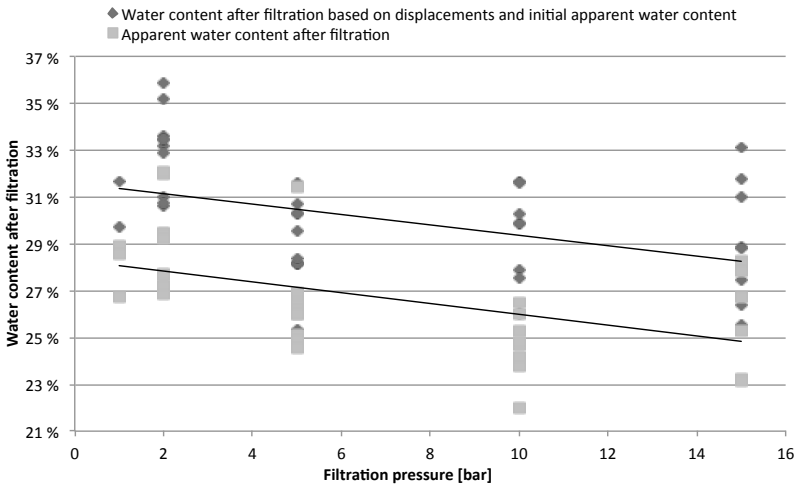

(b)

Figure 4.3: Water content after filtration versus...
(a)...initial apparent water content
(b)...filtration pressure

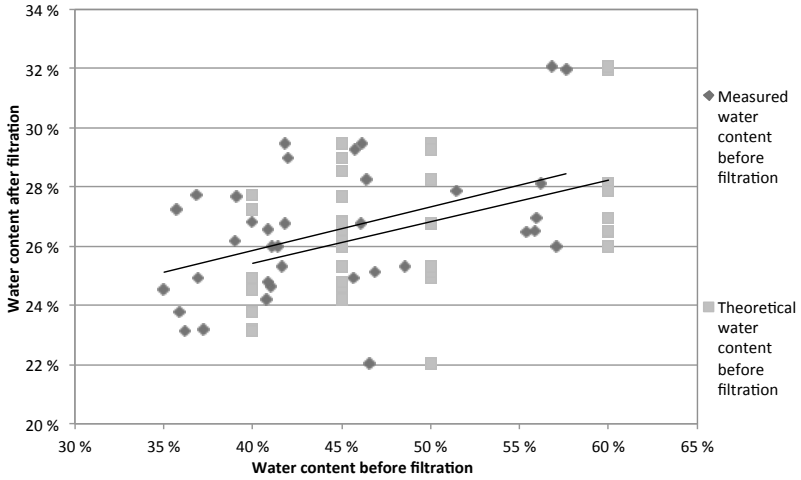

Figure 4.4: Water content before versus after filtration

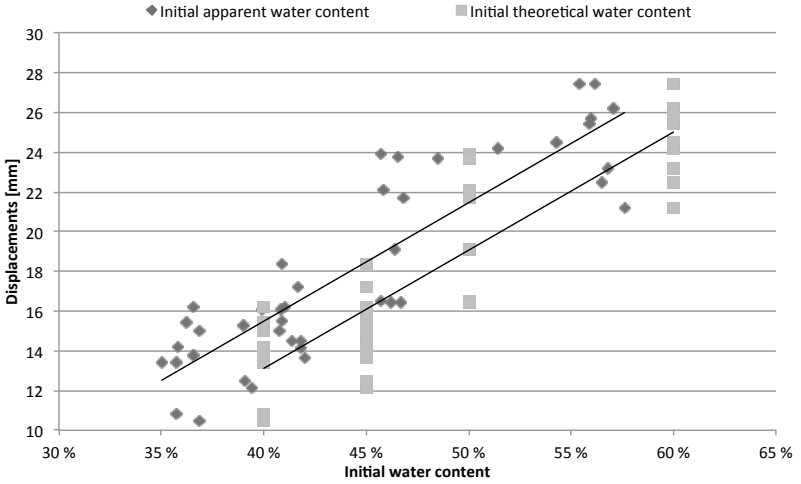

Figure 4.5: Displacements during filtration versus water content

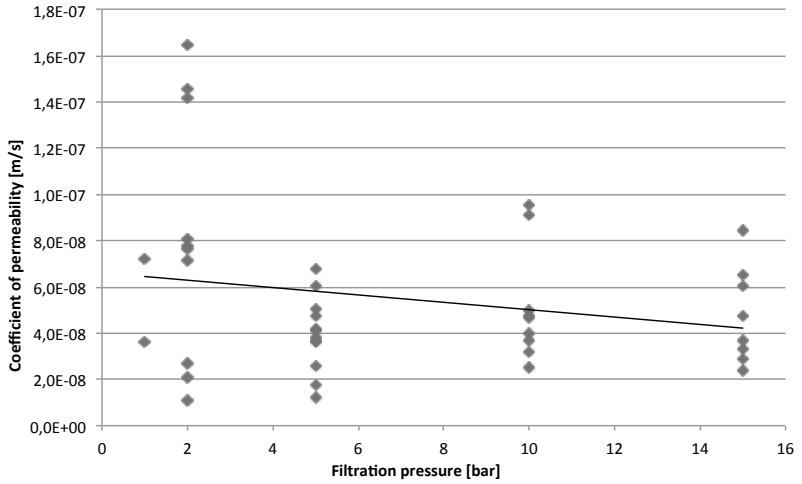

Figure 4.6: Permeabilities versus filtration pressure

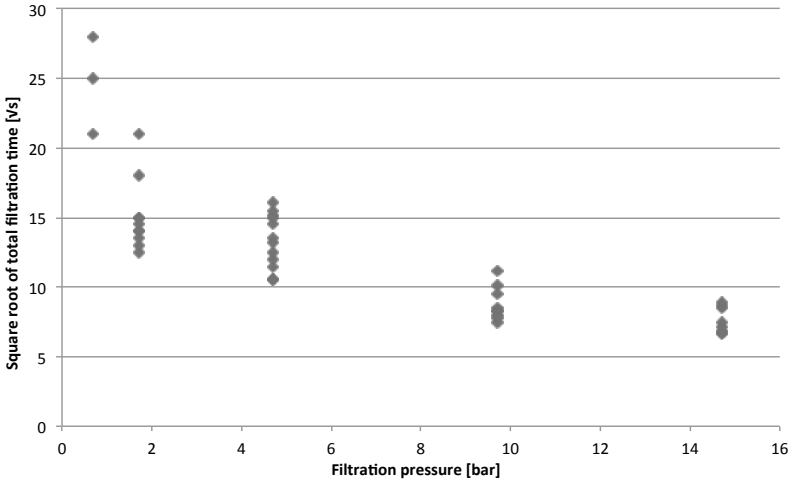

Figure 4.7: Square root of total filtration time versus filtration pressure

4.2 Permeability tests

During most of the tests a slight decrease in pressure (approximately 5-15 kPa) was experienced, probably due to friction between the piston and the cylinder. A mean pressure head was used in the calculations although it was found to make only a minor difference to the results.

Figure 4.8 shows the permeabilities measured during the permeability tests, based on the displacements of the top piston according to time. This corresponds well with the values calculated from the filtration tests, although the measured values are slightly higher than the values calculated from filtration tests. The straight line is drawn to show where the two permeabilities would be equal. Thus, there are good reasons to believe that Equation (2.6) yields trustworthy results, confirming the filtration model as an appropriate model for filtration tests.

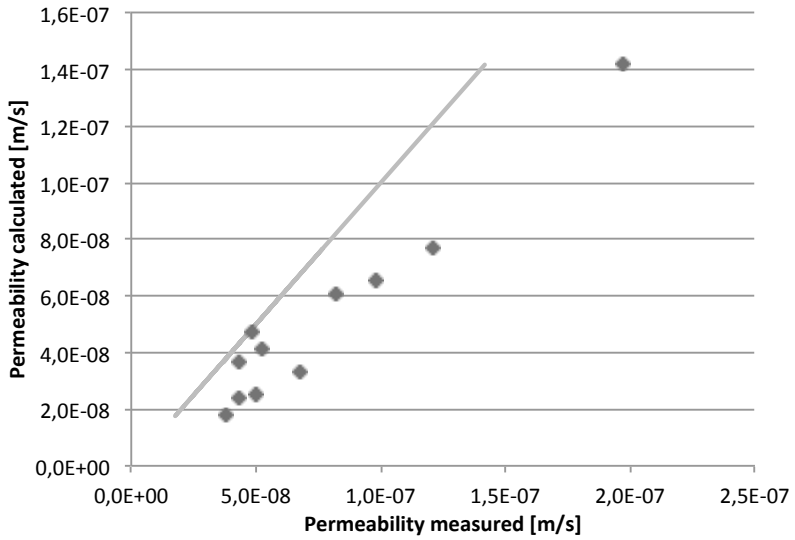

Figure 4.8: Permeability versus initial apparent water content measured in permeability tests

Comparing the measured permeability coefficients to the values in Table 2.1, it is clear that the permeability of the grout lies within the same order of magnitude as for pure silt.

4.3 Oedometer test results

During the oedometer tests the pore pressures were found to be very small and negligible (approximately 0-5 kPa) although the rate of strain was set to the maximum value of approximately 4% per hour. For the second clay test the pore pressures were found to be

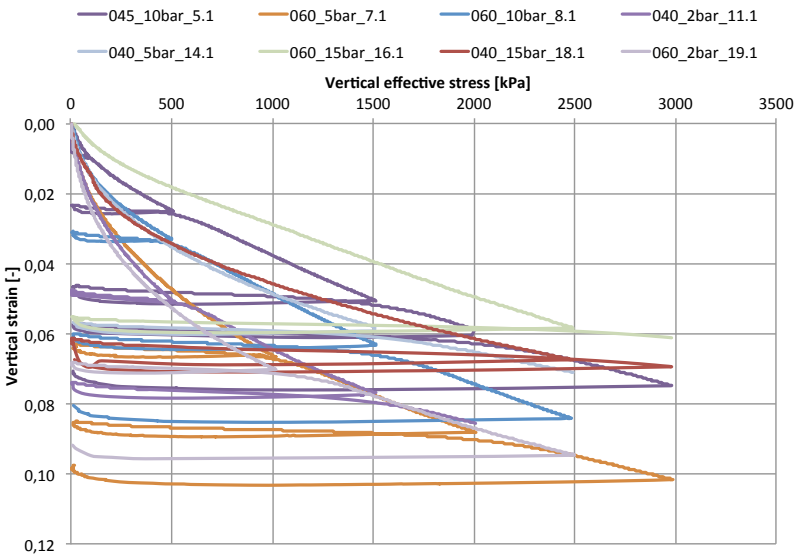

Figure 4.9: Vertical effective stress versus vertical strain

reasonable, running at 1,8 % per hour (see Appendix F). Ramberg (2009) stated leakage in the oedometer as a problem for the first tests she ran, but after applying blue silicone to the base and between the ring sections this problem was solved. The blue silicone was also used in the tests run for this thesis, and there were no observations of water coming out at the base or between the ring sections. As the permeability was found to resemble that of silt it is assumed that the pore pressures are low because the sample is drained to quickly for the pore pressures to build up. As the pore pressures were to low, the permeability and the coefficient of consolidation cannot be calculated.

Figure 4.9 shows the stress/strain curves for some of the oedometer tests, including unloading and reloading sequences. Clearly, there are differences in stiffness and from Figures 4.11, 4.10 and 4.12 we see that for the initial parts of the curves the stiffness clearly increases with the filtration pressure, yielding a modulus number at $\sigma'_v = 100$ kPa up to 260 (A reference level of 100 kPa vertical stress is chosen to better be able to compare the first time loading stiffness with the reloading stiffness). As the load increases, the modulus number is normalizing between 20-40, irrespective of the filtration pressure. Commonly, a modulus number in this range resembles that of a stiff or silty clay.

The increase in horizontal stress is approximately proportional to the increase in vertical stress during first time loading as illustrated in Figure 4.14. The lateral stress coefficient K'_0 versus vertical stress is shown in Figure 4.13. For most tests the initial K'_0 is very high ($> 0{,}5$), meaning that the horizontal stress is high compared to the vertical. This is caused by the tightening of the oedometer around the sample when building it into the oedometer, yielding a small horizontal prestress. After a while this prestress becomes negligible and we see that K'_0 stabilizes somewhere between 0,25-0,32 at the end of the tests.

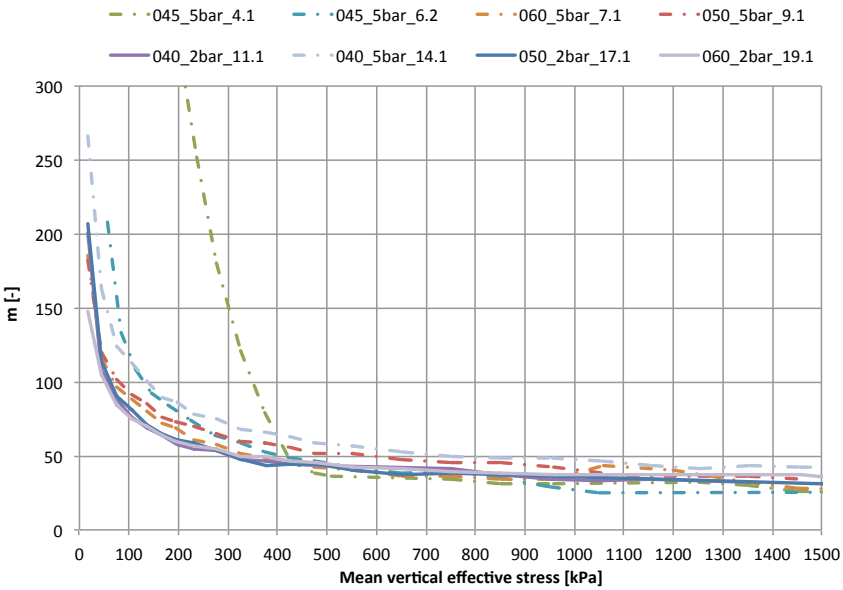

(a) Filtration pressure 2 bar (continuous lines) and 5 bar (dotted lines)

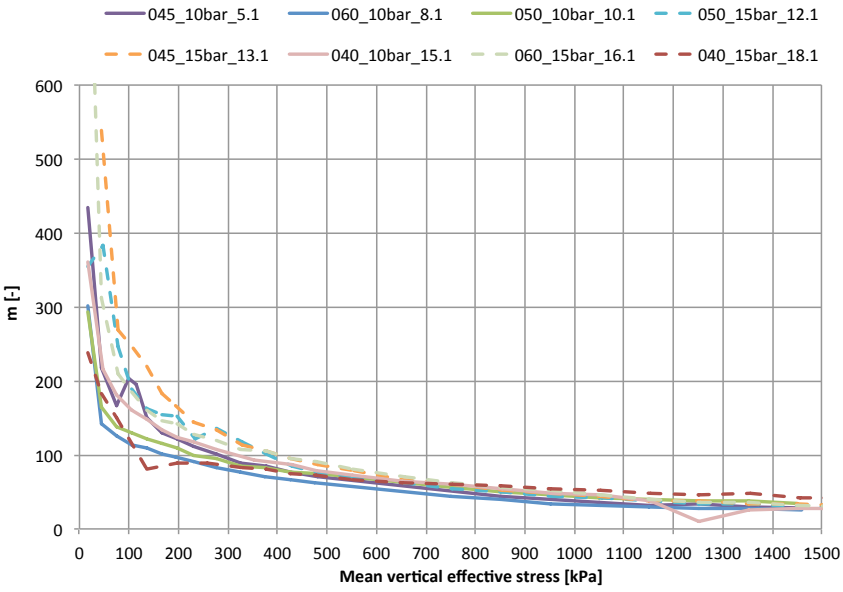

(b) Filtration pressure 10 bar (continuous lines) and 15 bar (dotted lines)

Figure 4.10: Vertical effective stress versus modulus number, m

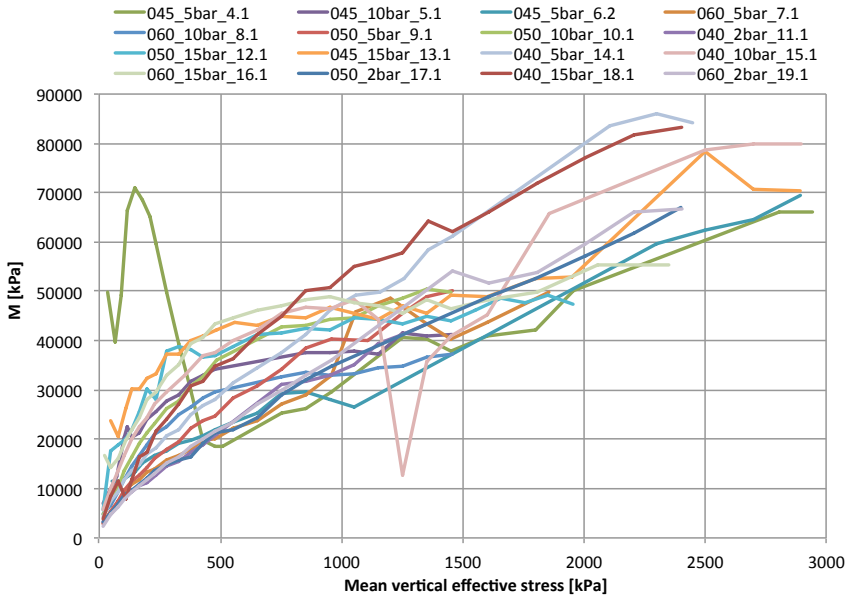

Figure 4.11: Vertical effective stress versus one-dimensional modulus, M

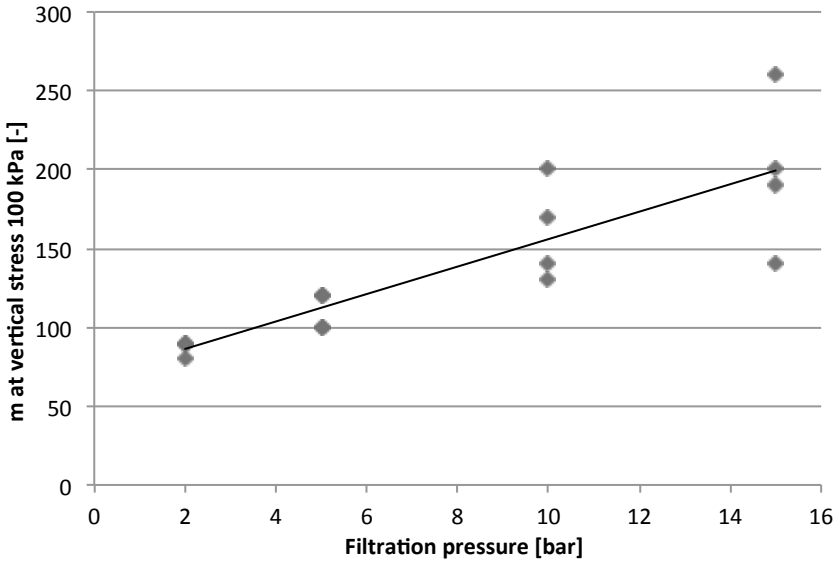

Figure 4.12: Modulus number at $\sigma'_v = 100\ kPa$ versus filtration pressure

More oedometer results can be found in Appendix B.

4.3.1 Unloading and reloading properties

For the unloading and reloading sequences, plots of the reloading stiffness were made (see Appendix D). In general it looks like the stiffness increases up to about 1/3 - 1/2 of the unloading stress, and then it decreases until the unloading/reloading effect is completely gone some few hundreds kPa above the unloading stress. The modulus number at $\sigma'_v =$ 100 kPa is found to be in the order of 1000-2000, decreasing towards the values for first time loading as the vertical stress approaches the unloading level. Surprisingly, the effect of preconsolidation directly in the oedometer is much higher than what was found for the filtration pressure - yielding a difference in modulus number at $\sigma'_v = 100$ kPa by at least a factor of four. The reason for this is not clear, but it could be because the friction between the steel cylinder and the top piston is to high to consolidate the filter cake properly. It could also be that the cement grout easily forgets it's stress history, either with time or as the sample is built into the oedometer. Additionally, curing of the cement could cause the grout to remember it's previous load level better, but this is considered unlikely in this case. The oedometer tests were executed on the first filter cake produced in a series, meaning that if considerable curing was evident in the oedometer sample, this should also be true for the second and third filtration tests in a series. Evidence on curing of the cement were however not found for any of the filtration tests.

When the sample had been unloaded, the horizontal stress did not go all the way down to zero. Thus, the lateral stress coefficient had to be calculated for incremental changes in horizontal and vertical stresses. A plot of this lateral stress coefficient versus vertical effective stress is shown in Figure 4.15. Clearly, the lateral response is high right after the reloading is started. It decreases as it approaches the unloading level, the minimum value being lower than the values for first time loading. The curves are made only for vertical stresses up to the unloading level except for the curves for tests 17.1 and 19.1, where $\Delta K'_0$ were plotted also for higher stress levels to better be able to see the effect of the unloading and reloading. When the stress level gets close to the unloading level $\Delta K'_0$ increases and stabilizes at the first time loading values some few hundreds kPa above the unloading stress level.

Further, studying Figure 4.14 it is evident that the reloading paths differ considerably from the unloading paths. During unloading the lateral response is very modest until almost half of the load is removed, whereafter the response increases rapidly. Additionally, as the vertical stress gets close to zero approximately 15-35 % of the horizontal stress seems to be encapsulated in the sample. For the reloading parts the lateral response is highest in the beginning, decreasing when approaching the unloading level. As the unloading stress level is exceeded, the lateral stress coefficient again increases and normalize at first time loading level. It is clear that the horizontal stress is lower after reloading than before unloading. Thus, in total the lateral response is higher during unloading than reloading.

In Figure 4.9 the unloading and reloading curves differ, producing hysteresis loops which resembles that of work hardening due to the Bauschinger effect. The materials stress/strain

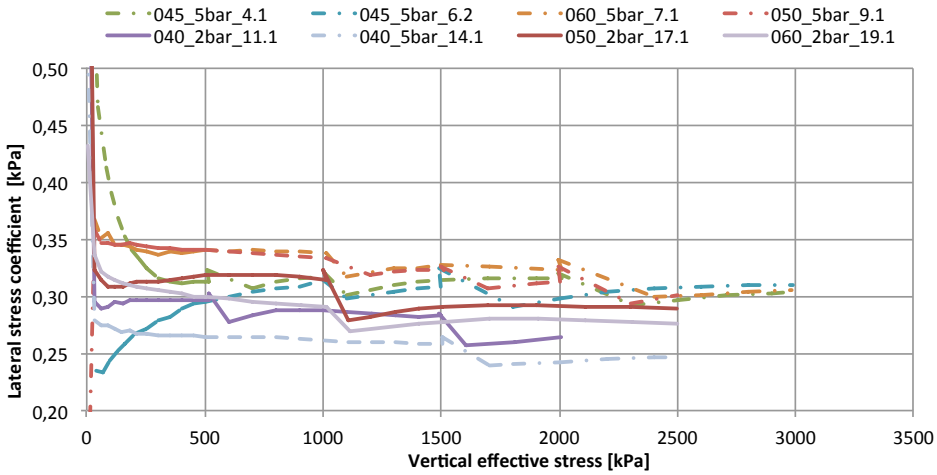

(a) Filtration pressures 2 bar (continuous lines) and 5 bar (dotted lines)

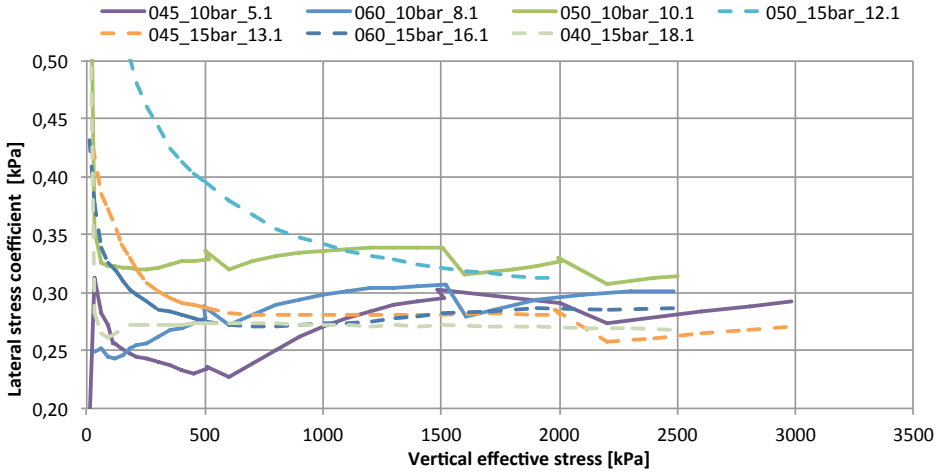

(b) Filtration pressures 10 bar (continuous lines) and 15 bar (dotted lines)

Figure 4.13: Vertical effective stress versus lateral stress coefficient

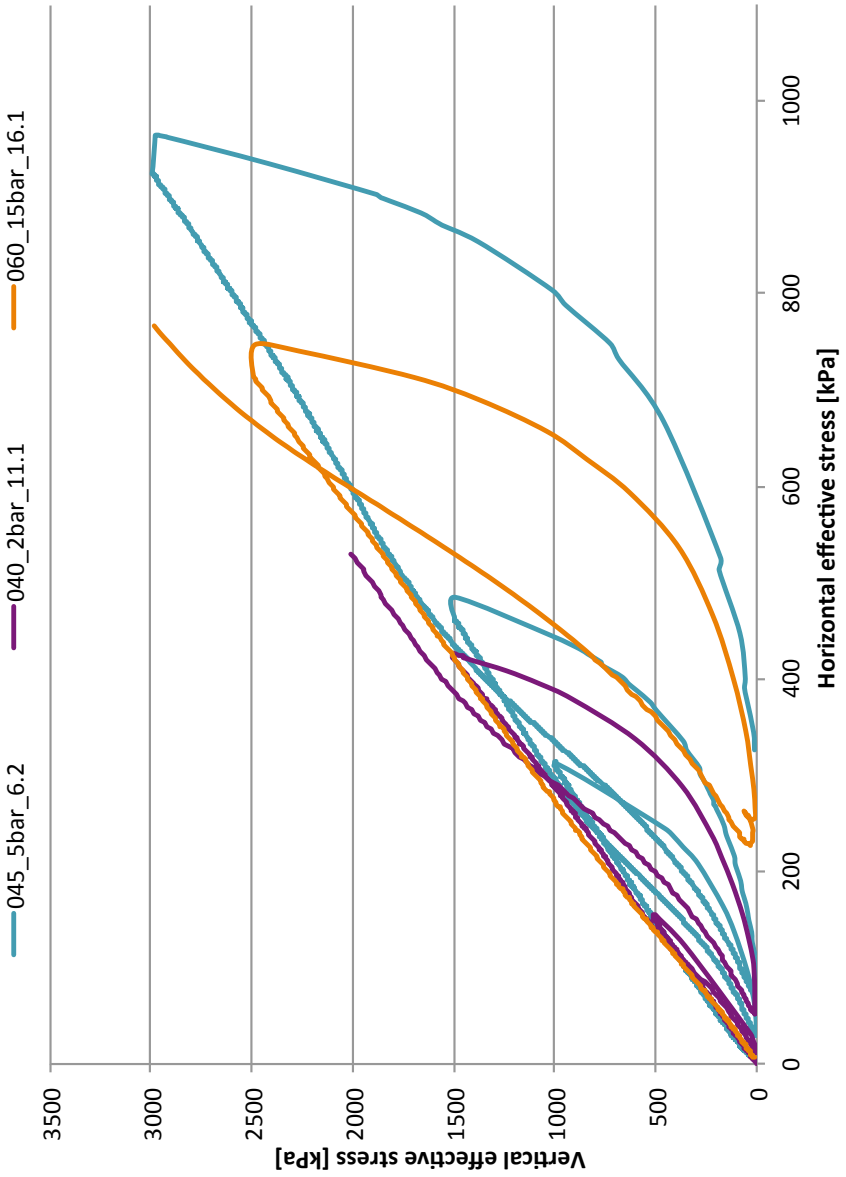

Figure 4.14: Horizontal versus vertical effective stress for three representative oedometer tests

characteristics change due to a shift in the yield surface with changes in the loading direction, producing different unloading and reloading stress paths. In metals this effect is related to movements of dislocations within the material structure (Kostryzhev, 2009, Lubliner, 2006). Probably, rearrangements in the material structure are also what cause the same effect in the filter cake material.

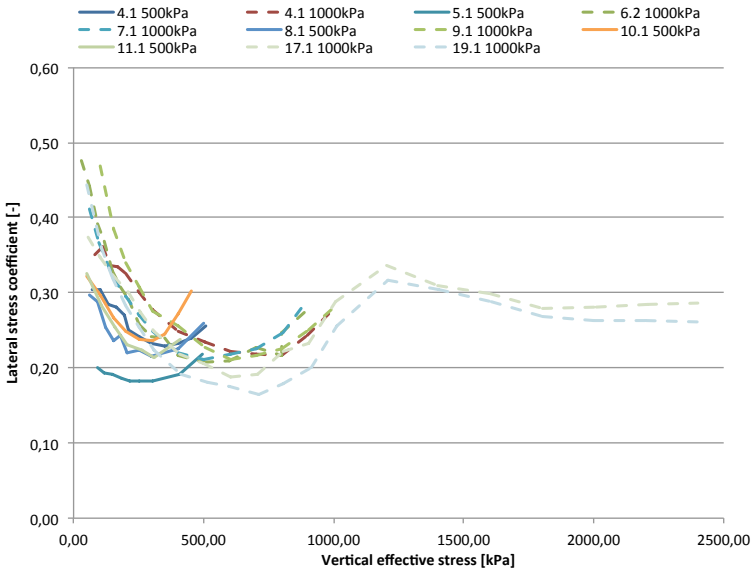

(a) Unloading level 500-1000 kPa

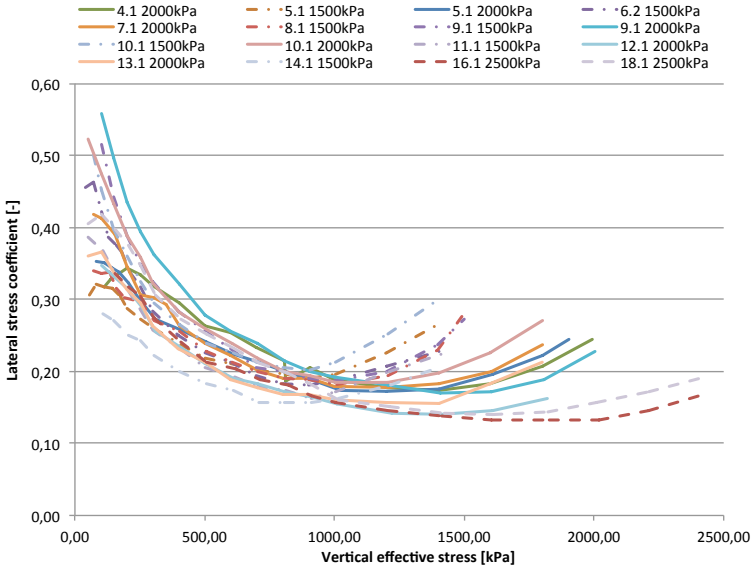

(b) Unloading level 1500-2500kPa

Figure 4.15: Vertical effective stress versus lateral stress coefficient

Chapter 5

Summary and concluding remarks

Firstly, it seems like the filtration model is an appropriate model for the filtration process as the filtration test results in general seem to correspond well with the predicted behaviour. Further, the water content, void ratio and permeability of the filter cake are found to be little affected by the filtration pressure. This is also evident from the oedometer results, showing only a minor increase in initial stiffness with increasing filtration pressures. The filtration process is however faster for high filtration pressures, but only up to a certain minimum value between approximately 5-10 bar. Thus, as filtration pressures higher than 5 bar are common for pressure grouting in non-cohesive soils, not much time can be saved by choosing higher pressures. Neither the initial water content seem to affect the properties of the filter cake material to a great extent although there is a slight increase in both the final water content, void ratio and permeability. Thus, irrespective of the grouting pressure and initial water content approximately the same material is produced every time, simplifying the design of grout anchors. The effect of filtration pressure may be stronger for really low pressures (<5 bar) but as this is rarely used in practice when grouting in non-cohesive soils it is not considered relevant.

The mechanical properties of the filter cake resembles that of a silt or a silty clay, both with respect to stiffness (modulus number), lateral stress coefficient and permeability. The filter cake remembers some of it's previous load level by yielding a much higher stiffness at reloading than at first time loading. The increase in reloading stiffness may however just be temporary as it is stronger when unloading and reloading directly in the oedometer than for reloading up to the filtration pressure right after the sample was built into the oedometer. Additionally, there is hysteresis during unloading and reloading. A Bauschinger effect indicates a shift in the yield surface with changes in loading direction, also known as kinematic hardening. Thus, although little can be said about the position of the yield surface from oedometer results, a kinematic hardening model seems appropriate for modelling the unloading/reloading behaviour.

Although the sample is vertically free of load approximately 15-35% of the horizontal stress seems to remain in the sample. Thus, the speculations considering a lock-in of pressure in the grout after filtration, followed by an increase in pull-out load of ground anchors seem reasonable. The lateral response is approximately constant for first time loading, yielding a lateral stress coefficient of 0,25-0,32. During reloading, the lateral response is more complicated.

For the future it could be interesting to check the filter cakes mechanical properties related to strength, e.g. by testing in a triaxial apparatus. To be able to develop a good mechanical model for cement grout, as many properties as possible should be investigated. Especially an investigation of the yield strength during first time loading versus unloading and reloading needs further investigation to be able to verify if the kinematic hardening model really is appropriate, as indicated by the results in this thesis. When the properties related to strength is more clear, a numerical analysis of the grouting process of anchors in sand and subsequent loading of the anchors can be performed.

Bibliography

European Committee for Standardisation (1999). *EN 1537: Execution of special geotechnical Work - Ground Anchors*.

Kostryzhev, A. G. (2009). *Bauschinger Effect in Nb and V microalloyed Line Pipe Steels*, PhD thesis, The University of Birmingham.

Lubliner, J. (2006). *Plasticity Theory*.

McKinley, J. D. (1993). *Grouted Ground Anchors and the Soil Mechanics Aspects of Cement Grouting*, PhD thesis, University of Cambridge.

Nordal, S. (2011). Geotechnical engineering advanced course, Compendium for the course TBA4115 Advanced Course in Geotechnics at the Norwegian University of Science and Technology.

Ramberg, S. (2009). *Splittet ring ødometer - spenningsforhold i prekonsolidert område - laboratorieforsøk og numerisk simulering*, Master's thesis, Norwegian University of Science and Technology.

Sandveen, R. and Department of Geotechnics at NTNU (2010). Soil investigations, Compendium for the course TBA4110 Soil Investigation at the Norwegian University of Science and Technology.

Smoltzcyk and Ulrich (eds) (2002). *Geotechnical Engineering Handbook*, John Wiley and Sons.

Statens Vegvesen (1997). *Håndbok 014 Laboratorieundersøkelser*.

Svaan, O., Sandveen, R. and Moen, A. (1992). *Brukerbeskrivelser for splittet ring ødometerforsøk. Forsøksrutiner—programanvendelse.*

Warner, J. (ed.) (2004). *Practical Handbook of Grouting - Soil, Rock and Structures*, John Wiley and Sons.

Xanthakos, P. P. (1991). *Ground Anchors and anchored Structures*, Wiley Interscience.

Appendices

Appendix A

More filtration and permeability test results

In this appendix results from filtration and permeability tests that were not given in the previous chapters are shown.
In Figure A.1 the results from all water content measurements and calculations are shown for each test individually.
Figure A.2 shows the water contents measured in different sections of the filter cake and after oedometer testing. Clearly, the variations of water content within a sample is small compared to the difference in water content before and after filtration, as assumed.
Figure A.3 shows the total displacements after filtration against the filtration pressure.
In Figure A.4 the initial water content is plotted against the square root of time used from start till end of filtration. Figure A.5 is a plot of the initial apparent water content against void ratio before and after filtration.
Figures A.6 and A.7 show filtration pressure plotted against the void ratio after filtration and permeabilities measured in the permeability tests, respectively. In Figure A.8 the permeabilities from both the permeability tests and filtration tests on the same filter cake are plotted against initial apparent water content.
In Figure A.9 the time divided by displacements are plotted against piston displacements. Here, all tests are plotted in one figure, making it hard to distinguish between each curve. However, this figure is only interesting in a trend illustration perspective so it is not considered important to be able to read specific values from each curve.
Figures A.10 and A.11 are plots of the square root of time used since start of filtration versus the piston displacements. The results are divided into four bulks sorted by initial water content to increase the readability.
Finally, Figures A.12 and A.13 shows the measured pore pressure versus deformation and square root of time, respectively. In these plots no color encoding was applied to the curves, as they are meant for illustrating the development of the pore pressure during the tests, and not for the relations between the filtration pressure versus time and deformation (these have been shown many times already).

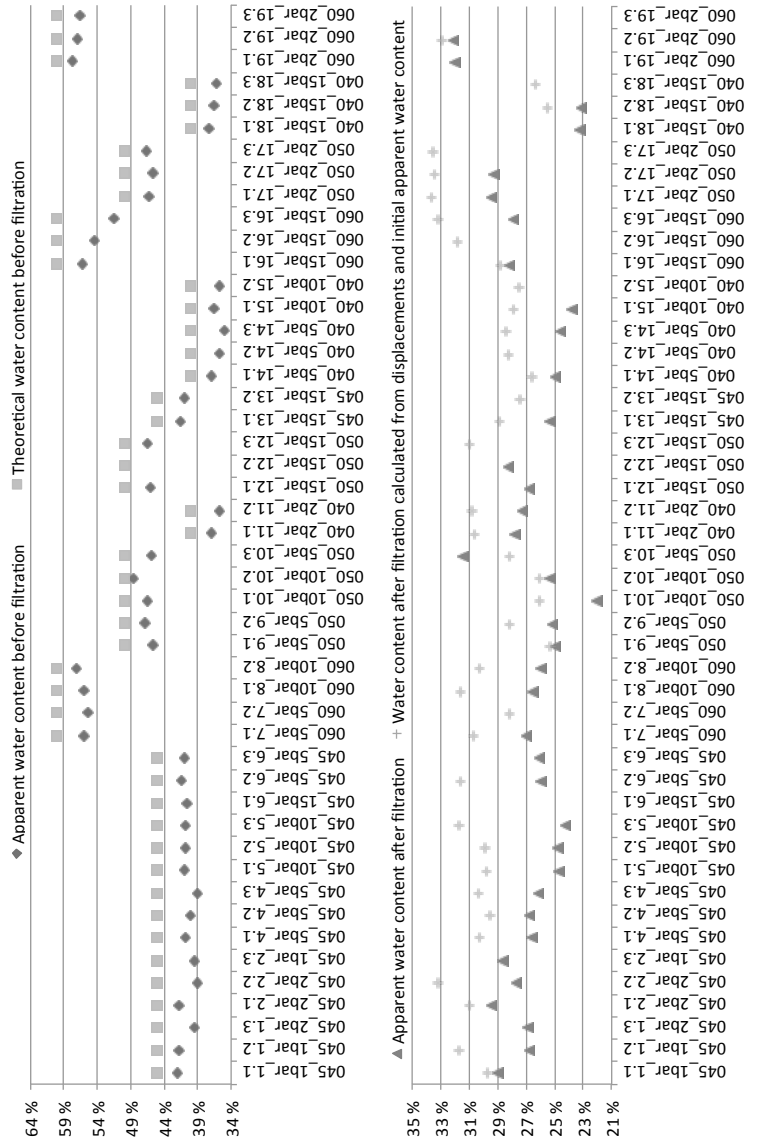

(a) Water contents for each test before filtration

(b) Water contents for each test after filtration

Figure A.1: Water contents for each test

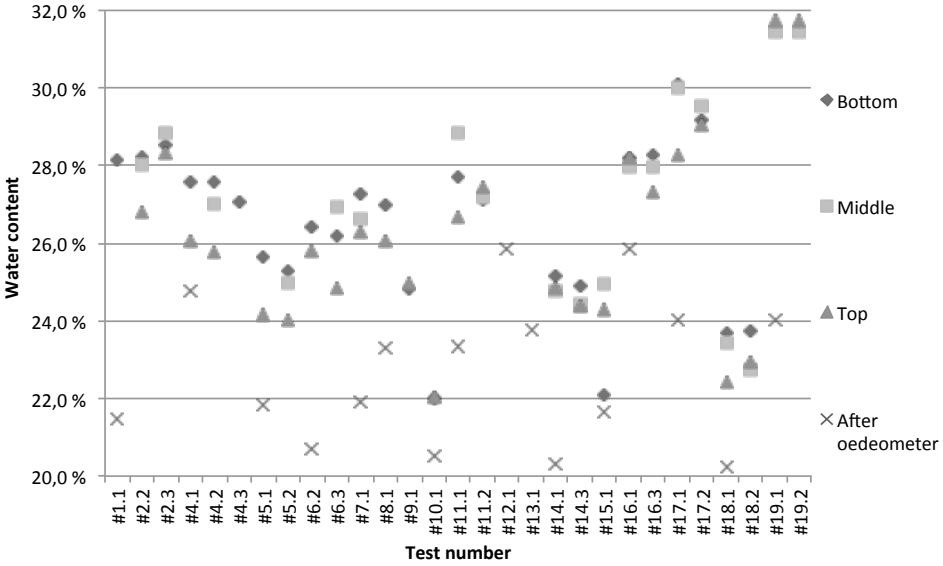

Figure A.2: Water content for different parts in a filter cake and after oedometer

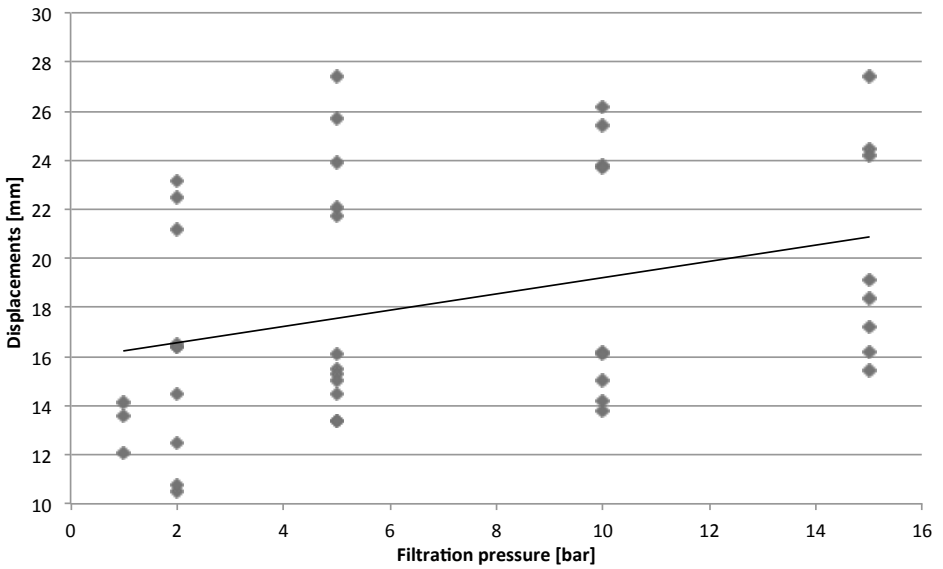

Figure A.3: Displacements during filtration versus filtration pressure

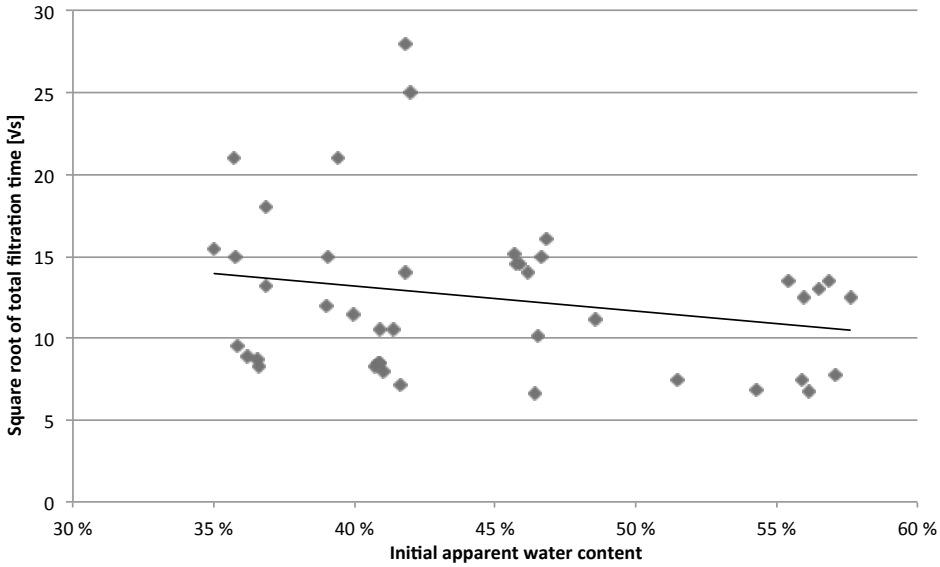

Figure A.4: Square root of total filtration time versus initial apparent water content

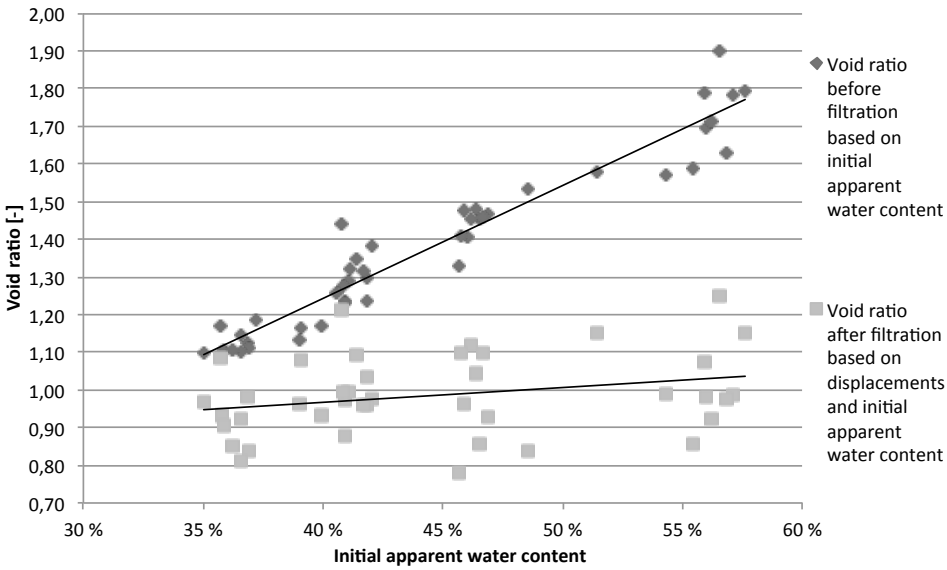

Figure A.5: Void ratios before and after filtration versus initial apparent water content

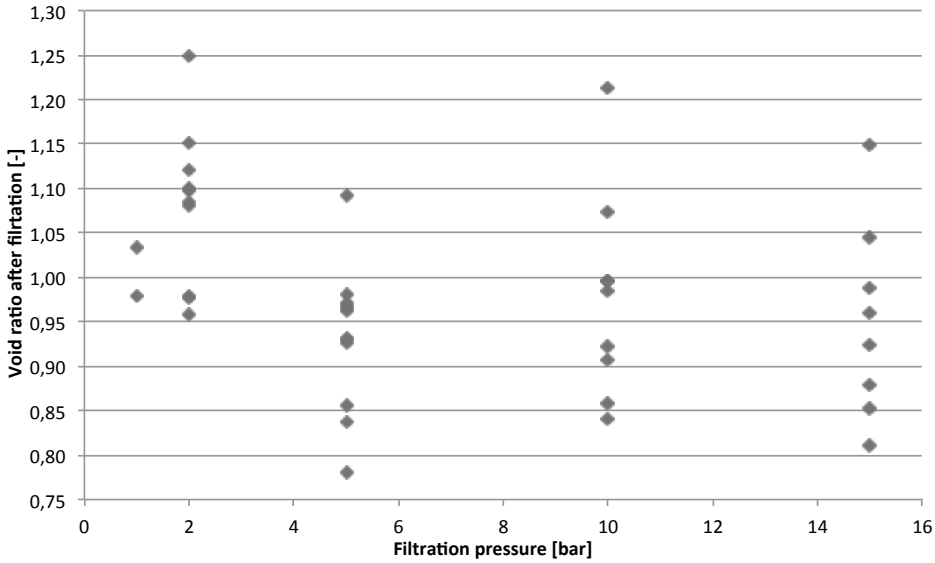

Figure A.6: Void ratios after filtration versus filtration pressure

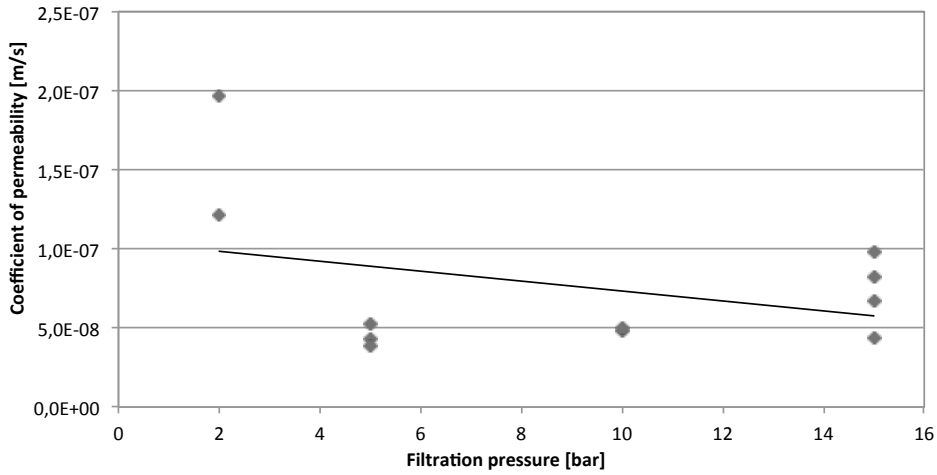

Figure A.7: Permeabilities measured in permeability tests versus filtration pressure

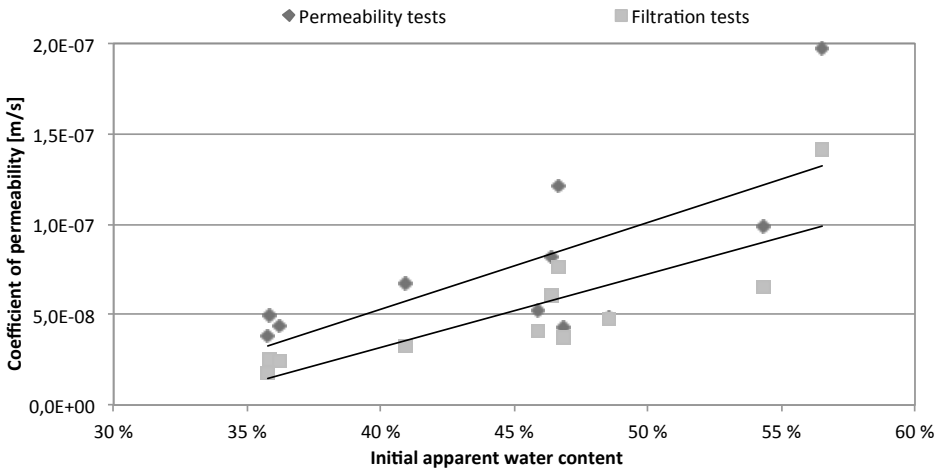

Figure A.8: Initial water content versus permeability

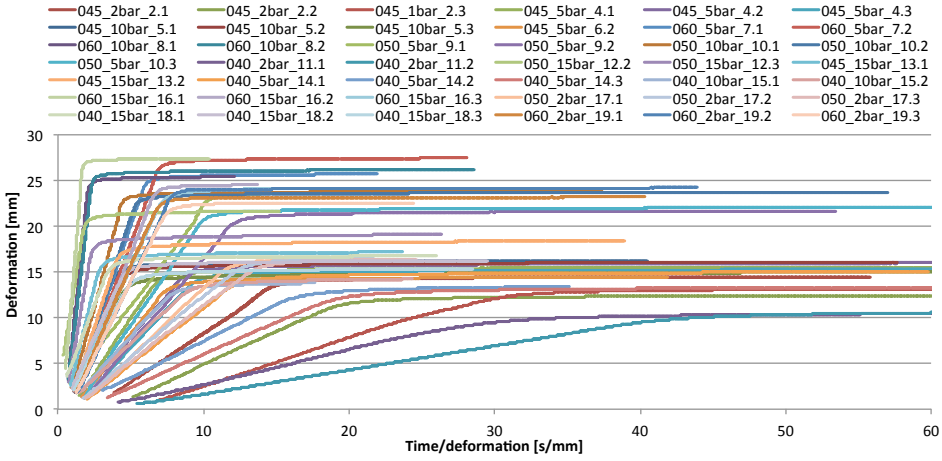

Figure A.9: Time divided by displacements versus displacements

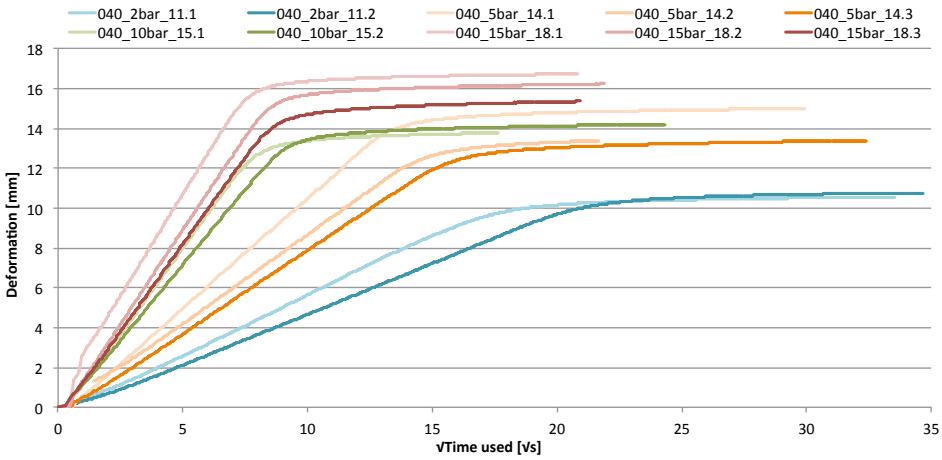

(a) Tests with initial water content of 40%

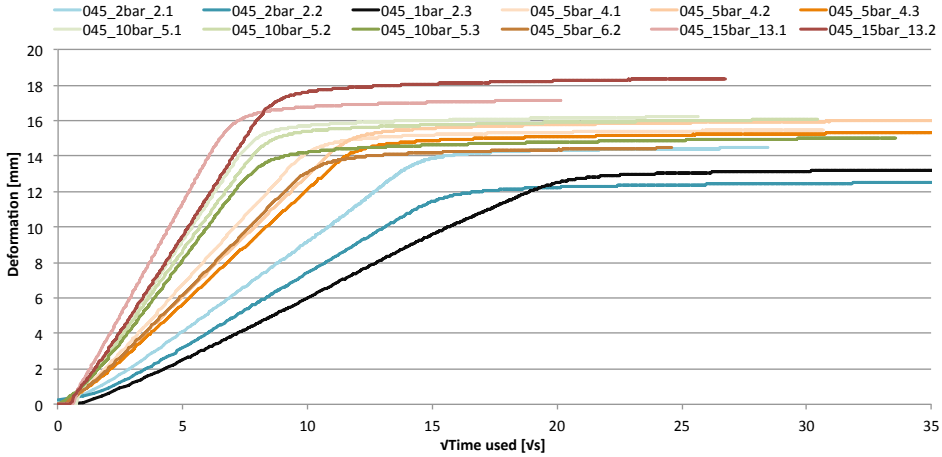

(b) Tests with initial water content of 45%

Figure A.10: Square root of time versus piston displacements.
Colour encoding: red=15 bar, green=10 bar, orange=5 bar, blue=2 bar and black=1 bar

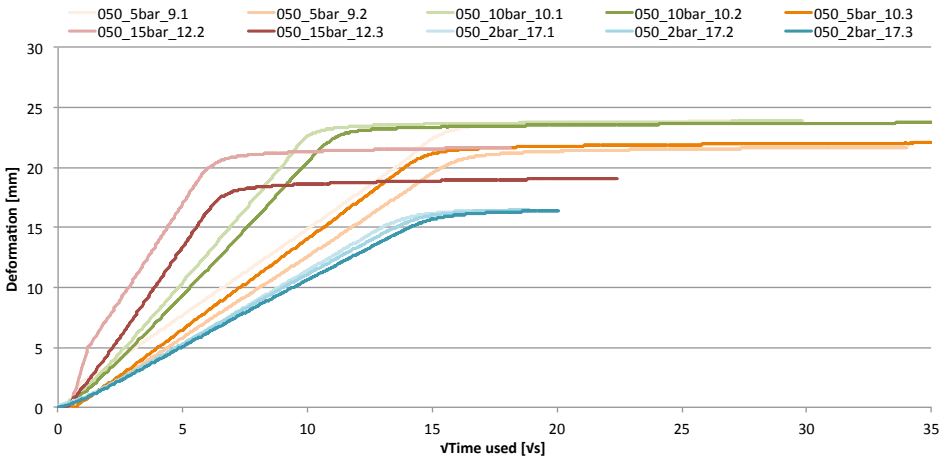

(a) Tests with initial water content of 50%

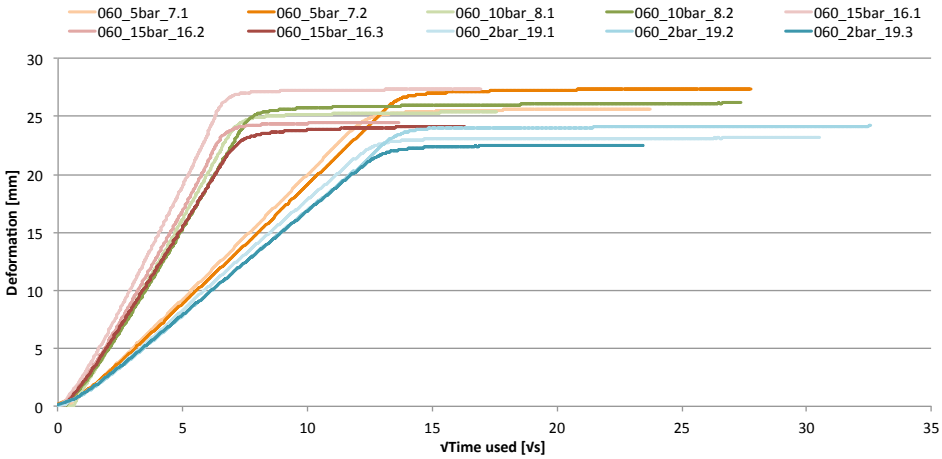

(b) Tests with initial water content of 60%

Figure A.11: Square root of time versus piston displacements.
Colour encoding: red=15 bar, green=10 bar, orange=5 bar and blue=2 bar

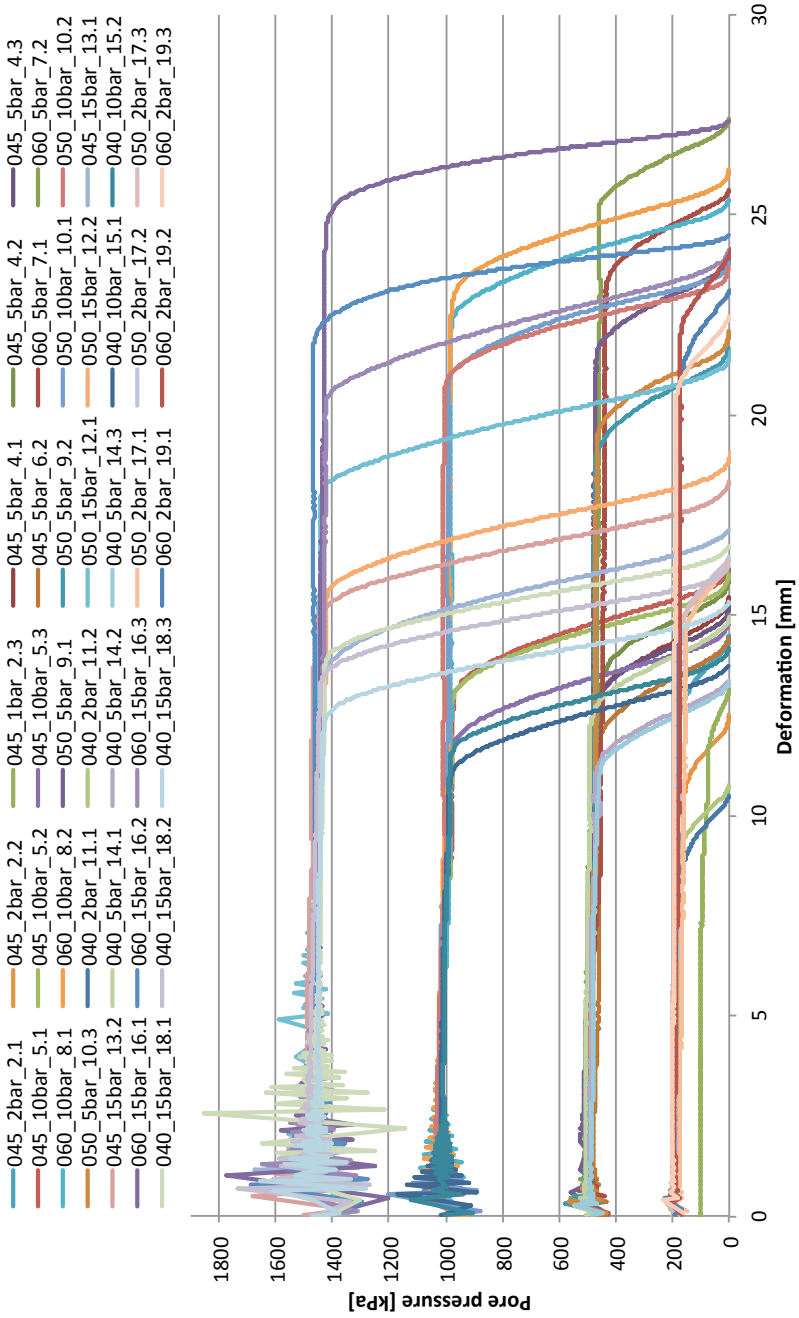

Figure A.12: Displacements versus pore pressure

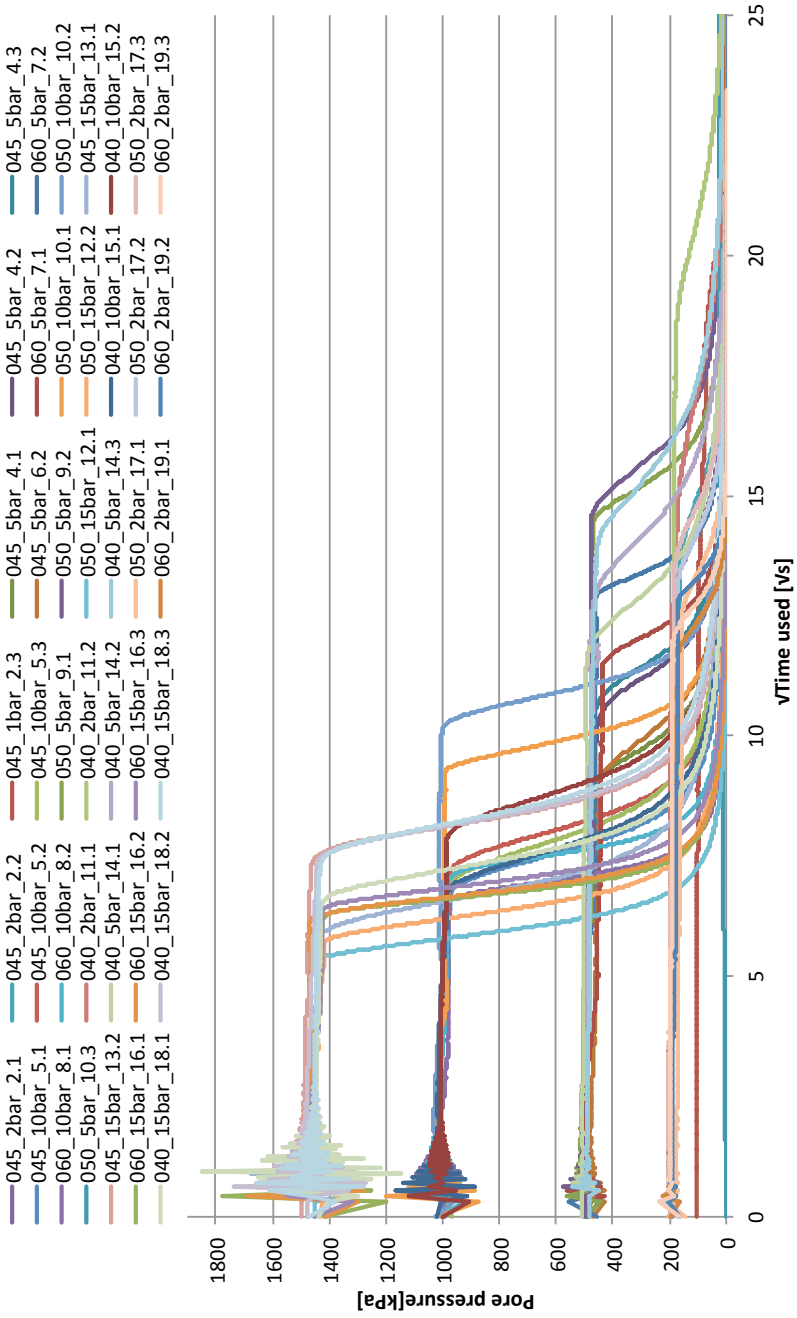

Figure A.13: Square root of time versus pore pressure

Appendix B

More oedometer results

In this appendix, oedometer results that were not included in previous chapters are shown.

Figures B.1 and B.2 show the vertical effective stress versus vertical strain for all oedometer tests.
In Figure B.3 the apparent water content before and after filtration is plotted versus the modulus number at a vertical stress of 100 kPa.
Figures B.4 and B.5 show horizontal versus vertical effective stress for all oedometer tests.
In Figure B.6 the later stress coefficient K_0' is plotted against (a) water content and (b) filtration pressure.

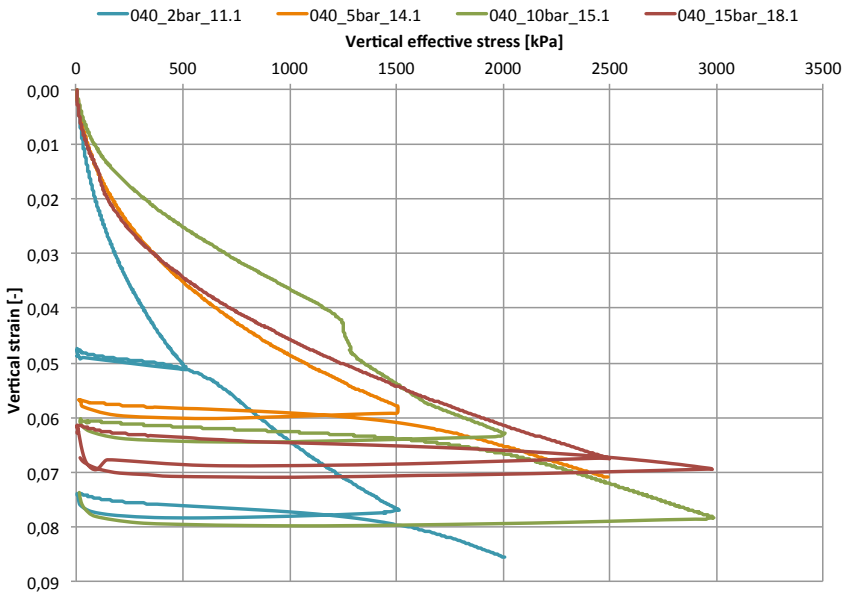

(a) Tests with initial water content of 40%

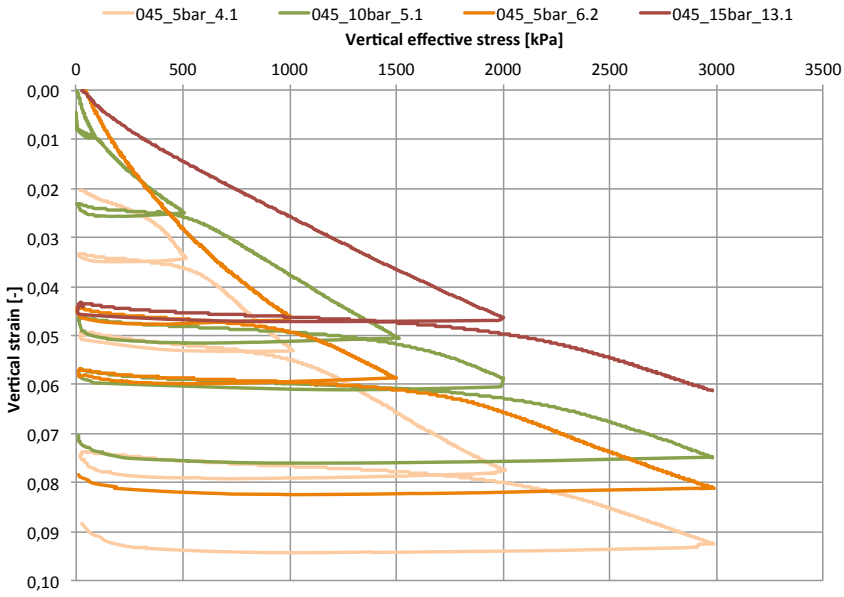

(b) Tests with initial water content of 45%

Figure B.1: Vertical effective stress versus vertical strain
Colour encoding: red=15 bar, green=10 bar, orange=5 bar and blue=2bar

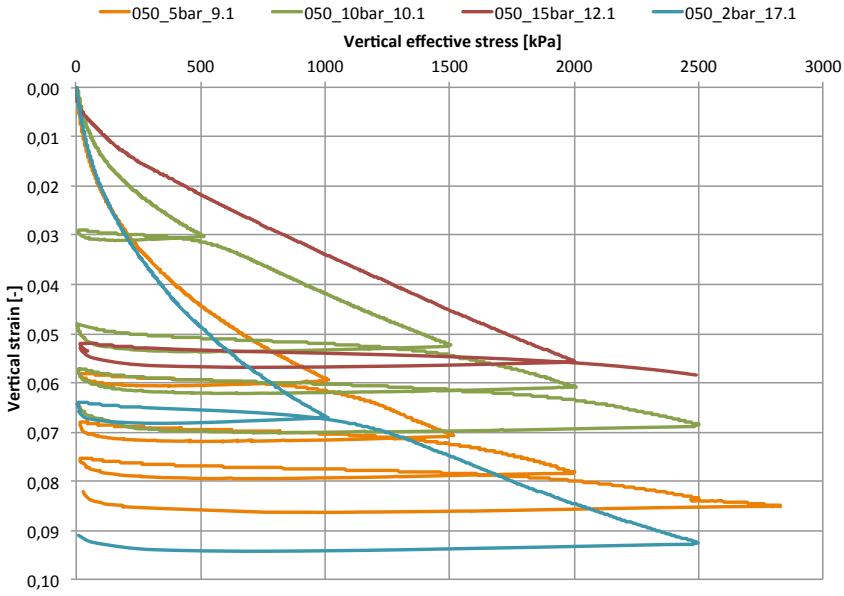

(a) Tests with initial water content of 50%

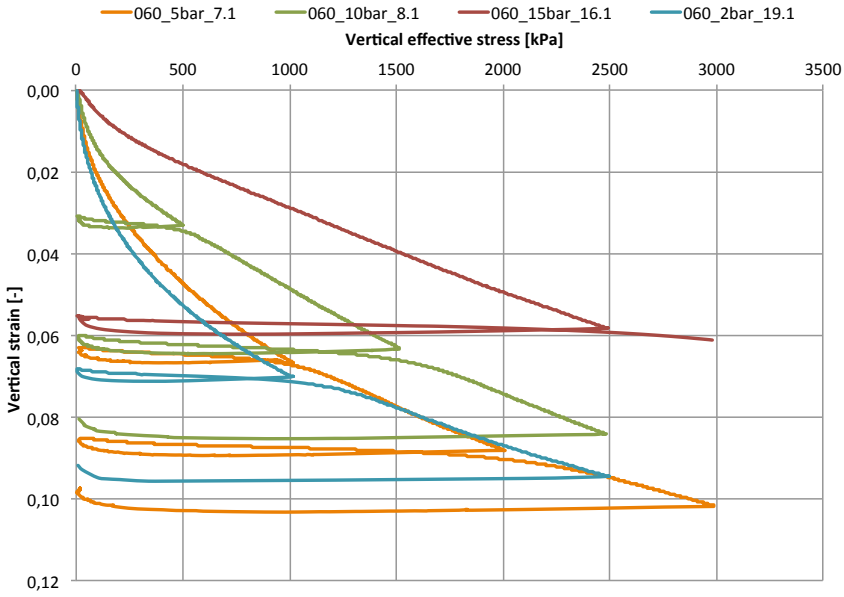

(b) Tests with initial water content of 60%

Figure B.2: Vertical effective stress versus vertical strain
Colour encoding: red=15 bar, green=10 bar, orange=5 bar and blue=2bar

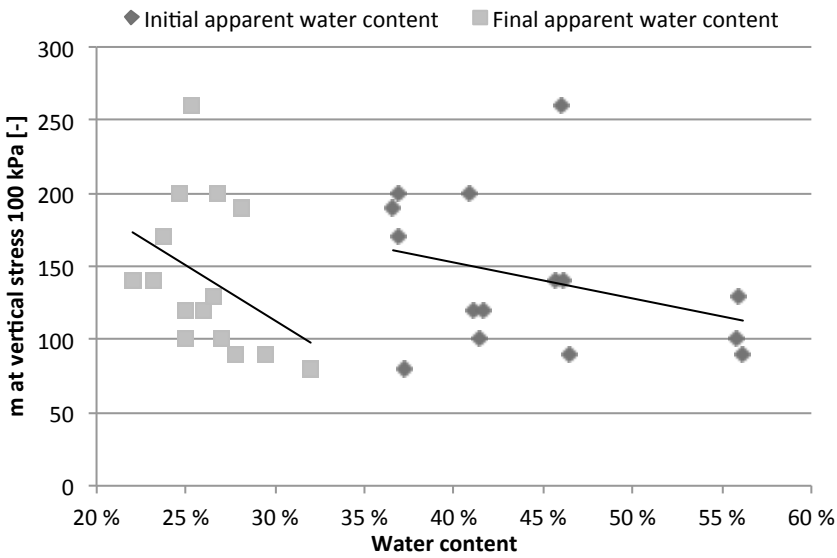

Figure B.3: Modulus number at vertical stress 100 kPa versus apparent water content before and after filtration

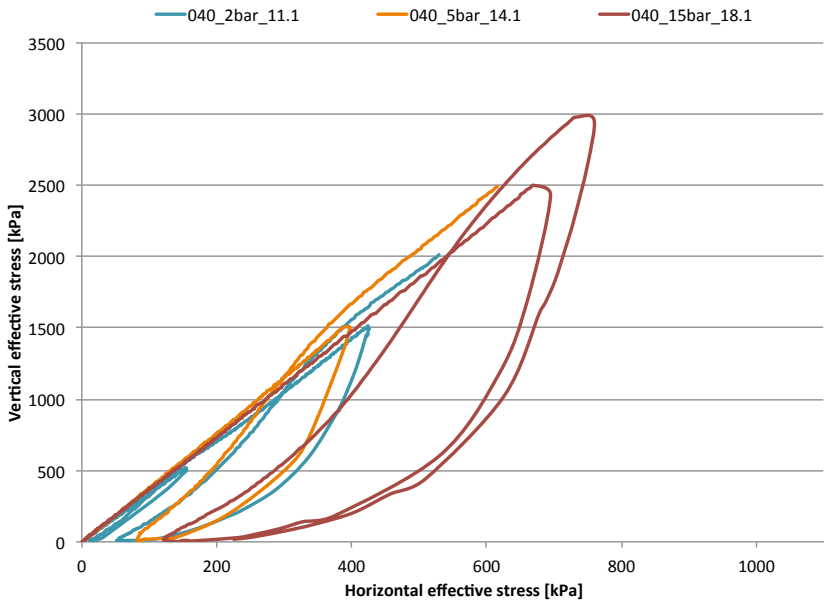

(a) Tests with initial water content of 40%

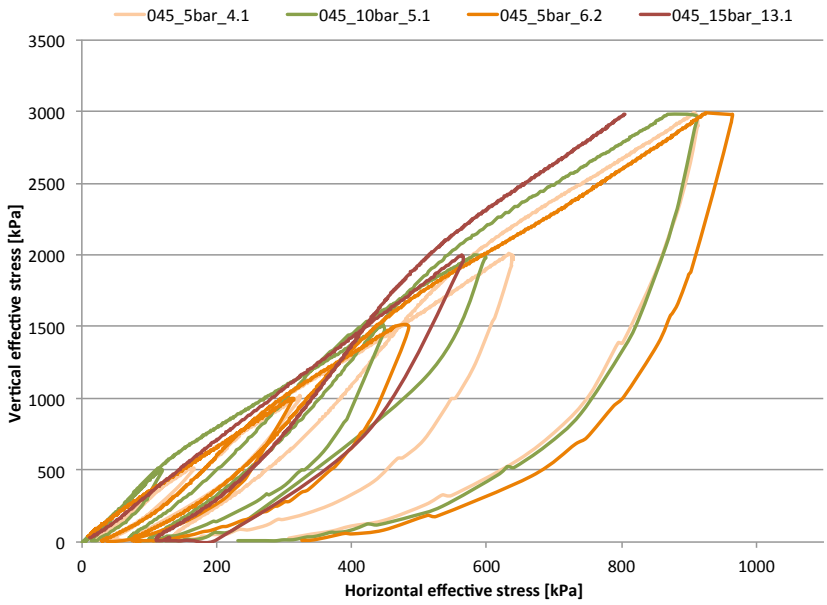

(b) Tests with initial water content of 45%

Figure B.4: Horizontal versus vertical effective stress
Colour encoding: red=15 bar, green=10 bar, orange=5 bar and blue=2bar

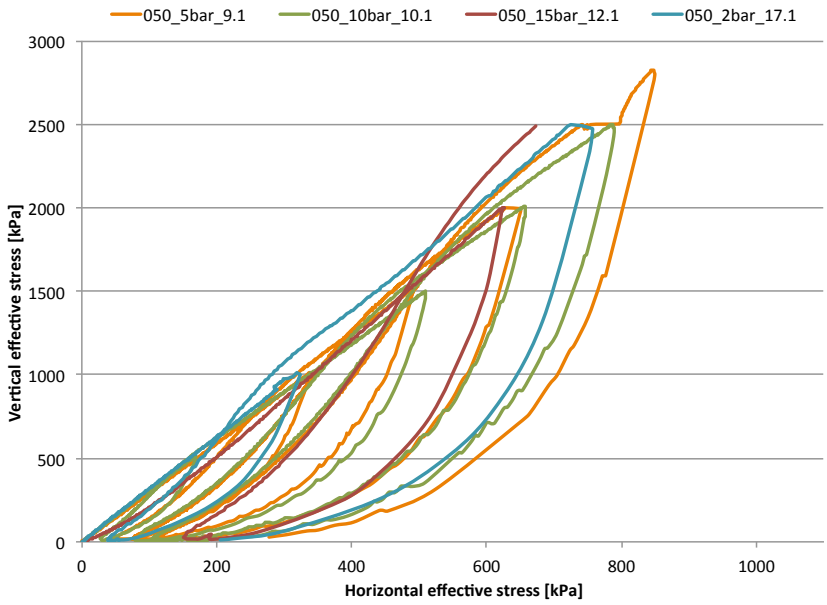

(a) Tests with initial water content of 50%

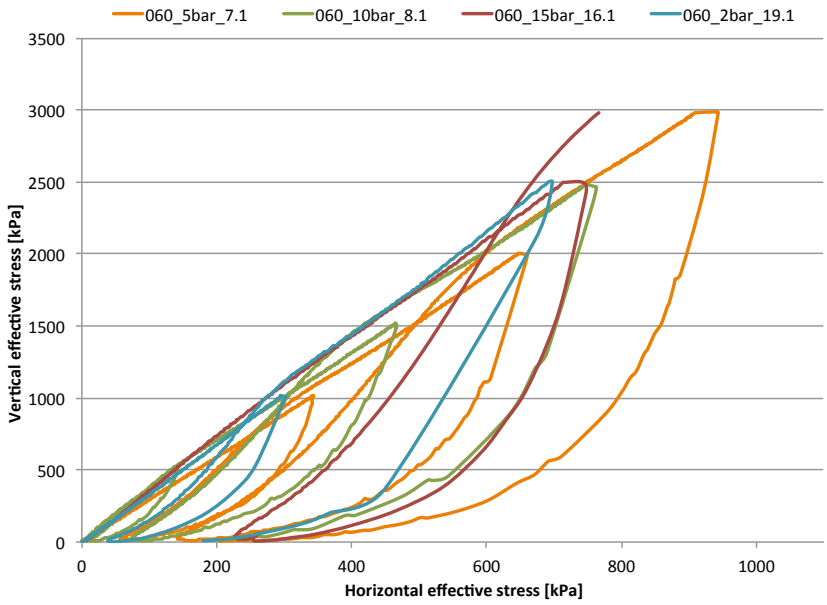

(b) Tests with initial water content of 60%

Figure B.5: Horizontal versus vertical effective stress
Colour encoding: red=15 bar, green=10 bar, orange=5 bar and blue=2bar

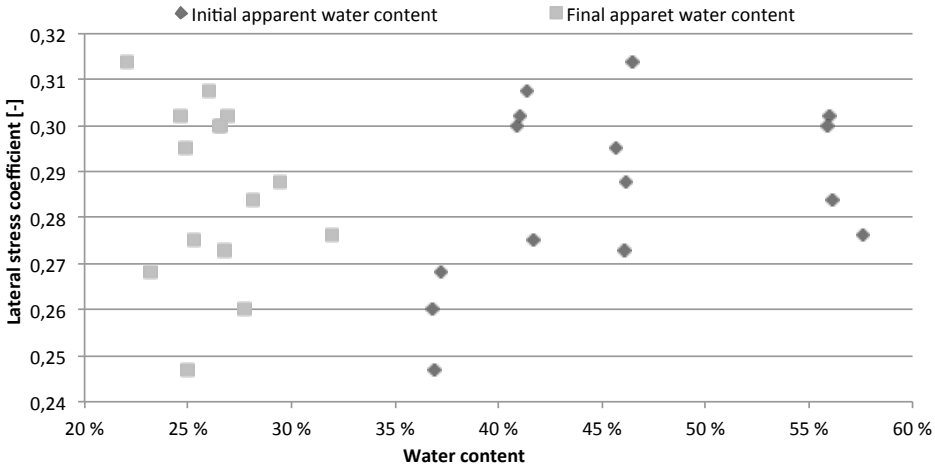

(a)

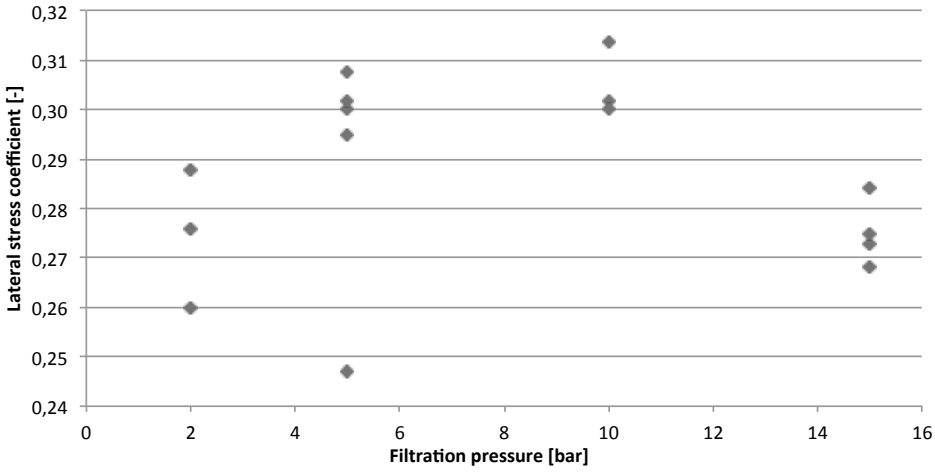

(b)

Figure B.6: Lateral stress coefficient versus water content and filtration pressure

Appendix C

Original and altered displacements for oedometer tests

When the oedometer reaches the desired maximum vertical stress it will stop further loading. Yet displacements are recorded due to creep and after some time there will be a minor stress relief. Thus, when the stresses become small enough the oedometer will start loading again until it again reaches the desired stress level. If the oedometer is left alone like this for some time the deformations will be larger than they should be. Thus, the portions of the results where the vertical stress level was constant were cut out, and the difference in displacements between the start and the end of these sequences zeroed, trying to recreate how the results would be if the tests were run without the oedometer stopping. The resulting shifts in displacements are illustrated in Figures C.1, C.2 and C.3.

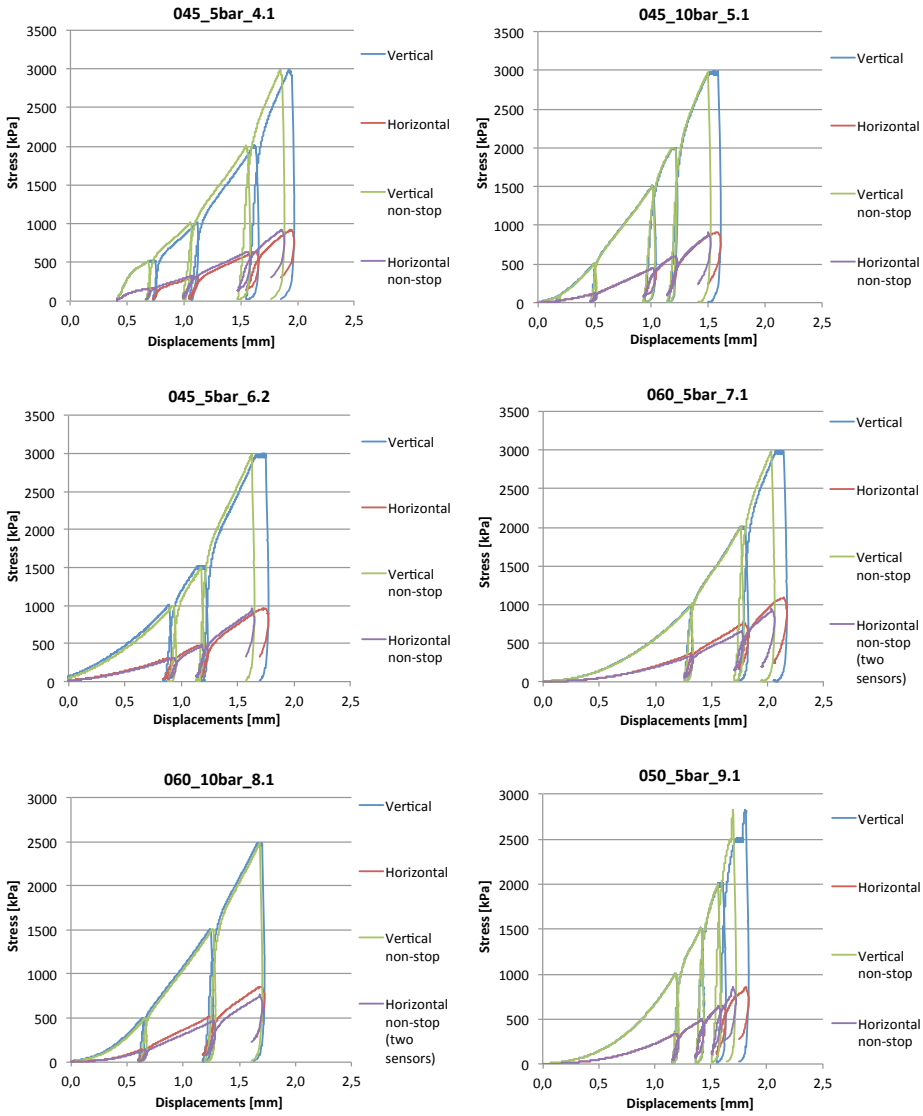

Figure C.1: Original and altered displacements versus vertical effective stress for test series 4 to 9

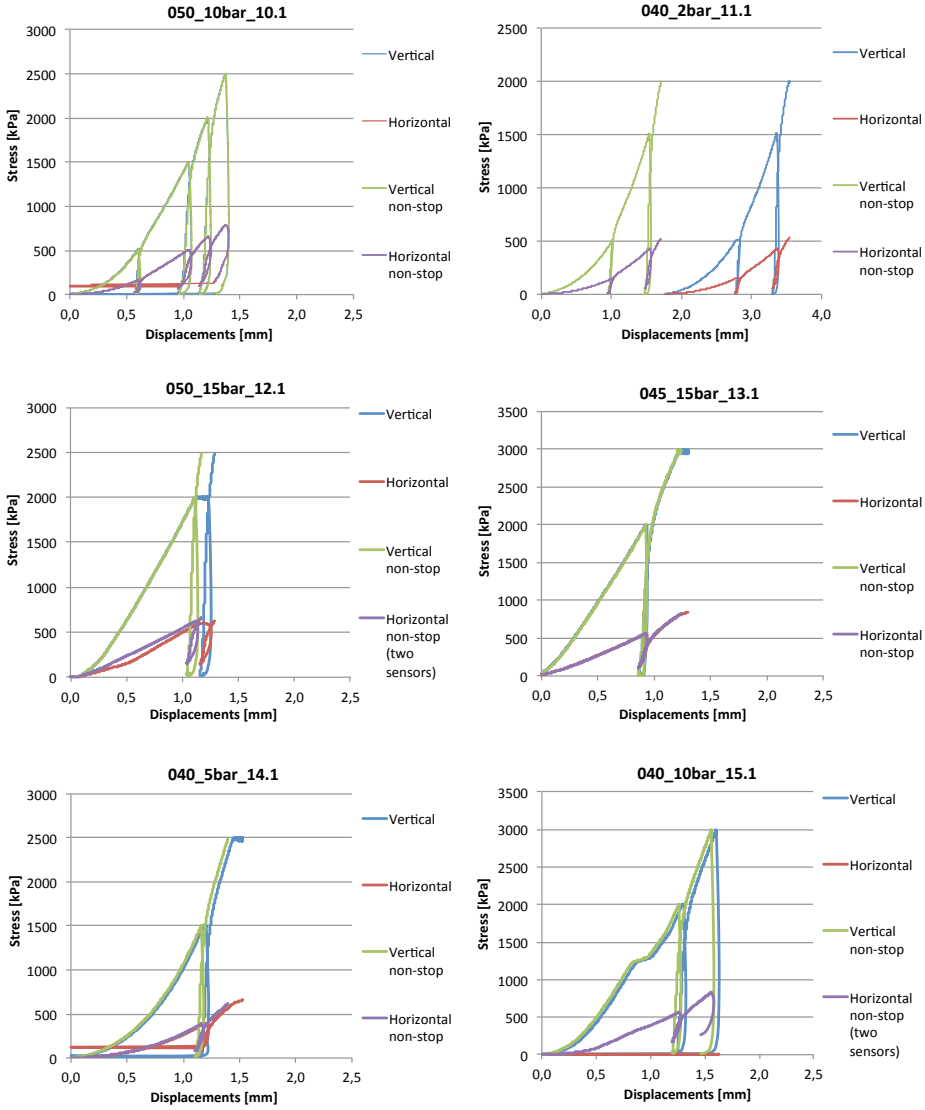

Figure C.2: Original and altered displacements versus vertical effective stress for test series 10 to 15

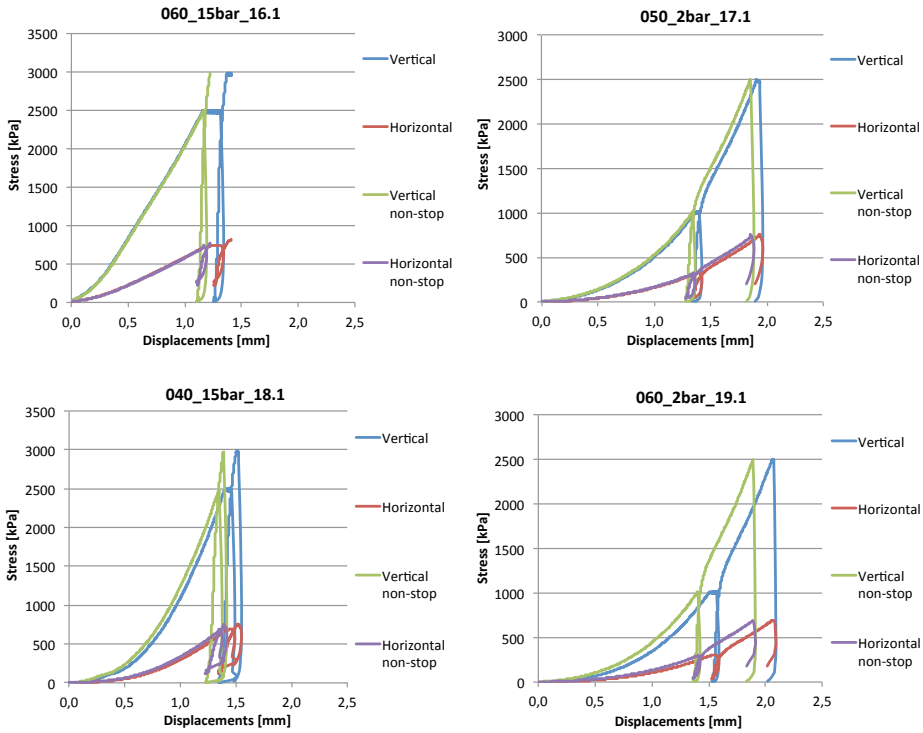

Figure C.3: Original and altered displacements versus vertical effective stress for test series 16 to 19

Appendix D

Reloading stiffness for oedometer tests

The oedometer modulus for each reloading sequence is shown in Figures D.1, D.2 and D.3. The corresponding modulus numbers (assuming a=0 in the modulus forumula) are shown in Figures D.4, D.5 and D.6. For tests 17.1 and 19.1 the results are also plotted after the reloading sequence has finished to illustrate the smooth transition between a reloading and first time loading stage.

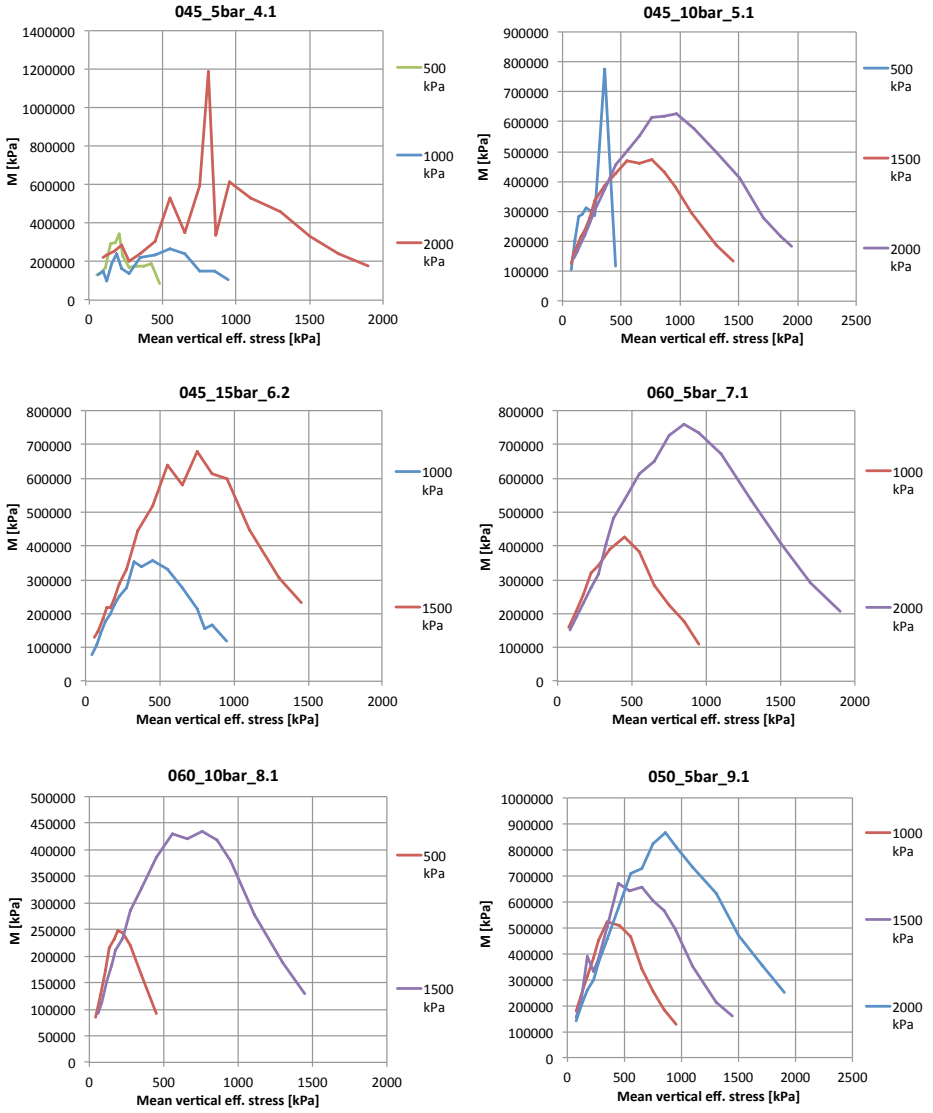

Figure D.1: Reloading stiffness versus vertical effective stress for test series 4 to 9

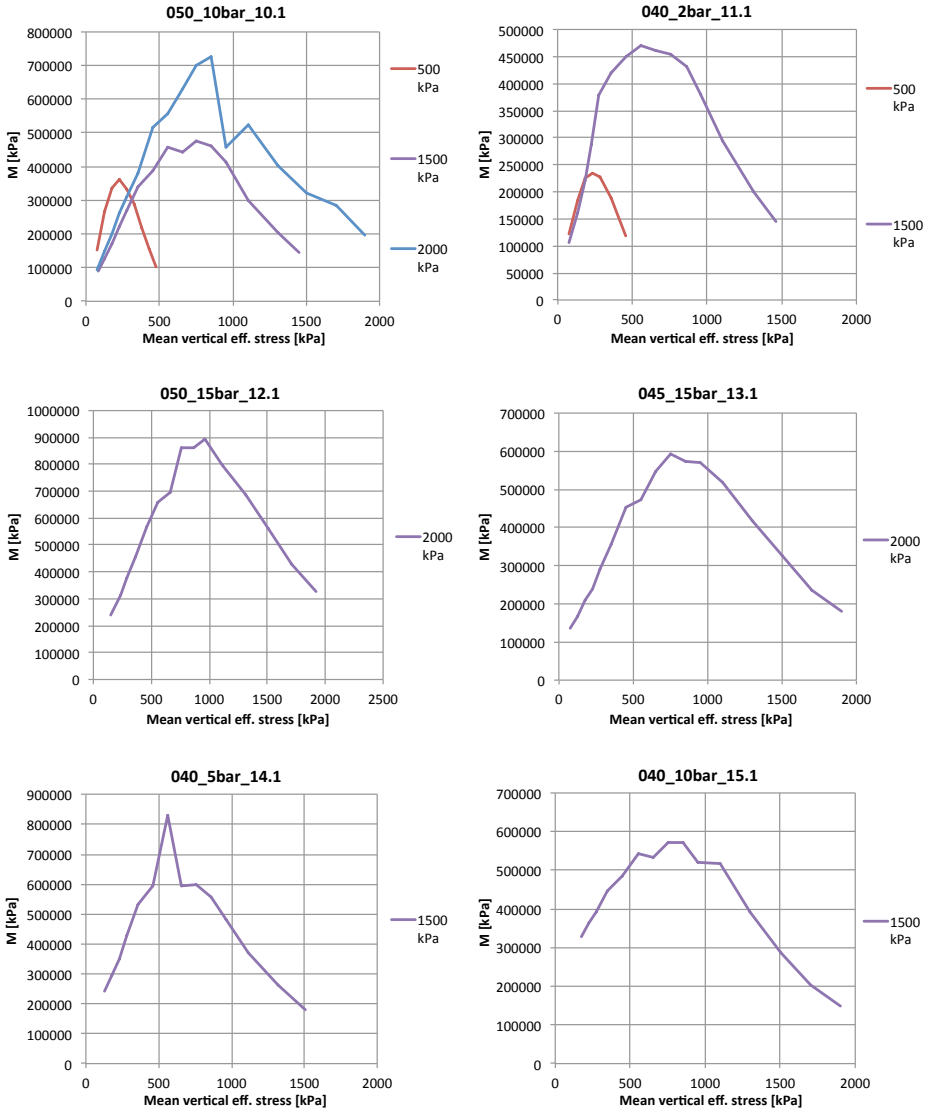

Figure D.2: Reloading stiffness versus vertical effective stress for test series 10 to 15

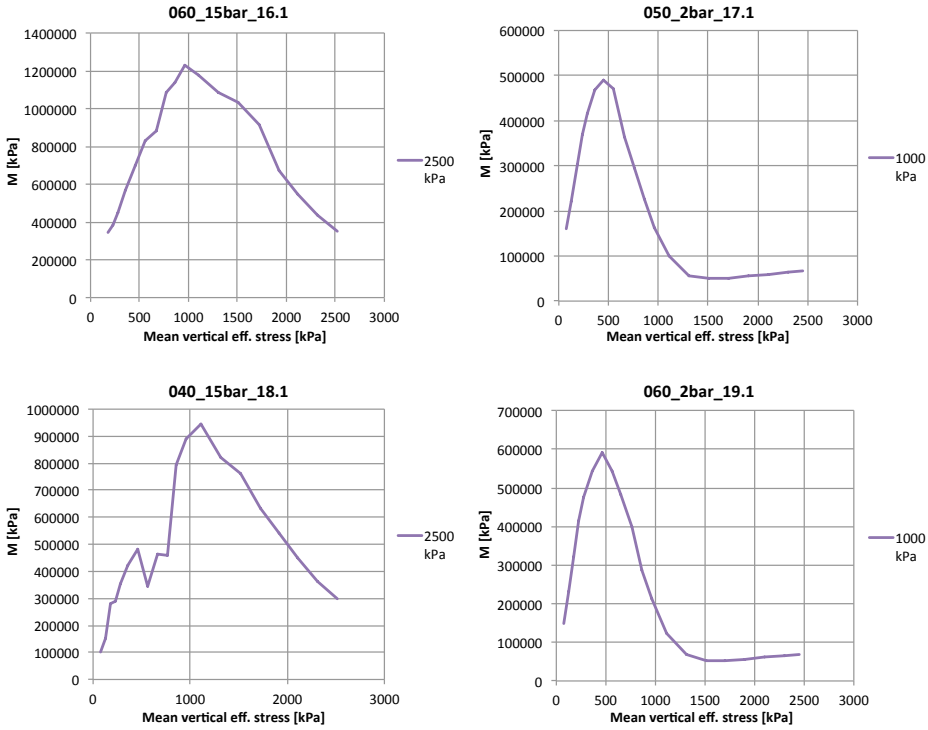

Figure D.3: Reloading stiffness versus vertical effective stress for test series 16 to 19

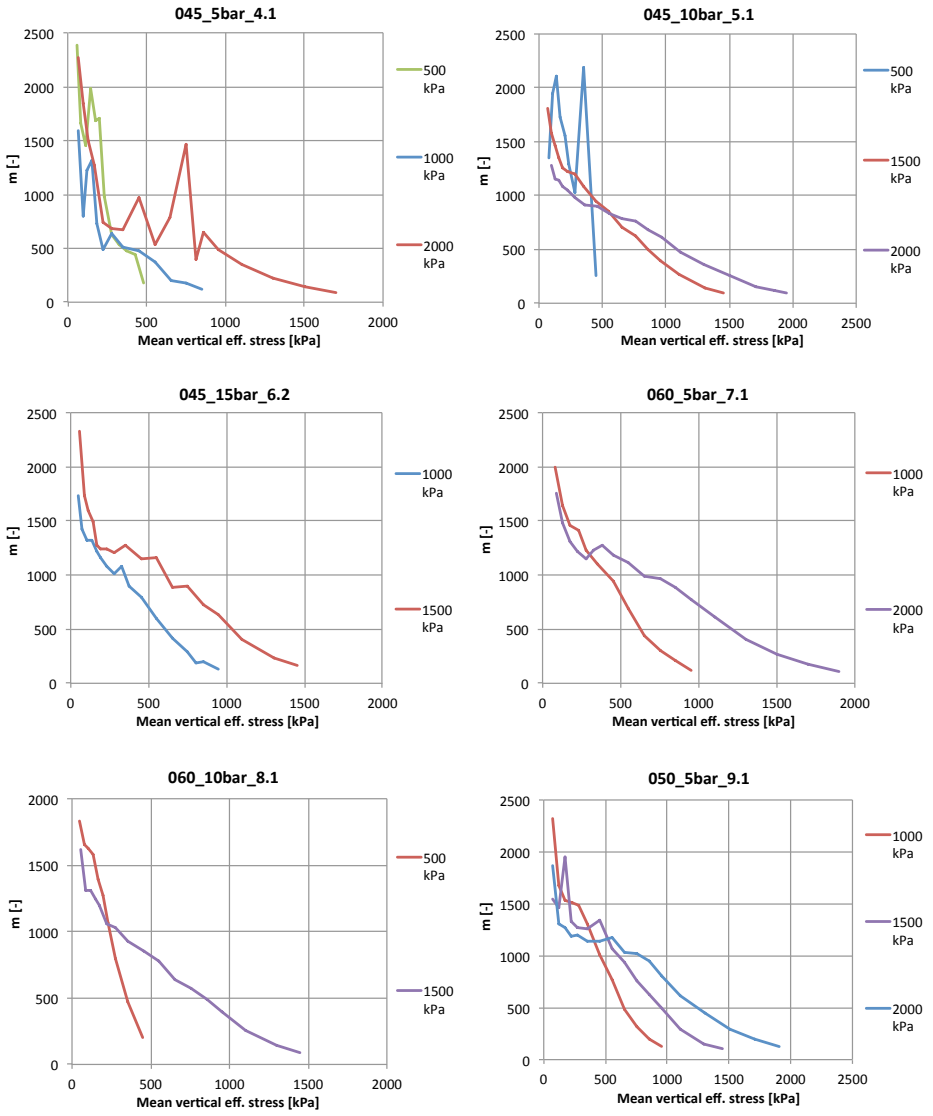

Figure D.4: Reloading modulus number versus vertical effective stress for test series 4 to 9

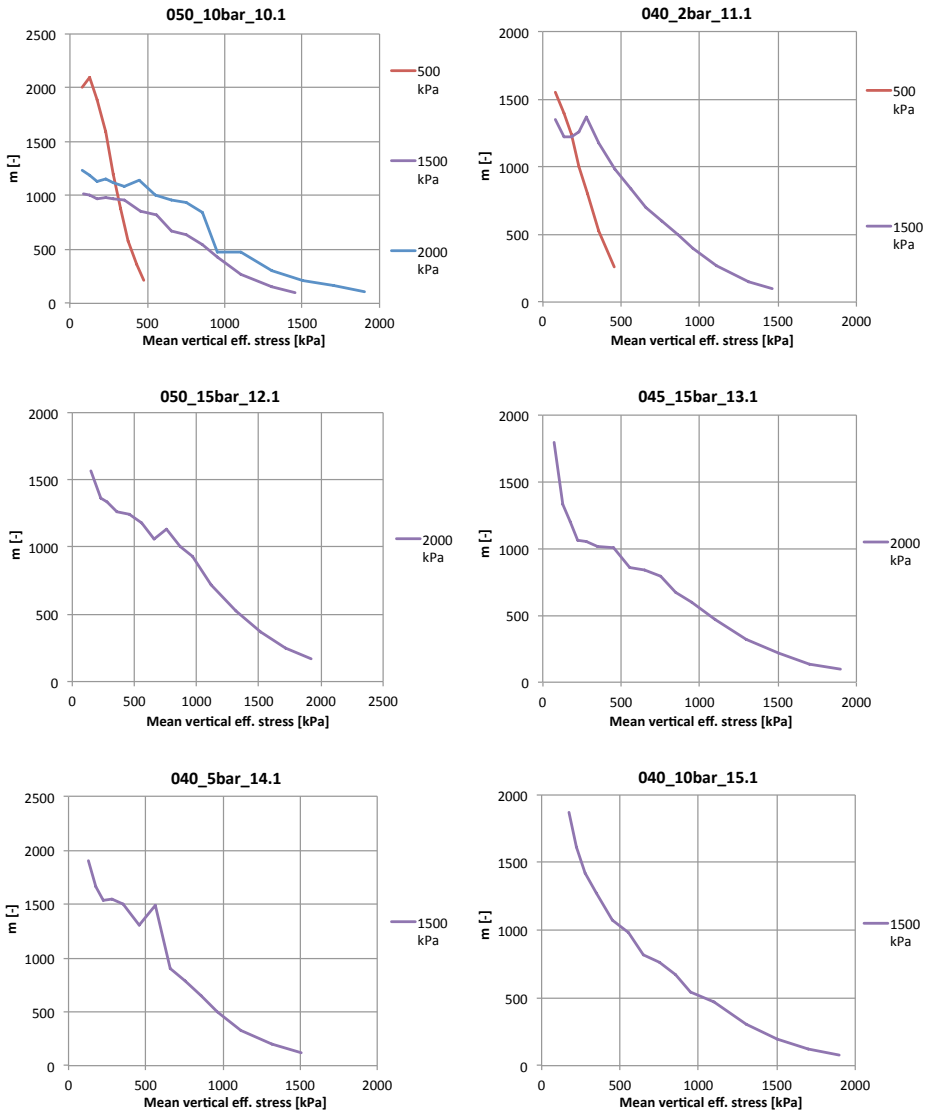

Figure D.5: Reloading modulus number versus vertical effective stress for test series 10 to 15

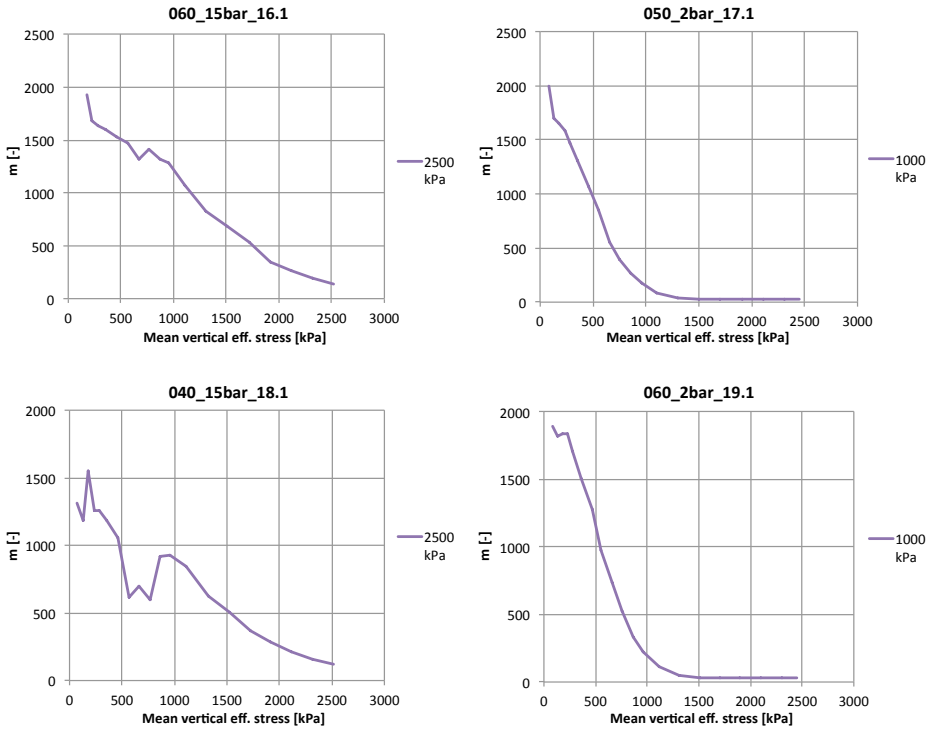

Figure D.6: Reloading modulus number versus vertical effective stress for test series 16 to 19

Appendix E

Calibration of the oedometer

During the seventh test series a disturbance in radial sensor three was suspected, probably due to a minor damage in a cable connected to the sensor. Calculating the horizontal stresses measured by each individual sensor and plotting against the vertical stress makes it possible to see if there are big differences between the sensors. According to Figures E.2, E.3 and E.4 the third sensor yields much bigger horizontal stresses than sensor one and two in test 7.1 and 8.1, but strangely not for test 9.1 and 10.1. The oedometer was re-calibrated before test 11.1, and the calibration factor was found to have changed from 2100 kPa/V to 1600 kPa/V. The calibration process was difficult to perform satisfactory, as the balloons were old and tended to burst before reaching higher pressures than 500kPa, which is only half of the maximum allowed horizontal stress. The result from the calibration test can be seen in Table E.1 and Figure E.2. The results for the tests after calibration are varying, and especially tests 12.1 and 15.1 seem strange. It seems like the third sensor is no longer trustworthy, and should be neglected if it causes major alternations in the results. Thus, for tests 7.1, 8.1 and 12.1 a horizontal stress based exclusively on radial sensor one and two are used in the calculations. Test 15.1 show some strange behaviour in both cases (there is also a sudden increase in vertical stress in this test) and was therefore excluded from the calculations related to the horizontal stress. Horizontal versus vertical stress for tests 7.1, 8.1, 12.1 and 15.1 are plotted in Figures E.5, E.6, E.7 and E.8, respectively.

Table E.1: Calibration data

Horizontal pressure	1	2	3
0	-0,001	0,012	0,003
100	0,044	0,072	0,06
200	0,09	0,131	0,122
300	0,131	0,188	0,186
400	0,171	0,244	0,249
500	0,209	0,3	0,315

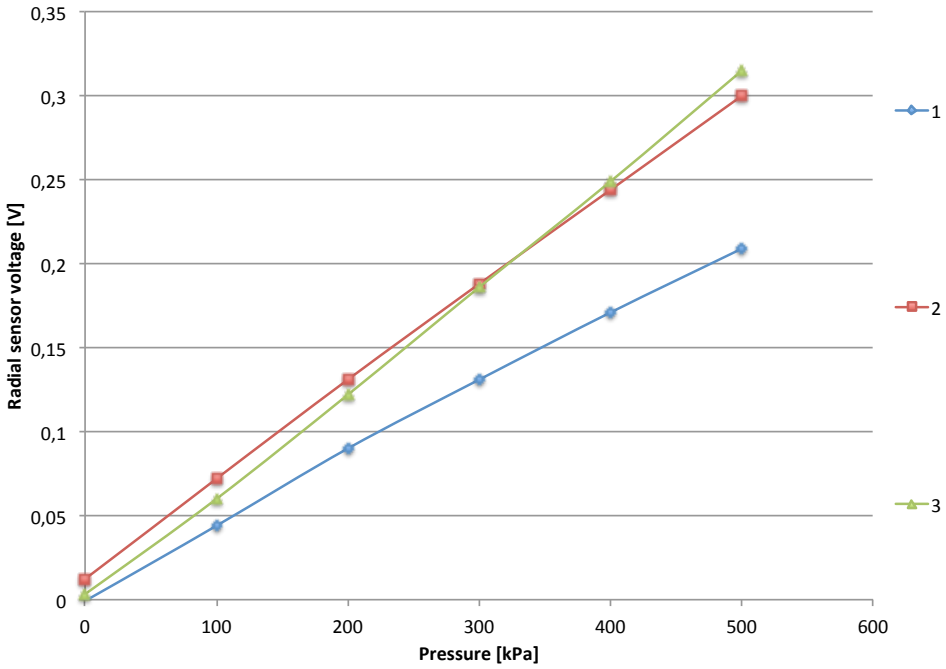

Figure E.1: Calibration curve

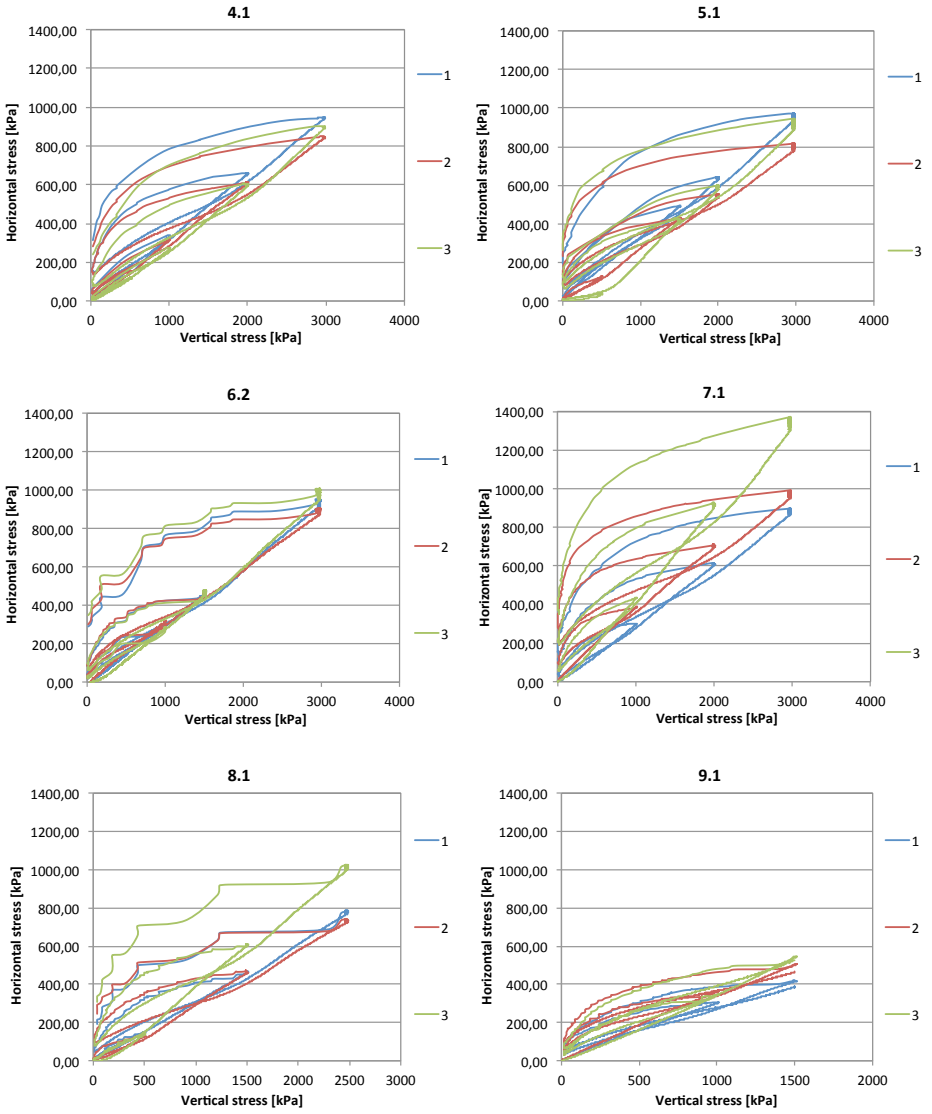

Figure E.2: Vertical versus horizontal stress for the individual radial sensors for test series 4 to 9

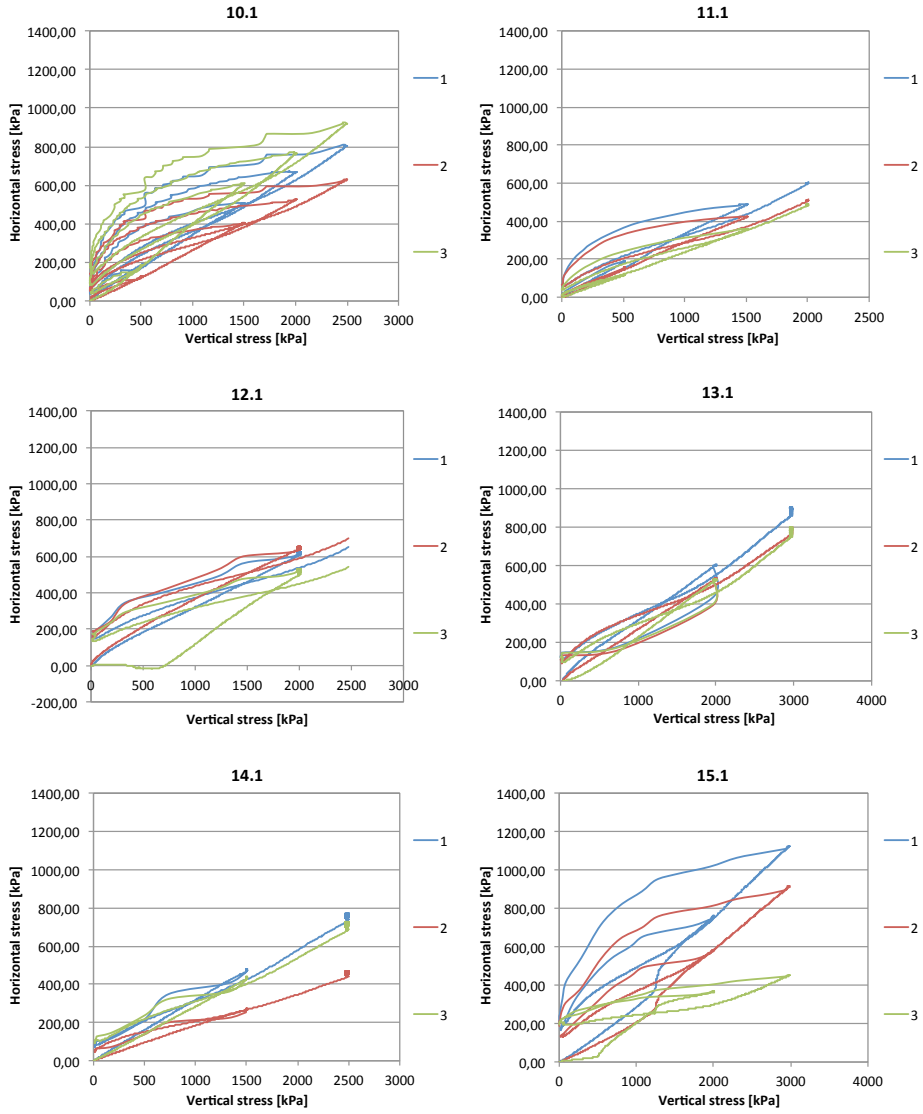

Figure E.3: Vertical versus horizontal stress for the individual radial sensors for test series 10 to 15

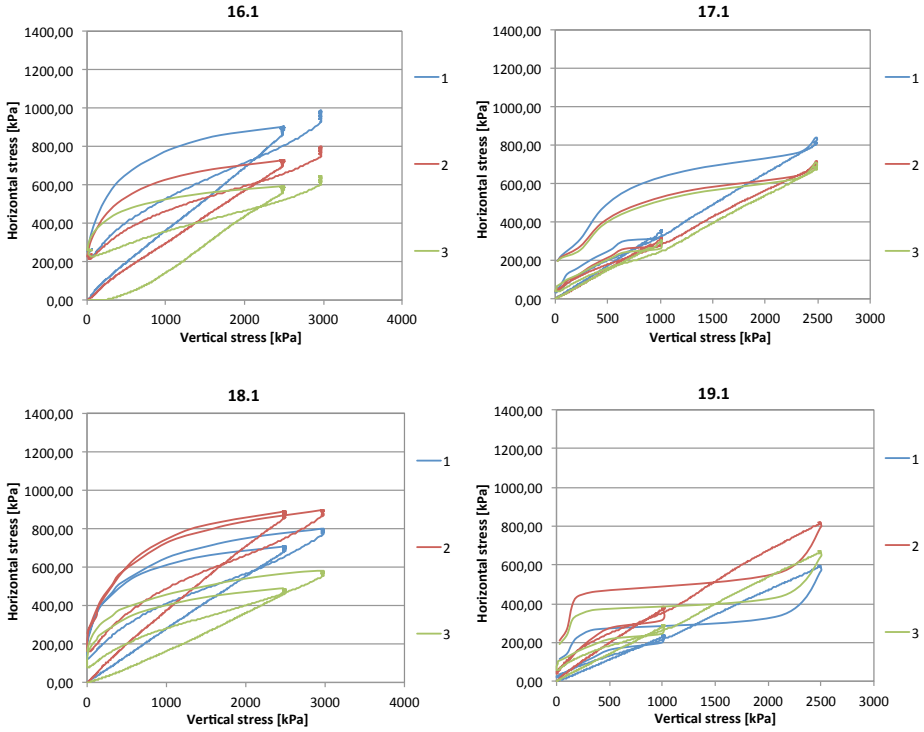

Figure E.4: Vertical versus horizontal stress for the individual radial sensors for test series 16 to 19

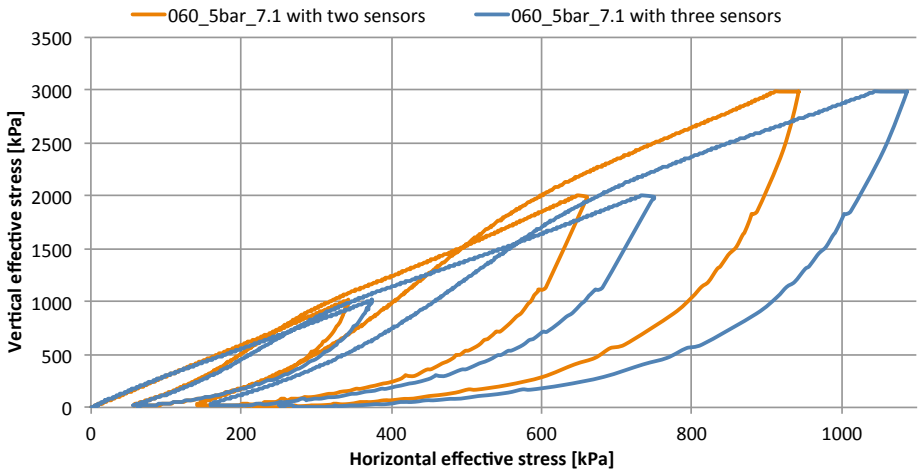

Figure E.5: Horizontal versus vertical stress for test 7.1

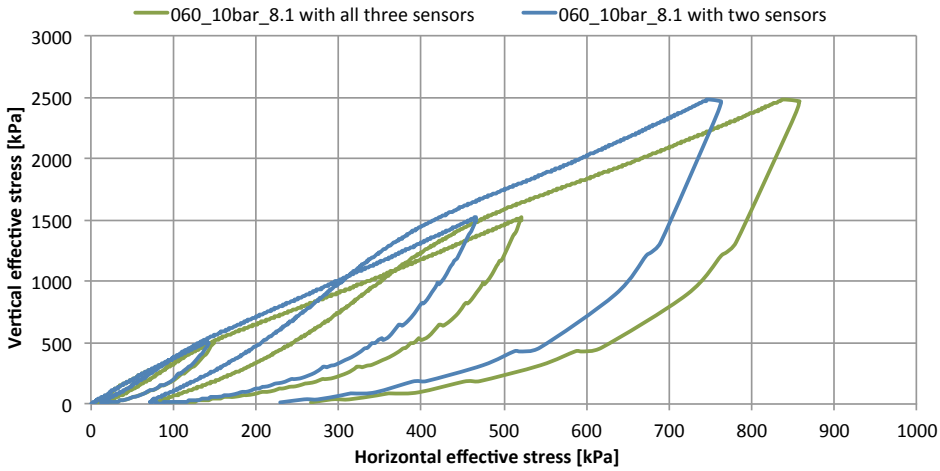

Figure E.6: Horizontal versus vertical stress for test 8.1

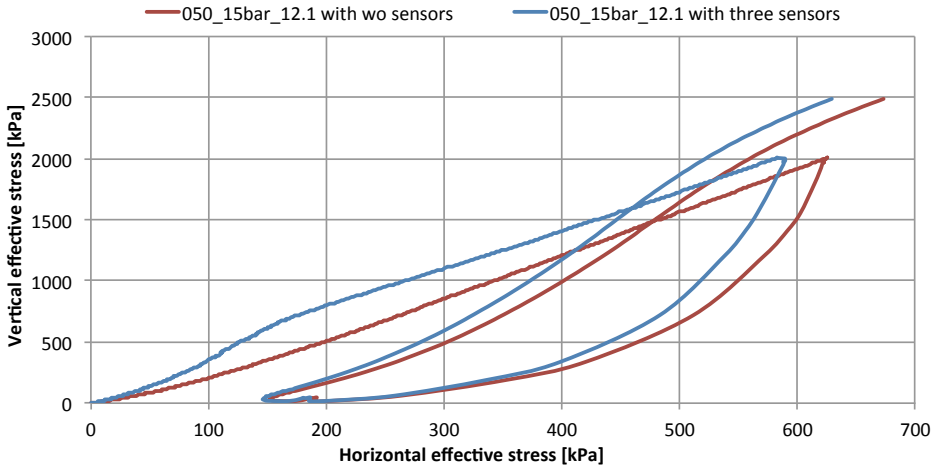

Figure E.7: Horizontal versus vertical stress for test 12.1

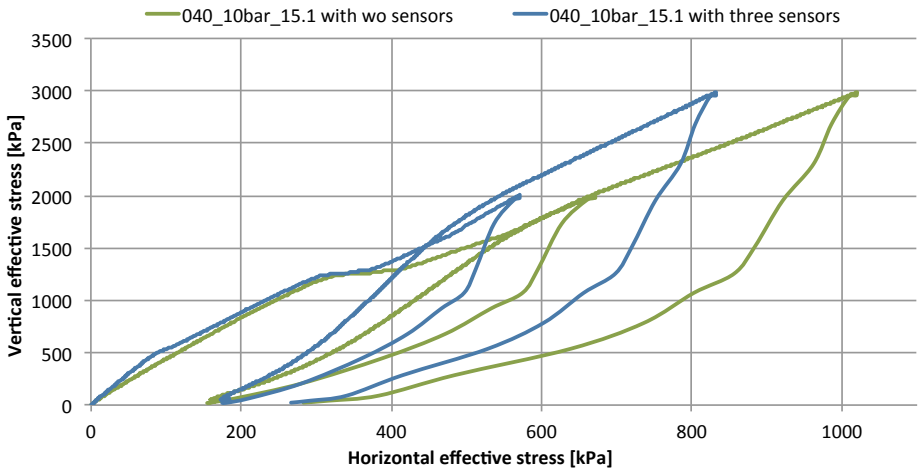

Figure E.8: Horizontal versus vertical stress for test 15.1

Appendix F

Oedometer results from tests on clay

In this appendix, results from two oedometer test on clay are presented. Figure F.1 shows the stress/strain curves. In Figures F.2 and F.3 the vertical effective stress is plotted against the oedometer modulus and the modulus number, respectively. The modulus numbers stabilize at approximately 20, which is normal for a medium stiff clay. The increase in horizontal stress is approximately proportional to the increase in vertical stress , as can be seen in Figure F.4. From Figure F.5 it is clear that the lateral stress coefficient stabilizes between 0,4-0,5, which also is common for a normally consolidated clay. In Figure F.6 the inclination of the curves gives the rate of strain applied to the clay samples. This corresponds to 1,2 %/hour for clay test 1 and 1,8 %/hour for clay test 2 (the samples initial height is 20 mm). As can be seen from Figure F.7 the pore pressure ratio is almost zero during the whole first test. This is probably due to the amount of silicone that was applied to the base of the oedometer and between the ring sections. For clay test 2 the amount of silicone was increased, yielding higher pore pressure ratios. The ratio is now higher and develops in a pattern which is expected from a CRS oedometer test with decreasing pore pressure ratios with increasing displacements. Also no leak was observed during testing, giving reasons to believe that the oedometer is tight and the pore pressure measurements reliable.

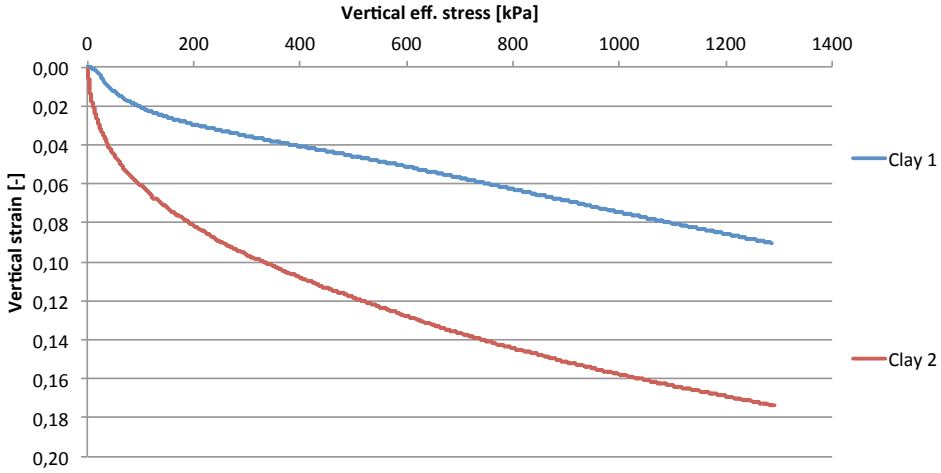

Figure F.1: Vertical effective stress versus vertical strain

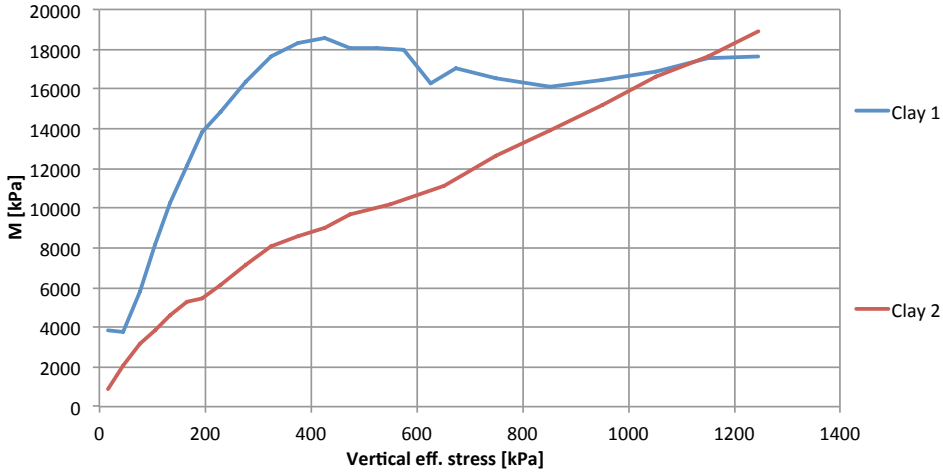

Figure F.2: Vertical effective stress versus oedometer modulus

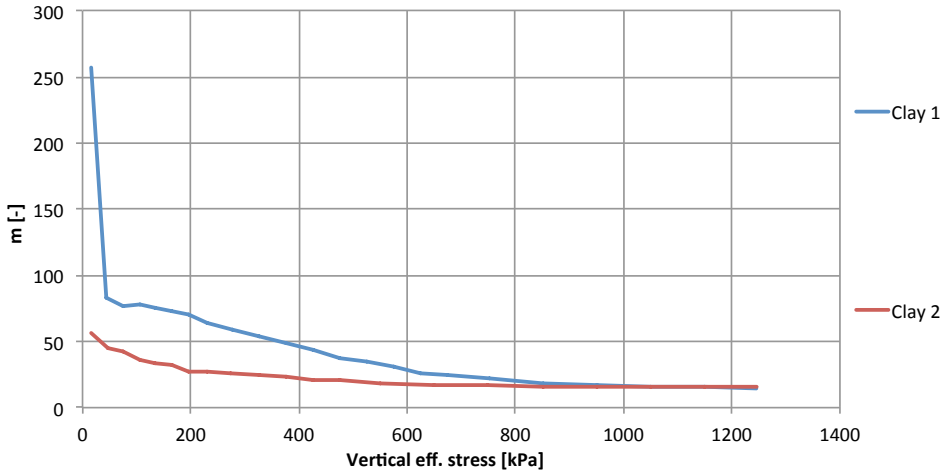

Figure F.3: Vertical effective stress versus modulus number

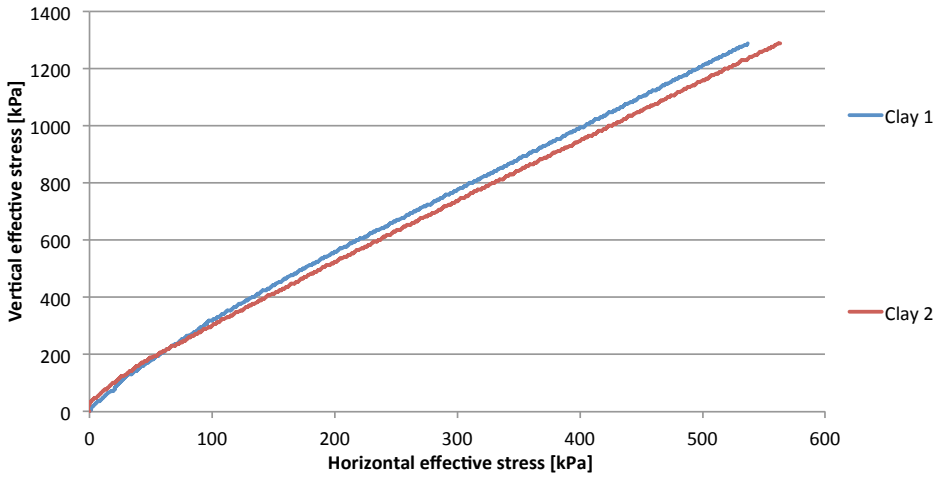

Figure F.4: Horizontal versus vertical effective stress

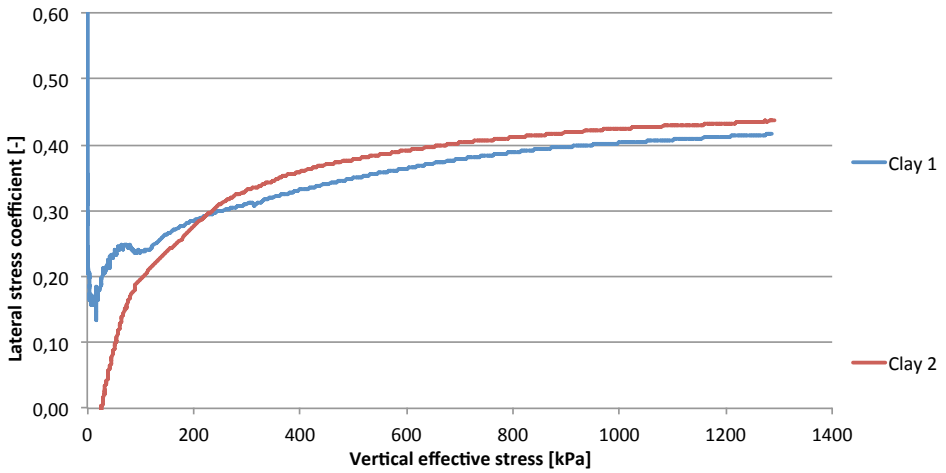

Figure F.5: Vertical effective stress versus lateral stress coefficient

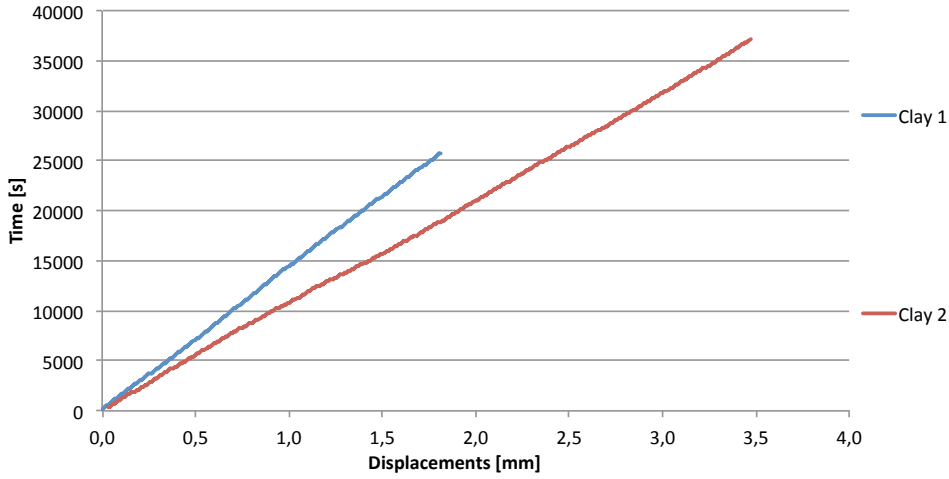

Figure F.6: Time after start versus displacements

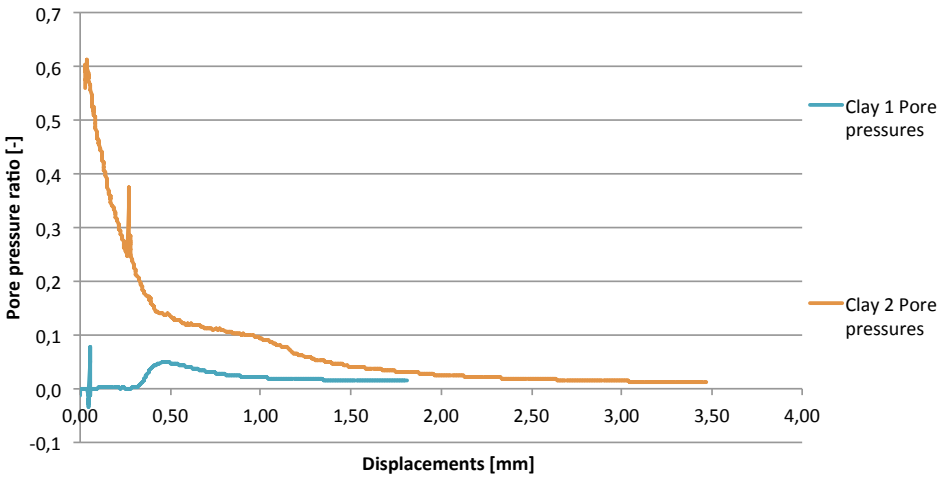

Figure F.7: Displacements versus pore pressure ratio

Appendix G

Detailed description of the planned experimental setup and aberrations

A detailed overview of how the experimental setup was planned is given in Tables G.1 and G.2. Test types F, P and O represent filtration, permeability and oedometer tests, respectively.

Table G.1: Detailed overview of experimental setup

Test number	Initial water content	Filtration pressure	Test type
1.1	0,45	1bar	F + O
1.2	0,45	1bar	F
1.3	0,45	2bar	F
2.1	0,45	2bar	F + O
2.2	0,45	2bar	F
2.3	0,45	1bar	F
4.1	0,45	5bar	F + O
4.2	0,45	5bar	F
4.3	0,45	5bar	F
5.1	0,40	10bar	F + O
5.2	0,40	10bar	F
5.3	0,40	10bar	F
6.1	0,45	15bar	F + O
6.2	0,45	5bar	F
6.3	0,45	5bar	F

Table G.2: Detailed overview of experimental setup continued

Test number	Initial water content	Filtration pressure	Test type
7.1	0,60	5bar	F + O
7.2	0,60	5bar	F + P
8.1	0,60	10bar	F + O
8.2	0,60	10bar	F + P
9.1	0,50	5bar	F + O
9.2	0,50	5bar	F + P
10.1	0,50	10bar	F + O
10.2	0,50	10bar	F + P
10.3	0,50	5bar	F + P
11.1	0,40	2bar	F + O
11.2	0,40	2bar	F
12.1	0,50	15bar	F + O
12.2	0,50	15bar	F
12.3	0,50	15bar	F + P
13.1	0,45	15bar	F + O
13.2	0,45	15bar	F + P
14.1	0,40	5bar	F + O
14.2	0,40	5bar	F + P
14.3	0,40	5bar	F
15.1	0,40	10bar	F + O
15.2	0,40	10bar	F + P
16.1	0,60	15bar	F + O
16.2	0,60	15bar	F + P
16.3	0,60	15bar	F
17.1	0,50	2bar	F + O
17.2	0,50	2bar	F
17.3	0,50	2bar	F + P
18.1	0,40	15bar	F + O
18.2	0,40	15bar	F
18.3	0,40	15bar	F + P
19.1	0,60	2bar	F + O
19.2	0,60	2bar	F
19.3	0,60	2bar	F + P

Occasionally some things may not have gone as planned, and any aberrations from the original plan are described in the following. Results may be excluded from interpretation due to these, in which case this is mentioned specifically. Also, results being excluded for other reasons are mentioned.

Test series 1 All tests were considered as tests run primarily to check the experimental procedure. Thus, due to procedural changes most of the results were omitted. However, the results related to water content measurements were spared. For test

045_2bar_1.3 the cylinder was not weighted before filtration.

045_2bar_2.1 The oedometer results were omitted due to procedural changes.

045_1bar_2.3 The cylinder filled with grout was not weighed before filtration, so the mass of wet grout in the cylinder is not known and parameters related to this could not be calculated.

Test series 3 Sand was used between the grout and the filter stone. Since it was difficult to obtain equal conditions between each test, more tests with sand was not executed. The results from the three tests were widely spread and the effect of using sand was not clear. Thus, the results were considered redundant and excluded.

045_5bar_4.1 The top filter stone were resting on the sides of the oedometer ring. This was discovered at an vertical stress of 300 kPa. The sample was then unloaded, the filter stone adjusted, and then reloaded. Thus, the initial part of the results will give reloading values.

045_15bar_6.1 The tube connected to the top piece was not properly connected to the pressure gauge, causing the tube to loosen so that the grout was spread around in the lab. Thus, only results for water contents before filtration are available., and the oedometer test for this series were instead run for the second test.

045_5bar_6.3 The deformation measurer in the filtration test was not properly set up, resulting in no deformation results.

060_5bar_7.2 Permeability test results were omitted due to procedural changes.

060_10bar_8.2 Permeability test results were omitted due to procedural changes.

040_2bar_11.2 Cylinder was not weighted after filtration, and the parameters based on this could therefore not be calculated.

050_15bar_12.1 Cement came out during filtration. Results affected by this were excluded.

050_15bar_12.2 Cement came out during filtration. Water content before filtration was not measured. After filtration, the top piece was stuck and the filter cake was destroyed during the effort of getting the top piece off. Thus, no usable results were obtained in this test.

040_10bar_15.1 The horizontal stress measured where very different than in all other tests. The reason for this is discussed in Appendix E, and the results related to the horizontal stress were not omitted. Also, there is a sudden increase in vertical strain at $\sigma'_v = 1000 - 1500$ kPa. Possibly the filter stone rested slightly on the side of the oedometer, yielding to high stiffness up to this level.

040_15bar_18.1 Some cement came out during filtration. Results affected by this were excluded.

040_15bar_18.2 Cylinder not weighed after filtration. Minor amount of cement came out during filtration, but this was considered negligible as the results looked okay.